Abstract

SANDERS, DILLON HUGH. Thermal Jamming in Glass Formers. (Under the direction of Dr. Jacob Eapen).

Theories of the glass transition generally attempt to describe the evolution of glass-forming liquids toward an amorphous solid state using an array of dynamical and thermodynamic properties. The focus of this work is to quantitatively describe the dynamical evolution of glass forming liquids, and ultimately the broader class of disordered states, in terms of "thermal jamming", a term that describes the level of kinetic frustration, which depends on the thermodynamic state and the fraction of atoms that effectively contribute to diffusion. Motivated by the Two-Phase Thermodynamic (2PT) Method for computing liquid thermodynamic properties, a hard sphere partitioning approach is proposed which partitions a liquid in such a way that its diffusive characteristics are encapsulated by an equivalent system of hard spheres, while its vibratory characteristics are modeled as a system of harmonic oscillators. This approach relies on a partitioning metric f which is defined as the ratio of effective hard spheres in the liquid to the total number of atoms in the liquid, and is postulated to be the inverse of the radial distribution function at the point of contact. The hard spheres represent the set of atoms whose dynamics are well-described using repulsive forces, while the harmonic oscillators symbolize the remaining set of atoms that interact through attractive forces. Thus, only a fraction of atoms denoted by the ratio f contribute to diffusive dynamics. The partitioning metric allows for the subsequent calculation of an effective packing fraction $\hat{\phi}$ of the liquid, and the excess entropy. These quantities are used to demonstrate two key predictions of the thermal jamming hypothesis: 1) the approach of $\hat{\phi}$ to a maximally-jammed value as the temperature of the liquid decreases towards the mode coupling or glass transition temperature, and 2) and a true universal scaling of dynamical quantities with excess entropy that holds among various thermodynamic states and across different materials.

Atomistic simulations are used to study several model systems which adequately recreate the dynamics of glassy liquids (Kob-Andersen, Weeks-Chandler-Andersen, harmonic spheres, and Dzugutov) are featured in this work. For these systems, the hard sphere partitioning (HSP) approach indicates that the effective packing fraction of the hard spheres, $\hat{\phi}$, asymptotically approaches the random-close-packed limit for the model glass formers with decreasing temperature. Furthermore, the HSP method is used to compute the excess entropy of the hard

sphere partition, as well as the excess entropy of the liquid. When plotted as a function of the excess entropy, the reduced dynamical quantities such as diffusivity portray a strict scaling behavior that establishes a direct relationship between the dynamical and thermodynamic properties of the liquids. In the context of quasi-universal and universal descriptions of liquid dynamics, the HSP approach reveals a new class of universal liquid behavior for all thermodynamic states.

In addition to the model systems studied using atomistic simulations, the application of the HSP approach to real glass formers is demonstrated. Eight glass forming liquids, for which the reported literature data extends to the glass transition temperature T_g and below, are investigated; these systems, which depict both fragile and strong behavior, allow a richer and a broader range of glassy dynamics than allowed by atomistic simulations. The analysis show that a true universal scaling with excess entropy is obeyed by all the eight glass formers. This universality principally rests on the partitioning of a system into equivalent hard spheres and harmonic oscillators, unlike the previous analyses that attempted to model the entire system into equivalent hard spheres. At a more fundamental level, the idea of a liquid solely represented by repulsive forces may need a revision, particularly for the supercooled states.

A separate analysis is conducted from the perspective of string-like cooperative motion, a ubiquitous feature of a broad range of jammed systems throughout nature. By conducting a novel analysis of string-like structures in four model glass-formers, a shift in the nature of the dynamics of strings is revealed as a non-monotonic variation of the population of "cooperative pairs" (two-member strings) at an important dynamic crossover that occurs at a temperature T_S for all model systems. Additionally, a novel "tracking analysis" is employed to examine the origins of this behavior in terms of the creation and annihilation of strings as the dynamics of the liquid evolves over time.

The twofold analysis of glassy systems in this work provides evidence for the concept of thermal jamming, in the form of (*i*) an effective packing fraction $\hat{\phi}$ from the HSP approach that demonstrates asymptotic convergence near critical temperatures in glass formers and (*ii*) the demonstration of a new class of universality in glass formers that envelops all thermodynamic states and interatomic/molecular interactions.

Thermal Jamming in Glass Formers

by

Dillon Hugh Sanders

A dissertation submitted to the Graduate Faculty of
North Carolina State University
in partial fulfillment of the
requirements for the degree of
Doctor of Philosophy

Nuclear Engineering

Raleigh, North Carolina

2019

APPROVED BY:

_____   _____
Dr. Jacob Eapen   Dr. Jerry Bernholc
Committee Chair

_____   _____
Dr. Mohamed Bourham   Dr. Nam Dinh

_____
Dr. Keith Gubbins

Dedication

This dissertation is dedicated to the memory of my father, Clarence Hugh Sanders, III. He passed away only months before I began the scientific journey that culminated in this work. I owe him my eternal gratitude for his devotion and encouragement, and for instilling in me a love of science from a young age. I know he would have been proud to read this dissertation.

Biography

Dillon H. Sanders was born in Hickory, North Carolina. He completed his B.S. in Physics at Wake Forest University in 2012, which culminated in his Honors Thesis "Particle Production in de Sitter Space and the Validity of the Semiclassical Approximation During Preheating." He then transitioned to the Department of Nuclear Engineering at North Carolina State University, completing his Master of Nuclear Engineering in 2015.

Table of Contents

List of Tables

List of Figures

Chapter 1: Introduction

Kinetically constrained or slow dynamics is commonly observed throughout nature, across a wide range of time and length scales. This dissertation focuses on uncovering dynamical and thermodynamic features of supercooled liquids and glasses [1-5], which are examples of kinetically-arrested matter at the atomic scale, and which have applications in nuclear engineering [6-8] and materials science.

Some key features of slow dynamics appear in diverse situations such as the movement of ants through their colonies [9], the behavior of foams and emulsions under shear stress [10-12], the flow of granular materials [13-15], superionic conduction [16-20], and cars moving on a busy highway [21, 22]. Slow dynamics at the atomic level [23], while obscure at first glance, is readily illustrated by many situations encountered in everyday life, and some common-sense intuitions can help to illustrate why atoms in these materials behave the way they do. For instance, a traffic slowdown during rush hour is a real-life illustration of kinetically constrained dynamics. On the highway, there will be some fast and more reckless drivers, and some slow and more cautious drivers. As faster drivers change lanes to move around slower cars, they might often realize they are coming upon the car in front of them too quickly and then hit the brakes or swerve quickly into the neighboring lane. Upon seeing the first car brake, other cars might overreact and brake too much, and the cars behind them might do the same. These sudden, collective movements can have consequences that reverberate backwards to the cars following behind, sometimes causing intermittent motion that varies across different length scales, dynamic clustering of cars with similar speeds, and even traffic jams that last for hours.

In the context of supercooled liquids and glasses, the origin and the mechanisms of kinetic arrest at the molecular level are not fully understood [24]. Glasses are formed when certain "glass-forming liquids", abbreviated as GFLs, are rapidly quenched, or supercooled, to temperatures below their melting points. Many quantitative or qualitative definitions for what exactly a glass is have been proposed, as outlined by Zanotto and Mauro [25]. For the purposes of this work, it is accurate enough to describe a glass as a non-equilibrium amorphous solid that lacks crystalline order. Rapid quenching allows the liquid to avoid crystallization at the melting temperature, which would normally occur with a sufficiently slow rate of cooling. Below the melting point,

supercooled liquids exist in a highly viscous state, usually in metastable thermodynamic equilibrium.

Common sand, silica (SiO_2), is perhaps the best-known glass former. When molten sand is removed from a furnace, it begins to cool quickly, usually fast enough to avoid crystallization. Glass blowers take advantage of the resulting viscous fluid and mold it into the desired object. In general, when a supercooled melt gets cooled, its enthalpy drops as shown in Figure 1-1 below. The enthalpy continues to drop until it reaches a certain characteristic "glass transition temperature" (T_g), at which the melt phase falls out of equilibrium and becomes a rigid, solid-like glass.
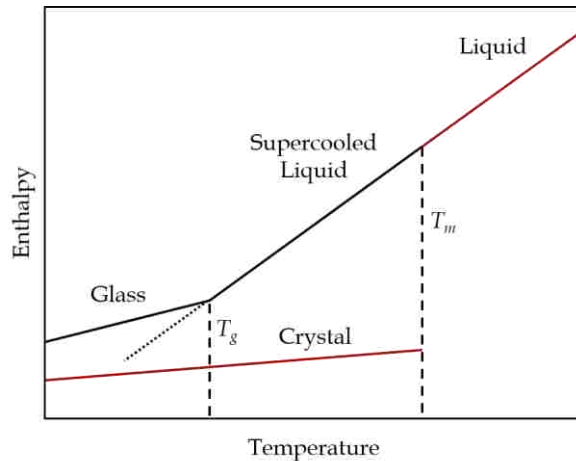
Figure 1-1:   Schematic depicting the change in enthalpy of a generic glass forming liquid (GFL) under rapid quenching [5, 25]. At the glass transition temperature T_g, which is less than T_m, the thermodynamic melting point, the supercooled liquid falls out of equilibrium and becomes a glass. A GFL does not have a unique T_g as it is typically dependent on the cooling rate. Quenching is not the only way to form a glass – other methods such as irradiation [26] and compression can also generate glassy states [2].

There are no unique ways to describe the glass transition temperature unambiguously. It is commonly observed that T_g occurs around $\frac{2}{3}T_m$, where T_m is the thermodynamic melting point [5]. Unlike the melting point, T_g is not unique and depends on how fast the melt is cooled. While T_g increases with increasing cooling rate, it does not depend *strongly* on the cooling rate; typically T_g changes by 3–5 K for an order of magnitude change in the cooling rate [5]. As evident in Figure 1-1, the glass transition is not a true first order thermodynamic transition because there is no

discontinuous change in the enthalpy, or a thermodynamic phase change with a measurable latent heat at T_g. However, the thermodynamic response function, specific heat, shows a distinct jump at T_g. The thermal signatures are typically weak for open-network or "strong" glasses such as GeO_2 and SiO_2 while they are more noticeable for "fragile" glasses such as glycerol as shown in Figure 1-2 [2].

The transition across T_g is irreversible – upon heating, a noticeable spike in the specific heat capacity occurs just above T_g. When going in the other direction by cooling from a high-temperature liquid, the specific heat capacity usually decreases monotonically. Thus, the glass transition is an irreversible process as indicated by the hysteresis in the heat capacity [27-29]. Although the heat capacity of the supercooled liquid is always higher than that of the corresponding crystal that would exist at the same temperature and pressure, the specific heat capacity of a glass is typically close to that of the underlying crystal (see right panel of Figure 1-2). The abrupt but continuous drop in the specific heat at T_g under quenching is often regarded as the key signature of a transition from an ergodic supercooled state to a non-ergodic glassy state [2, 30]. The rather close agreement suggests that the properties of the glassy state below T_g are dominated by molecular vibrations as in crystalline solids [31]. Thus, the glass transition is a manifestation of the breakdown of ergodicity, which is reflected by the loss of configurational degrees of freedom at T_g [30].

At the microscopic level, rapid quenching slows down the molecular motion, which is reflected as a dramatic increase in the viscosity of GFLs over a relatively small temperature interval. Angell [2] classified GFLs into two broad categories – "strong" and "fragile". As shown in Figure 1-3 [2], the strong GFLs, which have open-networked bonding structures, depict a near-exponential (Arrhenius) growth in viscosity while fragile GFLs, which typically interact through non-directional or van der Waals interactions, have a pronounced non-exponential increase as they near the glass transition temperature. Experiments show that many GFLs attain a viscosity of 10^{13} Poise (10^{12} Pa·s) at T_g, and thus this viscosity value is regarded as a *kinetic* marker for glass transition. Several crossover temperatures, which ostensibly correspond to different rate mechanisms, can be identified. While there is no universal consensus on the origin of these crossovers, the non-Arrhenius nature of fragile GFLs has attracted much attention over the last

several decades. At the glass transition temperature T_g the supercooled liquid attains a viscosity that is so high that it effectively acts like a solid, at which point it is said to finally be a glass.
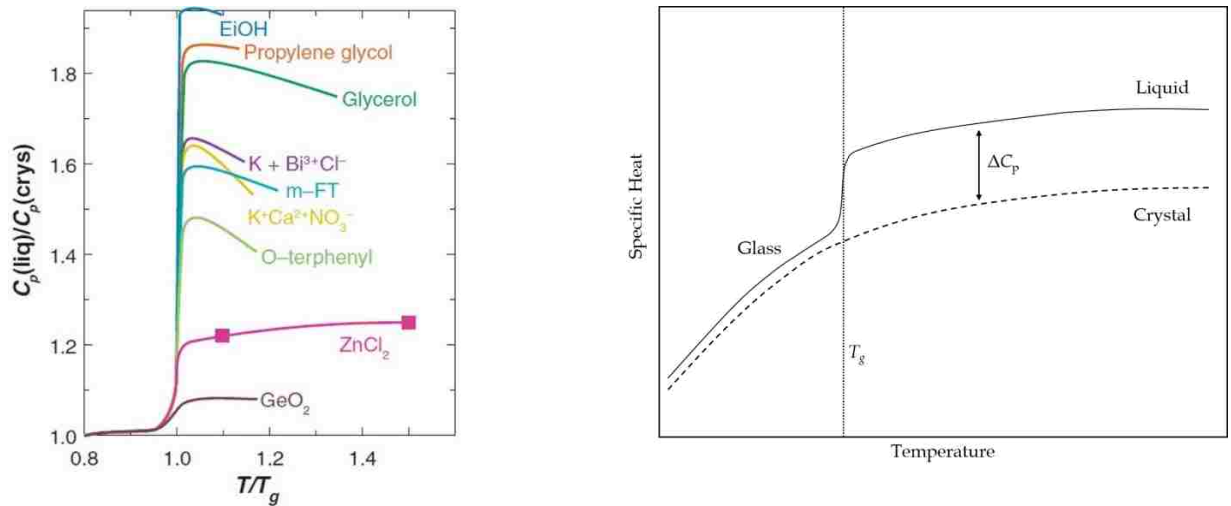
Figure 1-2:   (left) Abrupt drop in specific heat at T_g for several glass formers [1, 2]. (Right) Schematic showing the relative magnitudes of specific heats in the glass and the underlying crystal states [31]. The figure on the left is reproduced from [1].

Below T_g, the very high viscosity corresponds to a relaxation time for molecular rearrangement, which is the average time needed for atoms in the material to attain a state of thermodynamic equilibrium, that is too large to be measured in the laboratory. Thus the glass transition can be considered a type of kinetic arrest, and the falling out of equilibrium occurs when the relaxation time is $O(10^2 - 10^3)$ s. It is, however, important to understand that the glass transition is not a true first order thermodynamic phase transition. Rather, it signifies that liquid relaxation processes have become much slower than laboratory timescales [32, 33]. This transition to a non-equilibrium state is accompanied by loss of configurational degrees of freedom [30] that is manifested in changes in thermodynamic properties, such as the sharp but continuous drop in specific heat to values close to the corresponding crystal state [31].
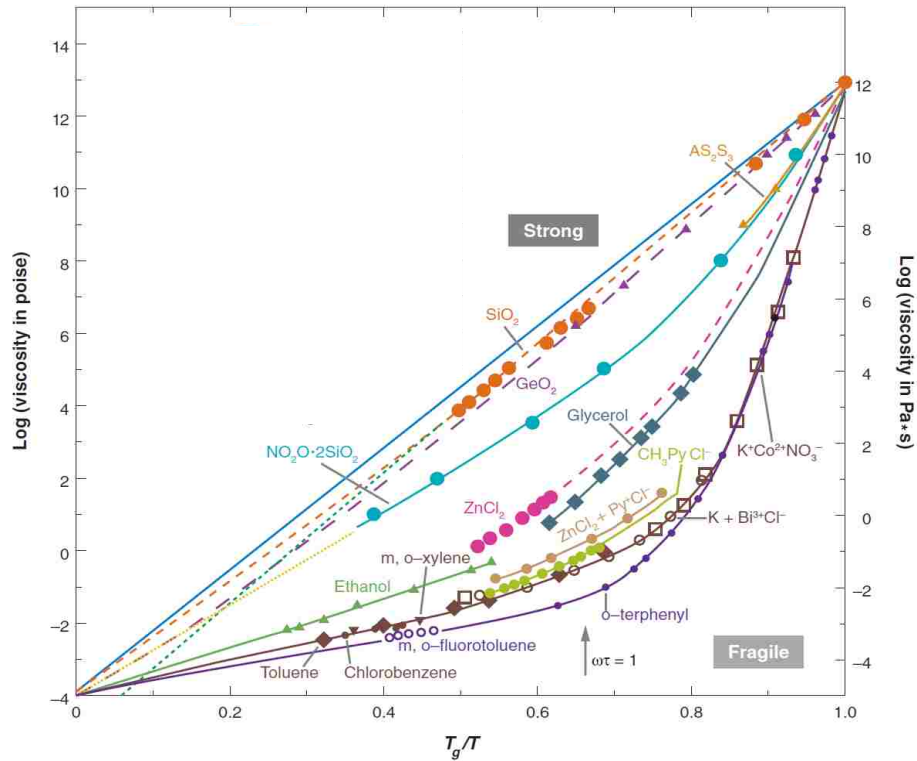
Figure 1-3:   Strong-Fragile classification of supercooled liquids according to Angell [1, 2]. The figure is reproduced from [1].

Section 1.1   Phenomenology of Supercooled Liquids

There are several interesting phenomenological attributes of supercooled liquids and glasses in addition to the features observed to occur at the glass transition as discussed previously. Some of these are briefly discussed below.

1.1.A   Temperature Crossovers and Transitions

Within the kinetic framework, the glass transition temperature T_g indicates a demarcation of experimentally accessible timescales in the supercooled liquid. As can be observed in Figure 1-3, the viscosity of the fragile GFLs shows changes in slope that are usually identified as temperature crossovers [34]. There is no firm consensus on the physical significance or location of these crossovers, although it is generally agreed-upon that a change of relaxation mechanisms occurs at the crossover temperatures.

5

In normal liquids, transport coefficients such as viscosity (η) or the self-diffusion coefficient (D) exhibit an Arrhenius variation with temperature. For example, the viscosity can be written as [23, 35]

$$\eta(T) = A(T)e^{\frac{E_A(T)}{k_B T}} \tag{1.1.1}$$

where $E_A(T)$ is the activation energy, k_B is Boltzmann's constant and $A(T)$ is a material-dependent constant. For normal liquids, both E_A and A are usually independent of temperature, which indicates that the viscosity is controlled by a single relaxation mechanism. Since the viscosity increases in an Arrhenius fashion in strong GFLs such as silica or germanium, as indicated in Figure 1-3, it can be inferred that there is a single dominant mechanism for viscous transport with a constant activation energy. For silica, it has been proposed that diffusion of silicon and oxygen atoms controls viscous transport [36]. Reliable viscosity measurements indicate an activation energy of 712 kJ/mol for temperatures ranging from 1400 °C to 1000 °C [36]. The activation energies for self-diffusion of silicon and oxygen atoms are of the same order of magnitude but are slightly smaller across the temperature range. It is also speculated that the transport of "defects" composed of silicon monoxide (SiO) in the silica melt influences the viscous transport at lower temperatures [36]. The concentration of the SiO molecules, or defects, however, is dependent on the open network structure of silica.

The close association between diffusive and viscous transport is encapsulated by the Stokes-Einstein relationship (SER), which posits that, the translational (self) diffusion coefficient D and viscosity η have the relationship [37, 38]

$$D\eta = \frac{k_B T}{6\pi R} \tag{1.1.2}$$

where R is the molecular radius [39]. The SER is remarkably observed to hold in both normal liquids and strong GFLs such as silica across wide range of diffusivities and viscosities.

So-called "fragile" glass-forming liquids, on the other hand, exhibit viscosity that grows faster than what is predicted by the Arrhenius Law [40], indicating a rapid increase in the activation energy that quickly becomes much higher than the energy associated with chemical bonds in the liquid. Thus, the activation energy of fragile glass-forming liquids corresponds not to the forming or breaking of individual chemical bonds, or the re-orientation of individual

atoms, but rather to one or more processes that involves groups of atoms. These collective processes are consistent with a picture of a supercooled liquid as a macroscopically homogeneous system where the movements of clusters of atoms are driving the system's most dominant relaxation process, which is also known as the α-relaxation. Theories of the glass transition, most-notably the model of Adam and Gibbs, place utmost importance on relaxation behavior of "cooperatively rearranging regions (CRRs)" [41, 42]. A kinetic "fragility" metric defined as $m \equiv d(\ln \eta)/d(1/T)$ [5] is often used to measure the sensitivity of the change in viscosity, or equivalently the α-relaxation time, with temperature. For strong GFLs, the kinetic fragility is typically small, and not unexpectedly, it shows a reasonable correlation to the attendant thermodynamic changes [43, 44].

The various temperature crossovers are illustrated using the prototypical viscosity variation of a fragile glass-forming liquid ortho-terphenyl (OTP) as shown in Figure 1-4. When a glass-forming liquid is quenched, there is some dynamic, structural, or thermodynamic process that prevents the liquid from crystallizing as it normally would at the melting point T_m. This process occurs above T_m at the "onset temperature" commonly denoted T_O; at this temperature, the first features appear that distinguish the supercooled liquid from the normal liquid [45].

The slow dynamics observed in supercooled liquids is elegantly described through the concept of transport across inherent structures (IS), which are local minima in the rugged 3N-dimensional potential energy landscape (PEL) with a large number of minima and saddle points [23]. The IS formulation of Stillinger and Weber [46, 47] follows the original idea of Goldstein [48]: that the dynamics of a supercooled or glass state can be described as predominantly vibrations at local potential energy minima. The slow relaxation observed in the glassy states can be described as a consequence of the system's occasional hopping between the inherent structures that are separated by "activation" energy barriers. The PEL is temperature-independent, but the thermodynamic state of the system determines which regions of the PEL are sampled by the system. At high temperatures, the system mostly traverses low energy barriers, and as the system becomes more supercooled, it encounters higher energy barriers which are temperature dependent.
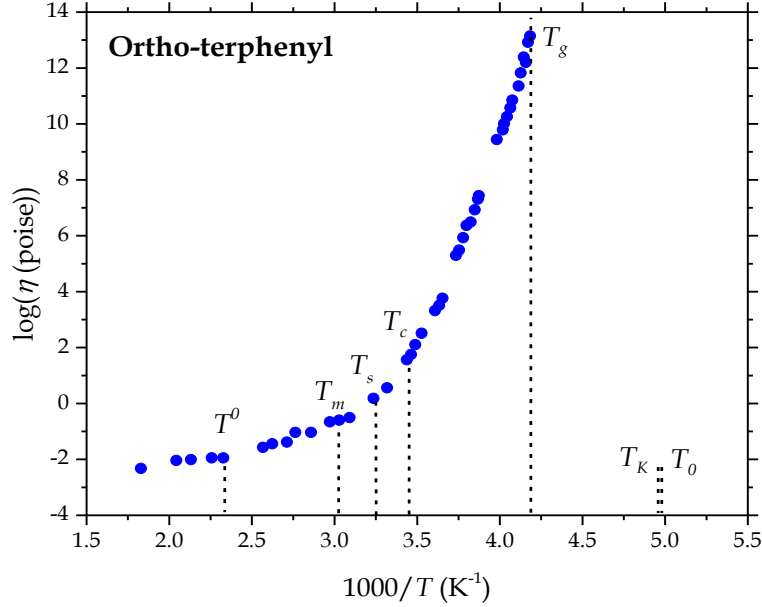
Figure 1-4:   The variation of viscosity of the glass-forming liquid ortho-terphenyl (OTP) [24], and the approximate location of various temperature crossovers or transitions. The onset of super Arrhenius behavior at temperature T^0 coincides with T^* of [24, 49], at which collective effects of supercooled liquids appear prominently. The Mode Coupling Theory (MCT) critical temperature T_c is coincident with the temperature T_x [31, 50] reported as the transition temperature that marks the approximate boundary between activated and non-activated dynamics. It also roughly fits the description of the crossover temperature T_d [51] or T_A [1] of the random first order transition theory (RFOT), below which the dynamics is landscape-dominated [1]. Using a derivative analysis [52], two characteristic temperatures T_A and T_B are sometimes reported in the study of viscosity data of GFLs. The former (T_A), which is a crossover to a non-Arrhenius form, is coincident with T^0, while the latter (T_B), which represents a dynamic crossover between one VFT (Vogel-Fulcher-Tammann) to another VFT form [53], is widely regarded to be same as T_c [34]. A milder crossover is more recently observed using atomistic simulations at T_s, which is above T_c. Several model GFLs show a breakdown in the Stokes-Einstein relationship (SER) at T_S although experimentally, this breakdown is regarded at take place at T_c. In this dissertation, additional dynamic and thermodynamic evidence based on theoretical modeling and simulations are provided in support of T_s, although it is quite close to T_c. The temperatures T_g and T_K represent the glass transition temperature and the Kauzmann temperature, respectively; the latter denotes a hypothetical temperature at which the configurational temperature of the glass vanishes [3]. For low temperatures, experimental data suggests a VFT form for the relaxation time given as $\tau = \tau_0 \exp\left(\frac{A}{T-T_0}\right)$ with T_0 nearly equal to T_K [54]. Other analytical forms that yield lower fitting errors [40] and representation of data, for example, based on T_c rather than on T_g [50], have also been proposed in recent years in the study of slow relaxation of GFLs.
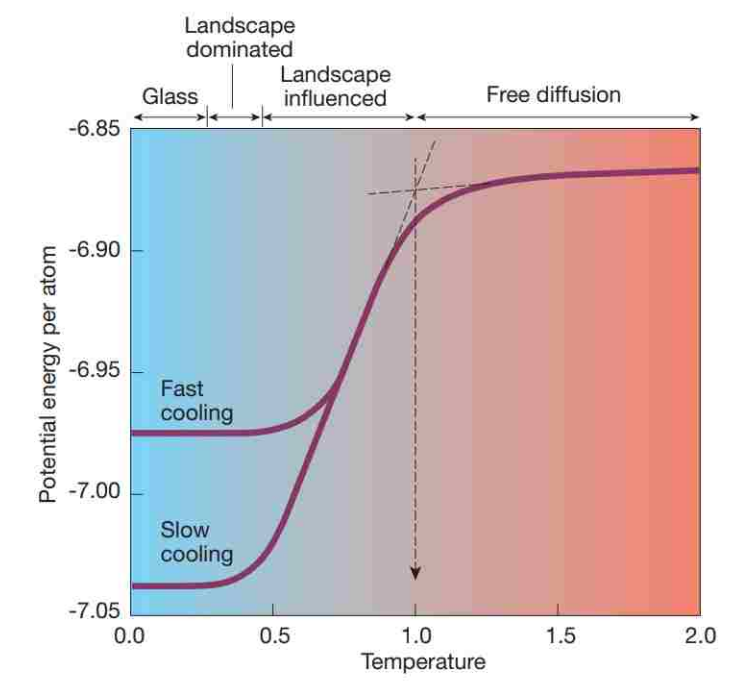
Figure 1-5: The variation of inherent structure (IS) energy demarcating the (potential energy) landscape-influenced and landscape dominated regions in a model supercooled liquid using atomistic simulations [5, 45]; the corresponding temperature is denoted as T_0. The figure is reproduced from [5].

The transition state, or kinetic rate, theory allows the calculation of the frequency of hopping from one IS to another. As is evident, the viscosity expression in Eqn. (1.1.1) can now be naturally accommodated into the PEL picture [23]. Using the PEL formalism, Sastry, Debenedetti, and Stillinger [45] noted that at high temperatures the IS energy is fairly constant, as shown in Figure 1-5. This regime corresponds to free diffusion that is a feature of simple liquids. The IS energy starts decreasing at a characteristic temperature, previously identified as T_0 – the onset of super-Arrhenius behavior for the viscosity. This regime, where viscosity increases modestly, is classified as (potential energy) landscape *influenced*. The IS energy continues to drop, which is accompanied by a rapid increase of viscosity. The regime where viscosity changes most is classified as landscape-*dominated*, and the transition temperature is usually denoted as T_c. The IS energy flattens out and becomes constant again with further reduction of temperature, and the system transitions into a glass at T_g. Thus Sastry, Debenedetti, and Stillinger, working under the energy landscape paradigm of Goldstein [48], frame the onset of glassy dynamics as a consequence of

9

the liquid settled deep in the landscape-influenced regime, as opposed to the normal liquid that is free to explore its configuration space with little to no constraint by the potential energy landscape.

The crossover to an "activated regime" where the dynamical processes and relaxation time are intimately tied to the activation energy barriers is marked by the temperature T_c. It is generally accepted that T_c also represents the critical temperature point of the mode coupling theory (MCT) [55, 56], which is described briefly in Section 1.2-B. MCT is a dynamic theory involving correlations of density fluctuations. Working with the static structure factor $S(\mathbf{q})$, the MCT equations entail a non-linear feedback mechanism between the structure and the dynamics, which strengthens with decreasing temperature. A key prediction is that the α-relaxation time diverges as a power law at a finite temperature as shown by

$$\tau = \left(T - T_c\right)^{-\gamma} \tag{1.1.3}$$

where T_c is the MCT critical temperature and γ is a system-dependent exponent [31]. It is now widely accepted that T_c represents a transition to an activated, or "hopping", dynamics regime; more recent versions of MCT incorporate the activated barrier crossing events [54]. Nevertheless, T_c marks the limit of MCT (without the hopping mechanism) and coincides with the start of the landscape-dominated regime. It is of interest to note that the numerical value of T_c is usually estimated from simulations using a fitting procedure that is performed over a small temperature range. Furthermore, the theoretical or ideal critical point $T_{c-ideal}$ is lower than what is estimated from simulations and is closer to T_0 [57].

As is expected, SER is violated for fragile GFLs much more prominently than in strong GFLs. Experimental data from 84 GFLs indicate that SER violation occurs below T_c with the SE relationship replaced by a fractional form $D \sim T\eta^{-0.85}$ [50]. Recently, atomistic simulations of several model GFLs have indicated that SER breaks down at a higher temperature $T_c < T_s < T_0$ [58, 59]. An earlier study revealed an interesting non-monotonic temperature variation of dynamic correlations in a model GFL comprising of harmonic spheres with a dynamic length scale peaking near T_s but below T_c [60]. The study involved the use of "point-to-set" correlations, where a subset of atoms was pinned in place to form a static wall, preventing any movement of these atoms but allowing them to interact with the rest of the atoms in the system, which were free to move. Dividing the simulation box into small subdivisions, the evolution of particle flow

10

was quantified with respect to the lateral distance z from the wall using an overlap function. By performing fits of a stretched exponential (KWW) form to these functions, the authors established a dynamic length scale ξ^{dyn} that is the distance required to move away from the static wall so that the equilibrium behavior of the system is recovered. A conclusion of this study is that the shapes of dynamically heterogeneous regions, which are related to the dynamical length scale, change at T_s. Subsequent investigations with three model glass-forming liquids confirmed changes in dynamics near T_s as well as a breakdown of SER [61]. This notion of a shift in the nature of heterogeneous dynamics – an important attribute of supercooled liquids and glasses [62] – will be addressed in the next section and further explored in Chapter 6 with analyses of stringlike cooperative motion in glass-forming liquids.

Interestingly, this high temperature crossover ($T_c < T_s < T_0$) has been reported in previous investigations. Using the Kob-Andersen model system [63], the statistical properties of "flow events" are observed to change appreciably near T_s [64]. For example, the shape of the flow event distribution displays a pronounced exponential form at temperatures below T_s but well above T_c. In this dissertation, additional dynamic and thermodynamic evidences are presented that can establish T_s to be a genuine crossover temperature that exists above T_c.

Below the glass transition temperature, T_g, two important transition temperatures exist - T_K and T_0. The former (T_K) is named after Kauzmann, who postulated the possibility of vanishing excess entropy between the liquid and crystal phases at this characteristic temperature, and the latter (T_0) is a fitting parameter of the Vogel-Fulcher-Tammann (VFT) form, which is commonly used to capture the variation of viscosity over a range of temperatures. Fascinatingly, both temperatures are found to be relatively close to each other while noticeably different from T_g [54]. While T_K has a thermodynamic origin, the physical significance of T_0 is strictly based on kinetic considerations. While Kauzmann never entertained the possibility of negative configurational entropy for glass – he merely postulated recrystallization as a recourse to the paradoxical situation – subsequent work by Gibbs and DiMarzio (GDM) [42] and Adam and Gibbs (AG) [41] led to the idea of thermodynamic glass transition, and relaxation of cooperative rearranging regions (CRRs). The viscosity variation with temperature in the AG model is Arrhenius and can be stated as

$$\eta = \eta_0 \exp\left(\frac{B}{TS_c}\right) \tag{1.1.4}$$

where S_c is the configurational entropy. By assuming that the change in specific heat is independent of temperature, S_c can be written as

$$S_c = \Delta c_p \left(\frac{T - T_K}{T_K}\right) \tag{1.1.5}$$

Finally, the viscosity can be shown to be

$$\eta = \eta_0 \exp\left(\frac{A}{T - T_K}\right) \tag{1.1.6}$$

which remarkably agrees with the VFT form

$$\eta = \eta_0 \exp\left(\frac{A}{T - T_0}\right) \tag{1.1.7}$$

Equations (1.1.6) and (1.1.7) are identical if $T_K = T_0$. The VFT law predicts the variation of viscosity η in terms of a characteristic temperature T_0, at which the viscosity diverges to infinity and total dynamical arrest of the liquid occurs. The VFT law has had considerable success at predicting the variation of viscosity by fitting to experimental data. The AG model establishes a theoretical basis for the VFT law in terms of the increasing size of correlation regions, and configurational entropy, which can ostensibly be extracted from specific heat data at T_g. Some have questioned the theoretical basis of the VFT Law and view it merely as a useful fitting equation [50]. For example, Mauro and co-workers [40], and the Dyre group [65], through the analysis of a large number of GFLs, found little or no reason to conclude that viscosity, or equivalently, the relaxation time, diverges at finite temperatures. Thus, empirical evidence does not lend a credible mechanistic basis to the VFT form; by association, the seminal idea of AG may also be questioned [66]. At the same time, one of the most successful theories of glass transition, namely, random first order transition theory (RFOT), also predicts a VFT-like divergence of relaxation time under certain assumptions [54].

1.1.B Configurational Entropy

Not all of the assumptions that go into the Adam-Gibbs Model rest on completely solid ground, as noted in some criticisms of the model [66], but it has seen considerable success in describing results from experiments and simulations [67-71], with the principal issue being that the configurational entropy is difficult to quantify in general, both in computer simulations and experiments. As previously described, the A-G Model establishes the decreasing configurational entropy as the driving cause of the rapid divergence of relaxation time (τ) when the liquid temperature approaches T_0. It has not always been entirely clear how to compute or determine the configurational entropy, which is the entropy associated with motion of atoms and contrasts with the vibrational entropy associated with the oscillatory movement of atoms around lattice sites. Conceptually, the excess entropy S_{ex} is defined as

$$S_{ex}(\rho,T) = S_{liquid}(\rho,T) - S_{cryst}(\rho,T) \tag{1.1.8}$$
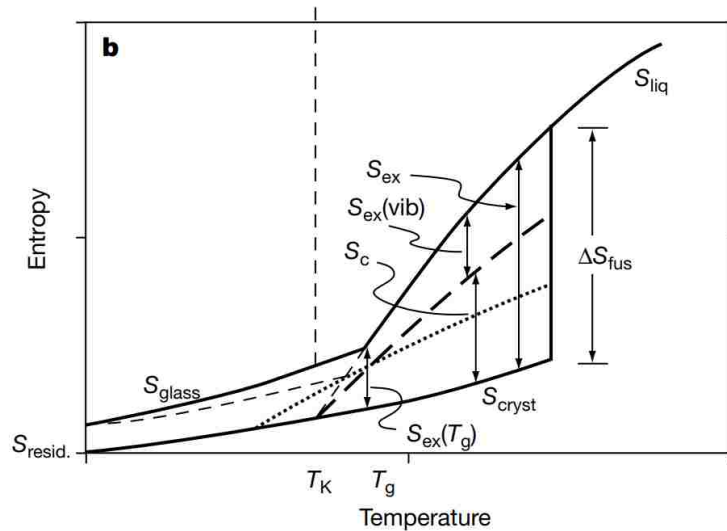
Figure 1-6: Schematic showing the relationships between different entropy components. The liquid state entropy can be divided into two components as $S_{liq} = S_{ex} + S_{cryst}$. Sometimes, the excess entropy S_{ex} is taken as the configurational entropy S_c, which is strictly incorrect. The excess entropy may be taken to be proportional to $S_c(T - T_K)$, where T_K is the Kauzmann temperature [43]. Figure reproduced from [43].

The excess entropy is a measure of the configurational entropy S_c, but they are not the same, as shown by the relationships between the various entropy components depicted in Figure 1-6. The vibrational entropy S_{vib} can be assumed to be the same as the entropy of the underlying crystal – that is, if there is indeed a well-defined crystalline structure at the same thermodynamic state (ρ, T) [24]. The liquid state entropy can be divided into two components as $S_{liq} = S_{ex} + S_{cryst}$. Sometimes, the excess entropy S_{ex} is taken as the configurational entropy S_c, which is strictly incorrect [30]. However, the excess entropy may be regarded to be proportional to $S_c(T - T_K)$, where T_K is the Kauzmann temperature [43], although the accuracy of proportionality is not fully established [68].

Experimentally, the most common method to estimate S_c is to use the change in specific heat capacity as [30, 68]

$$\tilde{S}_c(T) = \int_{T_m}^{T} \left(C_{p,liquid} - C_{p,crystal} \right) d\ln(T') + S_c(T_m) \tag{1.1.9}$$

The above expression involving the isobaric specific heat is only valid approximately, as the excess entropy also include excess vibrational entropy. The use of the above expression, which is strictly valid only under equilibrium thermodynamic conditions, becomes more questionable at and below T_g when the system falls out of equilibrium [30]. In the traditional viewpoint, S_c becomes "frozen" when the system transitions into a glassy state at T_g. Thus, the integrand in the above equation vanishes, leaving a residual entropy $S_c(T_m)$ evaluated at the melting point T_m or at some other reference temperature. The finite entropy, when extrapolated to 0 K, remains a point of contention in the glass community. Kivelson and Reis [72] have argued that entropy goes to zero at absolute zero Kelvin and the residual entropy is simply an artifact of calorimetric measurements along irreversible thermodynamic paths [73]. Mauro and coworkers [30, 74] have supported this argument by invoking the principle of "continuously broken" ergodicity at and below T_g. However, this viewpoint is not commonly accepted [75-78] and many practitioners in the glass field are comfortable with the notion that there is a residual entropy as shown in Figure 1-6 [79-81].

The inherent structure (IS) approach, discussed previously, can be used to access configurational entropy from atomistic simulations [82]. In this method, the supercooled liquid is simulated for a sufficiently long time that a large number of configuration samples can be

generated, and each configuration is minimized, for example, using a steepest-descent or conjugate gradient energy minimization method, which moves the system towards the nearest local minimum in the potential energy surface. These potential energy "basins" can be treated as a set of all points of the accessible configurational space [83]. The total partition function then can be expressed as a sum of IS partition functions. Since the number of inherent structures is equal to the number of distinct configurations, it will simply be a measure of the configurational entropy [83]. Recently, novel methods have been proposed for accessing configurational entropy from simulations [84]. In general, the configurational entropy is computed as $S_c = S_{total} - S_{vib}$ from numerical simulations; various methods are then devised to partition the states and compute the vibrational and total entropies.

1.1.C   Relaxation and Dynamical Heterogeneity

Diffusivity and viscosity can be theoretically expressed as the integral of time correlation functions, or equivalently, computed from the slope of the corresponding mean-square-displacements (MSD) [85]. In normal liquids, time correlation functions relax exponentially, which indicates that the system does not retain the memory of excitation. Further, this implies that different regions of the system relax with the same time constant, which signifies spatially homogenous dynamics. Correspondingly, the MSD depicts two broad stages; in the first stage, the atoms move ballistically, followed by the diffusive region where the MSD slope scales as the elapsed time. In contrast, a supercooled system shows a pronounced "plateau region" between the ballistic and diffusive regions, where the atoms are trapped in a "cage" formed by the neighboring atoms. The time correlation functions in the plateau region shows a discernible non-exponential temporal behavior, which can be expressed by a stretched exponential function given by

$$F(t) = C \exp\left[-\left(\frac{t}{\tau} \right)^{\beta} \right] \tag{1.1.10}$$

This is known as the Kohlrausch-Williams-Watts (KWW) form; in the above expression β denotes a material/temperature-specific exponent. Laboratory experiments on common glass-forming liquids such as ortho-terphenyl (OTP) and glycerol have demonstrated this relaxation behavior

[86]. The stretched exponential form for relaxation, which appears in various scenarios throughout nature, can be shown mathematically to result from a heterogeneous system wherein the various dynamically-distinct regions each decay in an exponential manner, but with different time constants or relaxation times τ [87]; it is also possible that the relaxation is inherently non-exponential even locally [54]. The super Arrhenius increase in the viscosity is closely correlated to the relaxation behavior of the system – non-exponentially relaxing systems usually depict large deviation from Arrhenius behavior [32].

Spatially distinct or heterogeneous dynamics is commonplace in nature. For example, in a traffic jam, one will often be sitting still behind a line of cars and experience a sense of frustration as a line of cars in the adjacent lane suddenly begin moving. This behavior, in which spatially distinct clusters of objects in jammed systems exhibit different dynamical behavior compared to the objects in nearby regions, is called dynamical heterogeneity (DH). A similar spatially heterogeneous dynamics is also observed in glasses and supercooled liquids, where dynamically similar groups of atoms form spatial clusters [62]. These spatially separated regions have a finite life time that is usually of the same order of magnitude as the a relaxation time [88, 89]. It is now widely regarded that DH is closely correlated to the super-Arrhenius increase of relaxation time with decreasing temperature, and the attendant non-exponential relaxation behavior.

DH is experimentally observed in diverse situations. Keys and coworkers studied a granular, two-dimensional system of metal ball bearings percolated by air [13]. By using a camera to track the trajectories of the ball bearings, they clearly observed the formation and disintegration of fast and slow regions in the system. Another experiment by Russell [90] involved measuring the dielectric constant of a very small region above the surface of a supercooled liquid. Within that small region, fluctuations were observed in time, indicating the presence of heterogenous dynamics. Complex "dynamic hole-burning" experiments have also demonstrated the existence of DH in several materials [91].

In the past few decades, the rapidly increasing practicality of atomistic computer simulations have made them instrumental in confirming the existence of dynamical heterogeneity in supercooled liquids. Several metrics have been proposed in recent years to quantify DH in GFLs. The simplest measure is the deviation from the Gaussian behavior expected

in simple liquids. When a liquid becomes supercooled, the non-Gaussian contribution α_2 also increases and is usually calculated in terms of the second and fourth moments as

$$\alpha_2(t) = \frac{2\langle r^4(t)\rangle}{5\langle r^2(t)\rangle^2} - 1 \tag{1.1.11}$$

The above non-Gaussian parameter shows a peak at a certain time when the presence of DH is maximal. Spatially heterogeneous dynamics also implies the existence of one or more length scales that characterizes the spatial correlations on the mobility of the atoms [92]. Sophisticated methods based on space-time multipoint correlations are usually employed to obtain length scales in computer simulations [54]. There are, however, no unique ways to define or extract length scales theoretically. For example, one can define both static and dynamic length scales. As noted in [92], length scales extracted from correlation functions and the attendant susceptibilities may not be the scales pertinent to the glass transition. In general, static lengths scale as the α-relaxation of the system and are much smaller than the dynamic length scales [93]. The dynamical behavior of the length scales can also be considerably different. As discussed previously, the dynamical length scale (ξ_{dyn}) identified in Kob, R-Vargas and Berthier, using point-to-set correlations, shows a peak at a characteristic temperature T_s while the static length scale (ξ_{stat}) shows a monotonic increase with temperature [60].

Perhaps the most striking illustration of DH is captured by quasi-one-dimensional or stringlike motion of atoms (or the constituents) in arrested states such as in granular media [13], supercooled liquids, colloids [94], and even at grain boundaries [95], and during homogeneous melting [96]. This kinetically constrained motion is observed both in experiments and simulations, as shown in Figure 1-7. An important study published in 1998 by Donati, Douglas, Kob, Plimpton, Poole, and Glotzer reported the existence of stringlike cooperative motion in the Kob-Andersen binary Lennard-Jones system [97]. Among the most mobile atoms in the system, correlated hops were observed that formed chains consisting of up to tens of atoms. The authors viewed this work as direct confirmation of the cooperatively-rearranging regions of the Adam-Gibbs Model [41, 98], described later in this chapter. DH has also been identified from simulations from so-called "propensity maps." Propensity refers to the trajectory of a molecule or system of molecules that evolves over an iso-configurational average, where many independent

simulations are run that start with the same configuration of atoms but with different initial velocities [99, 100].
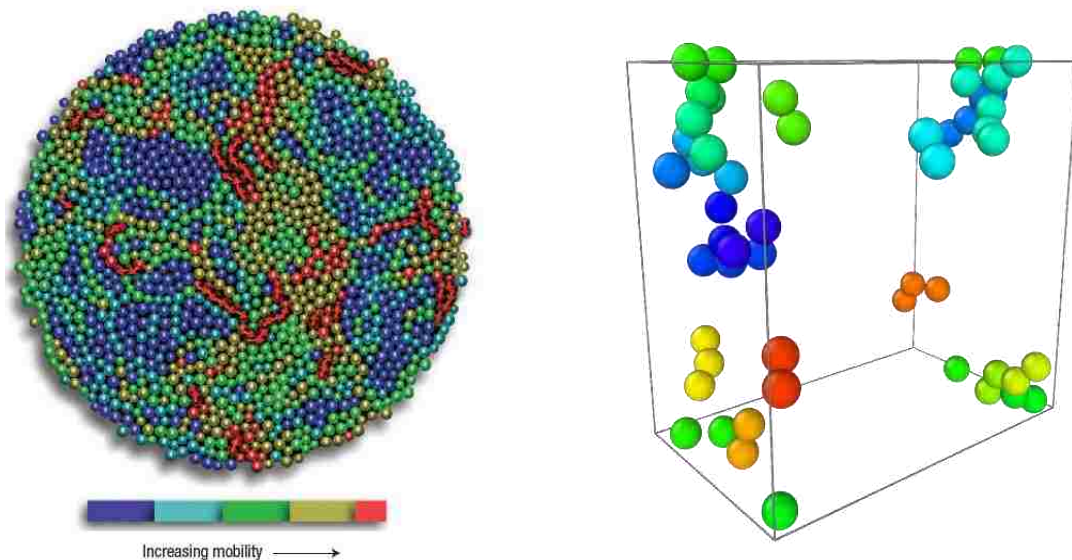
Figure 1-7:   Kinetically-constrained stringlike motion, for (left) granular media (reproduced from [13]) and (right) supercooled liquids. Each color denotes a separate string or cooperatively moving atoms. Stationary or non-cooperative atoms exist in the supercooled system (right) but are not shown.

The dynamic facilitation (DF) model proposed by Chandler and Garrahan [101] proposes that stringlike cooperative motion among atoms occurs as a natural consequence of facilitated, hierarchical dynamics [102]. It emphasizes the significance of "excitations," which are atoms that perform short hops typically on the order of an atomic diameter and persist in the new location for a relatively long time. A movement in which an atom breaks its nearest-neighbor cage, but then quickly moves back to its initial position, is not considered an excitation. The study conducted by Keys, *et al.*, of several model supercooled liquids revealed that the size of excitations has only a weak dependence on temperature and is almost always smaller than a couple atomic diameters [102]. Excitations facilitate other nearby excitations, resulting in hierarchical relaxation that gives rise to stringlike cooperative motion. The model is described in more detail later in this chapter.

An outstanding question is whether stringlike cooperative motion may be used to establish meaningful length scales that pertain to the slow dynamics [103]. The most straightforward length scale is the length of a string, which may be measured as simply the number of atoms in a string. However, strings rarely move in straight lines; they often contort and curl around on themselves, so the number of atoms in a string does not necessarily indicate the spatial extent of the string. Nevertheless, the average string length, which grows with decreasing temperature, may be considered a pertinent length scale associated with the growth in size of dynamically fast cooperating regions. A recent investigation by Starr, Douglas and Sastry has shown that string lengths can be construed as a metric for spatially heterogeneous dynamics and the length of the strings seem to be a quantitative yardstick of the CRRs in Adam and Gibbs model and RFOT theory [69].

Section 1.2   Models of Slow Dynamics and Glass Transition

The preceding descriptions of the most significant phenomenological hallmarks of dynamical and thermodynamic behavior in supercooled liquids represent the facts of the field as revealed by experiments and computer simulations. Many efforts have been made to assimilate these facts into coherent theories that seek to explain the mechanisms that culminate in the glass transition, or models that adopt some of the experimental observations and use them to explain other features and make predictions. Comprehensive reviews by Berthier and Biroli [54], Chandler and Garrahan [101], Cavagna [31], Kirkpatrick and Thirumalai [51], Stillinger and Debenedetti [4], Lubchenko and Wolynes [1], Karmakar, Dasgupta and Sastry [92], and Langer [104] address the strengths and weaknesses of nearly every glass theory in more detail than is provided here. Broadly speaking, theories of slowing down and the glass transition fall into two categories – they either have a thermodynamic origin and or a kinetic origin. It is important to note that in supercooled liquids, dynamical, structural, and thermodynamic processes are inextricably linked, so there is not really a theory or model that focuses entirely on one aspect without addressing the others.

1.2.A Free Volume Theories

Free volume models of the glass transition may be thought of as an attempt to begin with the fundamentals of diffusive motion in fluids. The simplest formulation of the free volume model involves the special system of identical hard spheres, which will be discussed in detail in Chapter 2. The success of the VFT form given in Eqn. (1.1.7) in predicting the variation of viscosity over several orders of magnitude prompted early theorists to propose a theory based on excess or free volume in the melt [36]. In one of the earlier formulations by Turnbull and Cohen [105] [106], it was postulated that the fluidity increases free volume, which is defined as the difference between the average volume of the molecule and the van der Waals volume associated with each molecule. The model begins with the idea that a particle's diffusive motion is really comprised of a cascade of short movements, where the particle's range of motion is constrained to its local free volume V within the "cage" of neighboring atoms. Using the hard sphere (HS) model, the diffusion coefficient can then be computed as [106]

$$D = \frac{1}{3}\bar{v}\int_0^\infty p(V)f(V)a(V)VdV \tag{1.2.1}$$

where $\bar{v}$ is the average velocity of particles in the fluid, $p(V)$ is the probability that the free volume lies between V and $V + dV$, $a(V)$ is a function of the free volume, and $f(V)$ is a correlation factor that accounts for the displacements as atoms bounce off their nearest neighbors within the cage inside the free volume. The correlation factor is critical to the free volume model for hard spheres at high density, and it is a process not considered by the successful but limited Enskog theory of hard spheres. For a random-walk trajectory which is only possible in an effuse, gas-like system of hard spheres, $f(V) = 1$. A completely jammed or solid state will consequently have $f(V) = 0$. Various free volume models may assume different functional forms for $f(V)$, provided they satisfy the above conditions in the limits of solid and effuse systems. Obtaining an accurate representation of the free volume of the material of interest is the primary challenge and potential drawback of free volume models. In [106], a step-function form is used for $f(V)$, and the jump distance is approximated as $a(V) = \alpha V$, a linear function of the free volume V. This assumption is reasonable as it is a simple reflection of the fact that a larger free volume allows for longer possible paths for a particle to move across that volume, and it results in an expression for the diffusion coefficient:

$$D = \left(\frac{\bar{v}\alpha}{3}\right)\left(V^* + \frac{V_f}{\gamma}\right)\exp\left(\frac{-\gamma V^*}{V_f}\right)$$ (1.2.2)

where V^* and V_f are the critical volume to allow the residence of another molecule and total free volume respectively, and the constant γ is numerical factor to correct the overlap of free volume which lies between ½ and 1. Typically, V^* is of the order of $10V_f$. The incorporation of backscattering into the free volume model is important, as it explains the shortcomings in equations of state for dense fluids that arise out of taking gas equations of state to high density limits and modeling the particles as hard spheres with finite size, most-notably the widely-used Carnahan-Starling equation which is derived from the virial expansion of the ideal gas law. Assuming the SER, the viscosity variation can be now be written as

$$\eta = \eta_0 \exp\left(\frac{B_1 V_0}{V_f}\right) = \eta_0 \exp\left(\frac{B}{T-T_0}\right)$$ (1.2.3)

where B_1 is a constant and V_0 is the volume of a molecule. If the free volume is assumed to follow the relationship $V_f = V_0(T - T_0)/T_0$, and with $B = B_1 T_0$, the viscosity can be expressed in the VFT form as shown above [36]. Thus, the early attractiveness of free volume theories stemmed from the ability to predict the VFT form, albeit with several approximations. Notably, the free volume approach was criticized by Goldstein [107], who proposed the potential energy barrier picture described in the earlier section, although some observations on pressure dependence are not strong enough to reject the free volume approach [36]. Recent work has shown that free volume can be treated as a natural variable to describe the variation of relaxation time with temperature [108].

1.2.B Mode-Coupling Theory

Mode-Coupling Theory (MCT) [55, 56, 109, 110] is the most prominent first-principles theory of the glass transition – in contrast to other phenomenological theories of the glass transition that rely on the existence of certain observed dynamical features of supercooled liquids. MCT has seen some significant successes in explaining both experimental and simulation results,

with some notable failures as well. The goal of MCT is to obtain an equation of motion for the density correlations of a liquid. The density at a position **r** in a N-atom system is computed as

$$\rho(\mathbf{r},t) = \sum_{i=1}^{N} \delta(\mathbf{r} - \mathbf{r}_i(t)) \tag{1.2.4}$$

where $\delta(\mathbf{r} - \mathbf{r}_i(t))$ is the Dirac delta function. The Fourier transform of the density is given by:

$$\rho(\mathbf{k},t) = \int d\mathbf{r}\, e^{i\mathbf{k}\cdot\mathbf{r}(t)} \rho(\mathbf{r},t) = \sum_{i} e^{i\mathbf{k}\cdot\mathbf{r}(t)} \tag{1.2.5}$$

The Dirac delta function conveniently eliminates the integral and reduces the expression to a sum of exponential terms in the reciprocal space. The density is now a function of the wave vector **k**. The density correlator or the so-called intermediate scattering function $F(k,t)$ is a correlation function in the reciprocal length $k = |\mathbf{k}|$ space, defined as

$$F(k,t) = \frac{1}{N}\left\langle \rho(-k,0)\rho(k,t) \right\rangle = \frac{1}{N}\sum_{i,j}\left\langle e^{-ikr_i(0)} e^{ikr_j(t)} \right\rangle \tag{1.2.6}$$

The density correlator, which is a measure of the system viscosity, decays to small values on a time scale indicated as the density relaxation time (often referred to as structural or α-relaxation) τ, which is sometimes defined as the time at which $F(k,t)$ attains one e-folding of its initial value. Using a series of steps, which are not outlined here, MCT ultimately results in the equation [54]

$$\frac{\partial^2 F(k,t)}{\partial t^2} + \frac{k^2 k_B T}{mS(k)} F(k,t) + \int_0^t d\tau M(k,\tau)\frac{d}{dt}F(k,t-\tau) = 0 \tag{1.2.7}$$

where M is the memory function or kernel, and $S(k)$ is the structure factor defined as $F(k,0)$, which is the only input that is needed in MCT. Solving the above equation yields the most important prediction of MCT: that the relaxation time diverges according to a power law as $\tau = A(T - T_c)^\gamma$. As described previously, T_c is called the mode-coupling critical temperature. In some range of temperatures, MCT does accurately describe the non-Arrhenius variation in relaxation time, one of the principal phenomena that must be encapsulated by any good supercooled liquid theory. As temperature approaches T_c, the original formulation of MCT predicts that the relaxation time diverges to infinity and the supercooled liquid has finally attained a completely *non-ergodic* state – in which the atoms can no longer achieve thermal equilibrium – and the system is said to be in a glassy state. For such a state, the intermediate scattering function will never

decay, remaining constant for exceedingly long time scales since the atoms cannot relax, and density fluctuations with length scales larger than those associated with vibrational motion remain correlated forever.

For temperatures above the mode-coupling critical temperature, MCT predicts three relaxation regimes (see Figure 1-8). As also described earlier in the context of mean squared displacement (MSD), at very short time scales atoms undergo ballistic motion where they vibrate and move across the free volume that exists between their neighboring atoms. At slightly longer time scales the atoms traverse their free volume and begin to collide with neighboring atoms. For normal liquids there is enough free volume that atoms can usually push through their neighboring atoms, but in dense supercooled liquids atoms are trapped in "cages" formed by their neighboring atoms. The time scale at which atoms leave the ballistic regime and rattle around in their nearest-neighbor cages is known as β-relaxation. Eventually atoms push through their neighbors and begin α-relaxation, which corresponds to diffusive motion. The β-relaxation process is unique to dense supercooled liquids. A fully constrained or non-ergodic state can be thought of as a state where the caging or β-relaxation is inordinately long, much longer than the timescales associated with typical laboratory measurements.

MCT has some important successes in when applied to explaining empirical results, one of which is the principle of temperature-time superposition that results naturally from the method. It states that in the α-relaxation regime, any correlation function $\Theta(t)$ can be scaled by the relaxation time $\tau(T)$ at that temperature so that it falls onto a master curve $\Psi(t,T)$ [110]

$$\Theta(t) = \Psi\left(\frac{t}{\tau(T)}\right)$$
(1.2.8)

This scaling has been widely confirmed in both simulations and experiments of supercooled liquids [111]. However, a significant drawback of MCT, that has also been uncovered in simulations and experiment, is that the temperature T_c at which complete dynamical arrest is predicted to occur is *higher* than the glass transition temperature T_g. This has simply not been observed in experiments or simulations. So, while MCT describes the dynamical features of supercooled liquids as they move towards the glass transition, there is some deficiency in the theory that prevents it from correctly predicting where the true glass transition should occur.

There are efforts in the glass community to identify other phenomena that may occur at the mode-coupling temperature [54]. Sastry notes that the mode-coupling temperature is thought to correspond to the onset of activated dynamics [112]; other studies have cast doubt on the notion that any dynamical or thermodynamic process occurs at T_c.
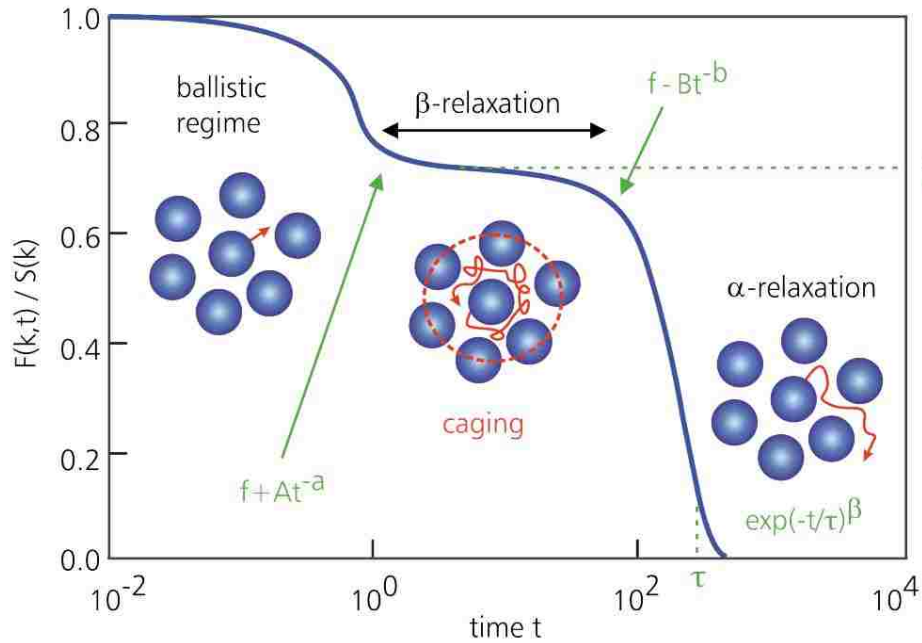
Figure 1-8: Predictions of the shape of the intermediate scattering function $F(k,t)$ made by MCT for supercooled liquids showing the two main relaxation behaviors. MCT predicts a diverging relaxation time at the mode coupling critical temperature T_c. Figure reproduced from [110].

1.2.C Random First-Order Transition Theory

Random First-Order Transition Theory, commonly abbreviated as RFOT Theory, is a mean-field description that is able to predict a very broad range of quantitative and qualitative features of supercooled liquids [1, 51], including the origin of non-Arrhenius viscosity variation, connection between liquid entropy and relaxation rates, and the glass transition temperature [113]. The theory, which has its origin in mean-field Potts and Ising spin glass models [114-116], is microscopic in nature, meaning that it begins by quantitatively defining the potential energy function that describes interactions between individual atoms. In principle, if the microscopic

functional form of molecular interactions is known, one may map out an analytic description of the potential energy surface of an arbitrarily large network of molecules. RFOT recognizes the fact that supercooled liquids, unlike crystals, have significant degeneracy in their potential energy surface. This means that there are a very large number of minima in the potential energy surface for supercooled liquids, below a certain characteristic temperature T_d [51] or T_A [1], which effectively coincides with the MCT T_c from a mean-field perspective [51]. For temperatures above T_d/T_A, the transport is dominated by collisional mechanisms, while below it is governed by activated or landscape-dominated transport. If activated events are completely neglected, then theoretically the system is trapped forever in a glassy state. Thus, without activated transport, the MCT T_c represents a glass-like state. In computer simulations $T_d/T_A/T_c$ all mark the transition to a very sluggish system, and hence this crossover is often considered as dynamic transition [51]. It is generally accepted that the RFOT and MCT approaches merge at the crossover temperature $T_d/T_A/T_c$. While RFOT is more appropriate at temperatures lower than $T_d/T_A/T_c$, MCT without activated transport is highly successful for describing the dynamics above $T_d/T_A/T_c$ [113].

In essence, RFOT is a thermodynamically rooted approach that seeks to extend the theory of the liquid-crystal first-order phase transition to the case of molecules with aperiodic, non-crystalline, randomized structures as seen in supercooled liquids. This is the origin of the "random" descriptor in RFOT. RFOT essentially states that the same microscopic processes that drive the liquid-crystal phase transition in normal liquids exist in supercooled liquids, but the first-order transition in supercooled liquids "looks" different in the mean-field limit due to the presence of random phases that are spatially and morphologically distinct [1]. This is why, for instance, there is no latent heat at the glass transition, and the heat capacity across the glass transition is smooth and appears closer to a second-order phase transition, in contrast to the discontinuity seen in the liquid-crystal phase transition [1]. The first-order transition predicted by RFOT occurs at T_d/T_A, at which point the system becomes activated. A second transition is predicted at the Kauzmann temperature T_K when correlation length becomes divergent and the supercooled liquid transitions to a glassy state.

When the system is in the activated regime, it can visit an exponentially large number of energy minima, which are statistically similar [92]. Thus, the system can be visualized as visiting a mosaic or patchwork of metastable states. Because there are interfaces between the mosaic states

there is an associated "surface tension" for generating these interfaces. Configurational entropy then acts as a driving force for the nucleation of "droplets" of metastable states [92]. The balance between the surface tension and the configurational entropy gives a critical length scale ξ, which is representative of the size of the CRRs; it can be expressed as [31]

$$\xi = \left(\frac{Y(T)}{TS_c(T)} \right)^{\frac{1}{d-\theta}}$$

(1.2.9)

where Y is a generalized surface tension and θ is a parameter less than or equal to $d - 1$, where d is the dimensionality of the system. Finally, it can be shown that [31]

$$\xi_{RFOT} = \left(\frac{1}{T - T_K} \right)^{\frac{1}{d-\theta}} \qquad \xi_{AG} = \left(\frac{1}{T - T_K} \right)^{\frac{1}{d}}$$

(1.2.10)

where T_K is the Kauzmann temperature. The above comparison shows that the RFOT length scale is sharper than that of Adam-Gibbs (AG) theory. Proceeding in the same way as done in Section 1.1, the viscosity variation with temperature can be expressed as

$$\eta = \eta_0 \exp\left(\frac{Y(T)^{\frac{1}{d-\theta}}}{T\left(TS_c(T)\right)^{\frac{1}{d-\theta}}} \right)$$

(1.2.11)

The above relationship, as previously mentioned, collapses to the VFT form with some additional assumptions.

Implicit in the above derivation is the assumed relationship between the configuration entropy S_c and the Kauzmann temperature given as $S_c = \Delta C_p \left(1 - \frac{T_K}{T} \right)$, where ΔC_p is the jump in the specific heat at the glass transition. Above the glass transition, the supercooled liquid has a higher entropy than the corresponding crystal phase that would have existed if the liquid had not been rapidly cooled. But the entropy of the supercooled liquid also decreases faster with temperature than the entropy of the crystal. As discussed previously, a small extrapolation of the excess entropy to lower temperatures from T_g will make the liquid entropy equal to that of the underlying crystal entropy – this temperature is denoted as the Kauzmann temperature T_K. Any further extrapolation of the liquid's entropy leads to the case in which the liquid entropy becomes *lower* than that of the corresponding crystal, which is improbable although within the bounds of

laws of thermodynamics. However, at some smaller non-zero temperature, the extrapolated liquid entropy reaches zero, seemingly a violation of the Third Law of Thermodynamics. Although this extrapolation results in a paradox, it is not necessarily problematic, as it not certain that such extrapolations of the liquid entropy are valid. Indeed, the liquid's entropy may turn sharply at some non-zero temperature and monotonically decrease until it disappears at absolute zero. The existence of a true first-order phase transition to a solid would save the "paradox" as Kauzmann originally postulated. In this case, the entropy would exhibit a sharp turn and decrease in the same manner of that as a solid, resulting in no violation of the Third Law of Thermodynamics.

As discussed previously, a finite configurational entropy at T_g if extended to 0 K, also remains a point of contention in the glass community. Kivelson, Reis and Mauro [72] [73] [30, 74] have argued that all entropy goes to zero at absolute zero Kelvin and any residual configurational entropy is simply an artifact of calorimetric measurements along irreversible thermodynamic paths. There is, however, considerable opposition to this view [75-78] [79-81] and the traditional viewpoint is that glass at absolute zero possesses a finite configurational entropy.

1.2.D   Dynamic Facilitation Model

An attempt to explain the glass transition in terms of processes driven by dynamical facilitation (DF) has been proposed by Garrahan and Chandler [117]. The model has its origins in early models of simple glass-like systems, in particular the Fredrickson-Andersen (FA) and East Models [118], which are variations on so-called "spin glasses" or Ising models that represent frustrated behavior in terms of interacting magnetic spins. In such models, the system attempts to attain a state of equilibrium indicated by the alignment of the magnetic spins. The East model is an Ising model where the spins (either "up" or "down") are flipped if right neighbor (east) spin is up; thus the excitations propagate in the leftward ("west") direction [119]. In the FA model, the spin flips if the left or right neighbor is in the up state [118]. Through this process of facilitation, spin excitations propagate across the chain in a hierarchical manner [118].

The DF model of the glass transition extends this idea to three-dimensional molecular kinetically arrested systems, where excitations are displacements of atoms from their "initial" positions that last for some significant time interval [102]. This definition of excitations excludes high-frequency rattling of atoms in the dynamic cages formed by their nearest neighbors, and also excludes fleeting hops by atoms out of their nearest-neighbor cage that are quickly reversed. Thus excitations correspond to the system crossing potential energy saddle points. As in the East model, these excitations are localized, meaning that the atom displacements they correspond to are fairly short, typically on the order of an atomic diameter and affecting only the nearest neighbors of the excited atoms, and the length scale associated with excitations is virtually temperature independent. Also, as in the East model, facilitation is directional and causes the propagation of dynamically heterogeneous regions throughout the supercooled liquid. In this sense, dynamical facilitation can be thought of as the impetus behind dynamical heterogeneity in the sense that the system dynamics is effectively controlled by dynamical facilitation [54, 102]. At a given time, some regions of the liquid will feature a higher concentration of excitations than the bulk, corresponding to dynamically fast regions of atoms that are undergoing cooperative rearrangements. The model assumes that the density of excitations follows the Boltzmann distribution, where the energy scale associated with excitations at a given length scale grows logarithmically with that length scale. This leads to the key prediction of the DF model - that the relaxation time varies with a parabolic form given by

$$\tau = \tau_0 \exp\left[J^2 \left(\frac{1}{T} - \frac{1}{T_o} \right)^2 \right] \tag{1.2.12}$$

where J is proportional to the logarithmically varying energy scale of excitations, T_O is the onset temperature of glassy dynamics, and τ_0 is the relaxation time at T_O. This parabolic law has shown good agreement to experimental data, with the significant caveat that it breaks down entirely above T_O – a worthy tradeoff since the goal is not necessarily to develop a model that encompasses high-temperature dynamics in the liquid. This parabolic form acts in competition with the predictions of relaxation time from MCT, the VFT law, the Adam-Gibbs Model, and other theories of the glass transition; the theory can also predict the calorimetric glass transition [120]. Striking images are presented in [102] (shown below in Figure 1-9) from simulations of the growing regions of excitations that are caused by dynamic facilitation. The notion of long-lived, persistent

local excitations will be called to mind in Chapter 6, when stringlike cooperative motion in supercooled liquids is discussed.

increasing displacement, $|r_i^{IS}(t) - r_i^{IS}(0)|$ →
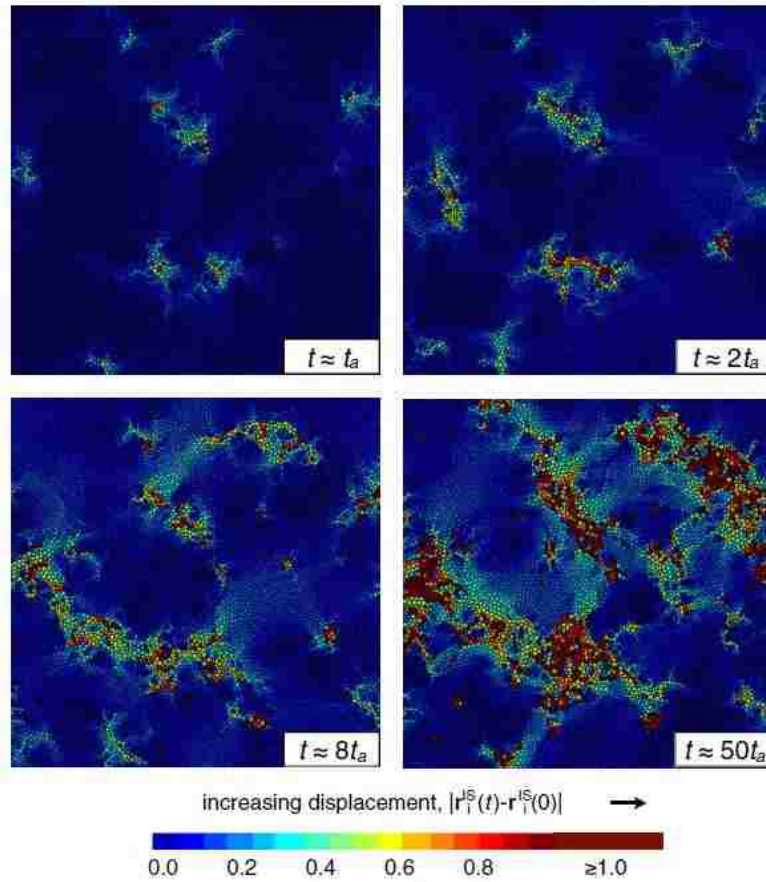
Figure 1-9:   Hierarchical dynamics from the dynamic facilitation (DF) model illustrating spatially expanding heterogeneous mobilities, reproduced from [102]. In the DF model, longer relaxation times at lower temperatures signifies increasing distance between elementary excitations, while in RFOT, the mosaic or cooperative rearranging regions (CRRs) grow in size with decreasing temperature.

Section 1.3   A Thermal Jamming Perspective

Although the debate as to whether the origins of the glass transition are thermodynamic or dynamical in nature is unresolved, the characteristic behavior of supercooled liquids entails some form of frustration at finite temperatures at the glass transition that confers mechanical rigidity to the glass. There are strong indicators of kinetic arrest in virtually every theory; for example, the ideal mode-coupling theory (MCT) emphasizes the role of dynamical caging of

atoms in inhibiting diffusive motion and leading to dynamical arrest at the critical temperature T_c. The free volume models predict dynamical arrest in a similar fashion to MCT by relating the slowing-down of molecules to rapidly decreasing accessible free volume. The Adam-Gibbs model and random first order theory (RFOT) relate the diverging relaxation time to the vanishing configuration entropy and a diverging length scale. Conceptually, the Adam-Gibbs model and RFOT assumes that activated transport, and not jamming, controls the slowing down of dynamics [33]. On one hand, kinetic arrest in real space is invoked in the dynamic facilitation models, which explicitly postulates that arrested regions stay arrested unless they are in close proximity to mobile regions. Thus, RFOT and DF bring out a conceptual dichotomy – the former works in the configurational space, while the latter is rooted in real space regions [101]. While jamming is well-understood in a static packing perspective [121, 122], none of the current theories described explicitly connects the jamming phenomena to the slowing down dynamics observed in supercooled liquids at finite temperatures. A central goal of this work, therefore, is to develop a theoretical framework for describing supercooled liquids in terms of the extent to which they are jammed at finite temperatures. The endeavor here is to conceptually consider glass forming liquids to be in a "thermally jammed" state with well-defined jamming metrics such as effective packing fraction and compressibility, and at the same time develop appropriate metrics to characterize the attendant dynamical slow down. The goal is to predict the ageing behavior of glass forming liquids all the way to glass transition; no attempt is made to rationalize the existence of crossovers associated with T_g or T_K or T_0.

In the case of rigid objects such as hard spheres, which will be discussed in detail in Chapter 2, jamming is a geometric phenomenon that may be unambiguously quantified by knowing the density or packing fraction ϕ of the system. Complete dynamical arrest in a system of monodisperse (identical) hard spheres occurs at approximately the random-close-packed configuration corresponding to $\phi_{RCP} \sim 0.64$, or if the system is carefully prepared so that it crystallizes; the packing fraction for the face-centered-cubic lattice is $\phi_{FCC} = 0.74$. It is intriguing that there is at least one scenario in which a fully-quantitative description of jamming is possible [121, 122].

In molecular glass formers that feature "soft" particles whose boundaries are not as clearly defined as hard spheres, other factors determine the extent of jamming. This situation is best

illustrated by considering an example seen in the "workhorse" model supercooled liquids, the binary Lennard-Jones system of Kob and Andersen (KA) [111]. Details of the system are provided in the reference, and in Chapter 5. Two features of the system primarily contribute to its status as a good model supercooled liquid: the disparate atomic radii and the heavily skewed ratio of atoms (80% are of type A, 20% of type B). These characteristics make the system extremely averse to crystallization even at low temperatures. The KA system is run at constant density, and the temperature and pressure are allowed to vary. As temperature decreases the phenomenological features of the glass transition begin to emerge. But since the density of the system doesn't change, the sluggish dynamics and non-Arrhenius variation of transport coefficients that *may* signify a jammed state cannot be as associated with the static jamming process that occurs in rigid systems – if ϕ were computed for the KA system using the atomic radii from the potential, it would never change. Instead, any jamming that accompanies the system's evolution towards the glass transition is related to the decreasing temperature or increasing pressure.

Thermal jamming descriptors such as the packing fraction that applies to hard spheres and rigid systems has not yet been similarly defined for molecular glasses. Consequently, there has not yet been a theory of the glass transition formulated in terms of jamming. But there are clues in the literature that suggest the route to be taken for establishing such a theory or model. An interesting result was observed experimentally for a number of supercooled liquids [53, 123] [124]. These studies showed that while dynamic crossovers indicated by shifts in the variation of relaxation time occur at very different temperatures depending on the choice of material or the pressure at which the sample is prepared, the *value* of the relaxation time at these crossovers is nearly identical. This result indicates that dynamical characteristics of supercooled liquids may be more informative than the thermodynamic state variables for describing the liquid's "distance" from dynamical arrest. In addition, the characteristic relaxation time in log scale for different temperatures and pressures can be collapsed to one master curve in thermodynamic $TV^{\propto}$ space, where T and V are the system temperature and volume, respectively, and $\propto$ is an empirical constant [125-127]. Dyre and coworkers extended the concept of a simple liquid [128] by incorporating the theory of isomorphs [129] that can explain this scaling in the thermodynamic space. In a simple liquid, as proposed, there exists strong correlations between the virial and potential energy [130]. Such liquids show a "hidden scale invariance" indicating the presence of isomorphs along which structure and dynamics are nearly identical [131]. Thus isomorphic

liquids at two different state points (T_1, V_1) and (T_2, V_2) show identical structure and dynamics. Similar scaling behavior has been noted where the relaxation behavior can be represented by a master curve with a single variable T/p, where p is the pressure of the system, emphasizing the role of both temperature and pressure on glass transition [132].

It is well-known that liquids can be approximated as a collection of hard spheres (HS) with a dominant repulsive potential and a weak attractive potential [37]. The collapse of structural and dynamic properties implies a quasi-universality in liquids that can be explained with model hard spheres [133, 134]. The quasi-universality in hard sphere systems indicates that if two liquids have similar structural and dynamical behavior, they both will map to a hard sphere system with the same effective packing fraction [134]. Thus, if an *effective* packing fraction can be defined and identified for all supercooled liquids, and in all thermodynamic states, then the associated structure and dynamics can be captured by this packing fraction, which will quantitatively describe the state of jamming in a thermally excited state. ***A primary objective of this dissertation is to develop a <u>thermal jamming framework</u> that will quantify the extent of jamming for any glass forming liquid (GLF) at any given thermodynamic state***. Central to this development is the idea of quasi-universality and the hard sphere paradigm [134], which is extended to supercooled liquids and GFLs. In the next chapter, basic concepts of hard sphere theory and jamming are presented.

Chapter 2: Hard Sphere Theory

The most basic conception of jammed matter can be visualized through randomly packed identical (monodisperse) spheres arranged inside a container. For a system of hard spheres, where the boundaries do not overlap, the extent to which the system volume is occupied by the spheres is determined by the "packing fraction" ϕ, which is the ratio of the total volume of the spheres to the total volume of the container. For such a system of hard spheres (HS), the compressibility $Z = p/\rho RT$, which is a dimensionless quantity expressed in terms of the pressure (p), number density (ρ), universal gas constant (R) (which is the product of Boltzmann constant k_B and Avogadro's number N_A), and temperature (T), indicates the extent to which the system behavior deviates from that of an ideal gas [85]. The volume or packing fraction of the spheres can be expressed as $\phi \equiv \frac{4}{3}\pi\rho\sigma_{HS}^3$, where σ_{HS} is the hard sphere diameter; it is directly proportional to a non-dimensional density, which is given by $\hat{\rho} \equiv \rho\sigma_{HS}^3 = 6\phi/\pi$. For the limiting case of $\phi = 0$, $Z = 1$ and the hard sphere system becomes identical to an ideal gas system – this may be conceptualized as an infinitely effuse system of hard spheres, or equivalently, hard spheres with a diameter of zero. Molecules in a real gas have finite volumes, which is reflected by a non-zero packing fraction. As ϕ increases, the spheres begin to act like a compressible fluid, and when ϕ exceeds approximately 0.49, an equilibrium hard sphere system can become partially crystallized [135]. Through a finite compression process, the hard sphere system can also be brought into a metastable state, analogous to that of a supercooled liquid [136]. It is remarkable that a simple system of monodisperse hard spheres can approximately represent such a wide range of fluidic behavior.

Section 2.1   Hard Sphere Phase Diagram and Jamming Transition

Figure 2-1 shows a "phase diagram" for hard spheres [121, 137], which relates the pressure (compressibility) of the system to the packing fraction. At $\phi_f \sim 0.49$, a situation analogous to freezing occurs where the spheres may only rearrange by making short movements, and two "branches" emerge on the phase diagram. Between $\phi_f \sim 0.49$ and $\phi_s \sim 0.55$, the hard sphere system undergoes a first order transition. The isotropic fluid branch is explored by carefully

arranging or percolating the hard spheres so that they may find optimal packing configurations. This leads to the densest-possible packing of a face-centered-cubic (FCC) lattice at $\phi_{FCC} \sim 0.74$. Other configurations such as $\phi_{BCC} \sim 0.68$ (BCC lattice) or $\phi_{SC} \sim 0.54$ (simple cubic lattice) can arise from this branch as well. These configurations are periodic arrangements of atoms that can be constructed by translational placements of unit cells along the Cartesian axes. A unit cell is the simplest "building block" of the periodic lattice by which the entire lattice can be built. The simple cubic unit cell, for instance, is a cubic box with eight atoms located on the eight vertices of the cube. The FCC unit cell features atoms on the eight vertices of a cube with six additional atoms on the centers of the six faces of the cube; the BCC unit cell also features atoms on the cubic vertices but has one additional atom in the center of the cube.
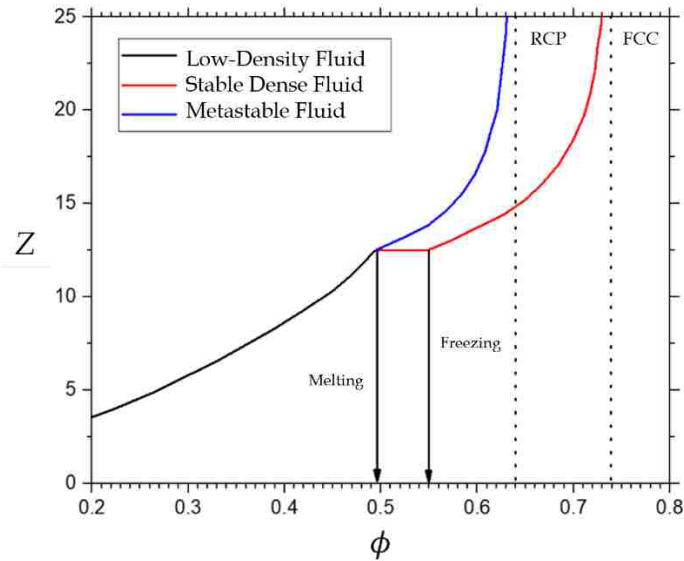
Figure 2-1:   A schematic of the phase diagram for hard spheres [137].

The metastable branch of the hard sphere phase diagram develops when the spheres are compressed rapidly. Having insufficient time to rearrange into optimal packing, the spheres will eventually obtain a "random close-packed configuration (RCP)" corresponding to $\phi_{RCP} \sim 0.64$ [121]. At this configuration, the hard sphere system can be said to undergo a hard sphere glass transition. The hard spheres have formed an amorphous solid that is completely jammed with only local vibrational modes surviving [134].

Molecular dynamics and Monte Carlo simulations [138] of hard spheres have been used to compute Z near the RCP limit for decades [139, 140], a feat that is arguably not possible in a laboratory experiment of hard spheres, since gravity, friction, and finite size effects are exceedingly difficult to correct for. Although the simulations can reasonably compute the compressibility to ϕ close to the RCP limit, the exact value of ϕ_{RCP} is not necessarily discernible even in simulations. The metrics of jamming in hard sphere systems are thus not unique, and a more precise classification of jamming allows for multiple jammed configurations such as locally, collectively, or strictly jammed; similarly, the ambiguous RCP configuration [121] is more precisely expressed as "maximally random jamming" (ϕ_{MRJ}) [122].
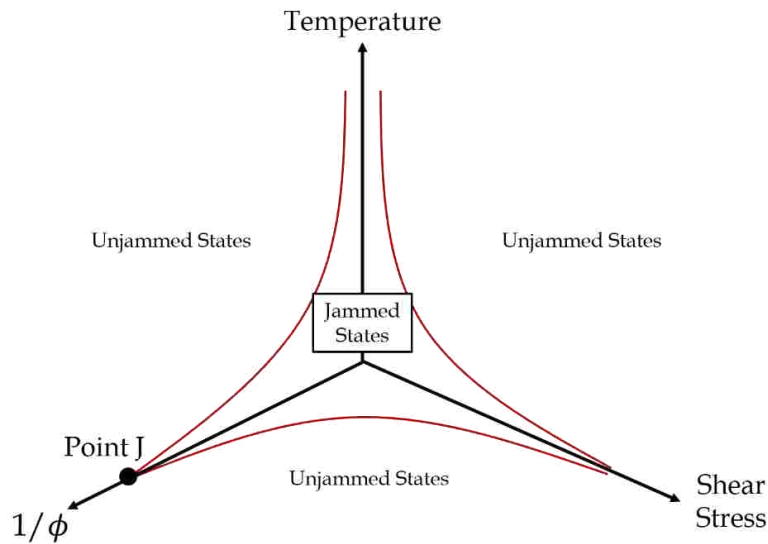
Figure 2-2:   Liu and Nagel's jamming phase diagram [141]. The interior of the surface bounded by the red curves corresponds to jammed states, which occur under sufficiently small temperature, shear stress, and reciprocal density.

Liu and Nagel [141, 142] proposed an important heuristic for understanding the behavior of jammed matter in general by proposing a higher-dimensional phase diagram, shown in Figure 2-2. Three variables – temperature, applied load or shear stress, and reciprocal density – are considered, and jammed states are demarcated by the surface bounded by the red curves. While qualitatively accurate, a quantitative boundary for the jamming surface has so far only been

defined at a single point, "*J*", which occurs only in the special case of zero applied load (shear stress) and zero temperature [141, 143]. At the point *J*, the hard sphere system achieves a jamming transition [144] with a power-law scaling that indicates a critical transition. Both thermodynamic variables such as temperature or shear stress can alter the jammed state. The jamming surface is not, however, sharply defined. As noted by Chaudhuri, Berthier and Sastry [145], who discovered a range of possible values for ϕ_{RCP} in the vicinity of 0.64 that correspond to the hard sphere glass transition, the point *J* is not unique, and it is dependent on the sample's preparation history. Other possible transitions in hard spheres are also known at packing fractions close to point *J*. A list of these transitions is provided in Table 2-1.

Table 2-1:   Static and dynamic transitions in monodisperse hard spheres in the vicinity of Point *J* [121]

ϕ	Definition	Value
ϕ_{MRJ}	Maximally random jammed configuration (geometrical)	~ 0.64
ϕ_d	Liquid HS state splits into an exponential number of states	~ 0.58
ϕ_K	Ideal HS glass transition	~ 0.62
ϕ_{MCT}	Mode-coupling transition in HS	~ 0.58
ϕ_g	HS glass transition density (compression-rate dependent)	0.58 – 0.62
ϕ_J	Point *J*	~ 0.64
ϕ_{RCP}	Random-close-packed configuration	~ 0.64

Section 2.2   Hard Sphere Theory

The monodisperse hard sphere system has long been the subject of intense theoretical development in the field of statistical mechanics, as it serves as a suitable approximation of the non-ideal gas. Since the hard sphere system is also the only case in which a firm, unambiguous jamming criterion may be established, an examination of hard sphere theory is a logical place to

begin with respect to understanding the jamming phase diagram. The interatomic potential energy of hard spheres is a step function at the hard sphere diameter σ_{HS} [85]:

$$U_{HS}(r) = \begin{cases} \infty & r \leq \sigma_{HS} \\ 0 & r > \sigma_{HS} \end{cases} \tag{2.2.1}$$

The equation-of-state (EoS) of a hard sphere system is expressed in terms of the compressibility and the packing fraction. In general, it can be written as [37, 146]

$$Z(\phi) = 1 + b\rho g(\sigma^+) \tag{2.2.2}$$

where ϕ is the packing fraction, σ^+ is the diameter of the hard spheres approached from the right as defined from the interatomic potential, and $g(\sigma^+)$ is the value of the radial distribution function at contact; i.e., at $r = \sigma^+$. The direction of approach is specified to avoid the divergence of the potential at σ^- (approached from the left). The value of $g(\sigma^+)$ may be computed from molecular dynamics or Monte Carlo simulations [146]. The area under the first peak of $g(r)$ is equal to the coordination number (CN), the average number of nearest neighbors for every atom in the system. It is given by [85]

$$CN = \int_0^{r_{min}} dr g(r) \tag{2.2.3}$$

where $g(r)$ is the radial (pair) distribution function. For a random-packed-configuration of hard spheres with frictionless contact, $CN = 6$ [147]. The term b in Equation (2.2.2) is the van der Waals co-volume, and in three dimensions $b = 2\pi\sigma_{HS}^3/3$. Another relationship that is commonly reported is given by [148]:

$$\phi = \frac{\pi\hat{\rho}}{6} = \frac{b\rho}{4} = \frac{\pi\sqrt{2}}{6}\left(\frac{V_0}{V}\right) \tag{2.2.4}$$

where V_0 is defined as the close-packed molar volume, and is given by

$$V_0 \equiv \frac{N\sigma_{HS}^3}{\sqrt{2}} \tag{2.2.5}$$

The compressibility now can be written as [85]

$$Z(\phi) = 1 + b\rho g(\sigma^+) = 1 + 4\phi g(\sigma^+) \tag{2.2.6}$$

The previous equation is a general thermodynamic relationship for the hard sphere fluid; it is can be expressed as in terms of a geometric packing fraction ϕ and $g(\sigma^+)$, which is purely a structural quantity. The most widely-used equation of state for hard spheres was obtained by Carnahan and Starling (CS) [149] which uses the following form for $g(\sigma^+)$

$$g(\sigma^+) = \frac{1 - \dfrac{\phi}{2}}{(1-\phi)^3} \tag{2.2.7}$$

The CS EoS then reduces to

$$Z(\phi) = \frac{1 + \phi + \phi^2 - \phi^3}{(1-\phi)^3} \tag{2.2.8}$$

The CS equation can be derived by using a truncated virial expansion of the pressure in the compressibility equation, and has been found to be highly accurate for hard spheres $\phi < 0.50$ [150]. However, the CS equation suffers from two limitations: for one, it allows for non-physical values of ϕ. The range of the CS equation is $0 < \phi < 1$, and in the context of physical hard spheres it is not possible to exceed the FCC packing limit of $\phi_{FCC} \sim 0.74$, as it is geometrically the densest packing configuration. Increasing the density further would either require the spheres to overlap, in which case they are no longer hard, or deform, in which case they are no longer spheres. A packing fraction of 1 is attainable only if the diameter of the hard spheres is zero, in which case this description is also rendered meaningless. The second issue with the CS equation is that it simply does not agree well with compressibility data obtained by simulations for dense hard sphere packings, since it predicts a divergence in the compressibility at $\phi = 1$ which is significantly higher than where it should diverge (near ϕ_{RCP} or ϕ_{FCC}, depending on which branch of the hard sphere phase diagram the system exists). This shortcoming has led many practitioners to propose other equations of state that better encompass the compressibility of hard spheres in the metastable branch of the hard sphere phase diagram. Some of these equations have been developed on the basis of theoretical arguments, others on the basis of fitting functions applied to compressibility data from numerical simulations, and yet others are obtained by a combination of the preceding approaches [136, 144, 151-157].

For the meta-stable fluid branch, several relationships have been proposed in the past. Many relationships are based on the free volume theory, which predicts a behavior of the form [144, 158, 159]:

$$Z(\phi) = \frac{d}{1 - \frac{\phi}{\phi^*}} \qquad (2.2.9)$$

where d is dimensionality of the system and ϕ^* is the maximal packing fraction, which is close to ϕ_{RCP}. Using a numerical protocol that is based on inherent structures, and later through compression, Speedy [151, 152] proposed an EoS of the following form:

$$Z^S(\phi) = \frac{d_S}{1 - \frac{\hat{\rho}_S}{\hat{\rho}_S^*}} = \frac{2.67}{1 - \frac{\hat{\rho}_S}{0.875}} \qquad (2.2.10)$$

Here d_S is close to 3, and $\hat{\rho}$ is the non-dimensional number density scaled to the FCC packing density $(\sqrt{2}\pi/6)$, which is given by $\sqrt{2}\hat{\rho}_S = \rho\sigma_{HS}^3 = 6\phi/\pi$. The above equation then can be formulated in packing fraction as

$$Z^S(\phi) = \frac{d_S}{1 - \frac{6\phi}{\sqrt{2}\pi\hat{\rho}_S^*}} = \frac{d_S}{1 - \frac{\phi}{\phi_S^*}} = \frac{2.67}{1 - \frac{\phi}{0.648}} \qquad (2.2.11)$$

The parameters for the power-law of Speedy is chosen to fit hard sphere compressibility data computed from 200 hard sphere metastable systems that have been thermalized. It features the parameter $\phi^* \sim 0.648$, which is very close to ϕ_{RCP} and indicates the value of ϕ at which the compressibility diverges for this EoS. While Speedy's equation is very accurate for hard spheres at high density [153], it is invalid for hard spheres at low density where the CS equation works well. Odriozola and Berthier (OB) [136] have more recently developed a relationship that is based on numerical simulations of fully thermalized polydisperse repulsive spheres and the free volume theory. It is very similar to Speedy's equation and is given by:

$$Z^{O-B}(\phi) = \frac{d_{OB}}{1 - \frac{\phi}{\phi_{OB}^*}} = \frac{2.82}{1 - \frac{\phi}{0.669}} \qquad (2.2.12)$$

39

Given that its functional form is identical to Speedy's equation, the Odriozola and Berthier EoS is also invalid for low values of ϕ.

Both Speedy and Berthier and coworkers [144] posit a kinetic glass transition before the maximally jammed state that occurs at $\phi = \phi^* \sim \phi_{RCP} \sim \phi_J$. According to Speedy [151, 152], the hard sphere glasses are reproducible, which implies that structural relaxation time diverges before the maximal packing fraction ϕ^* is achieved in the system, and the glass transition may have a thermodynamic basis [152]. In both approaches, a kinetic glass transition is identified at a packing fraction that is smaller than ϕ^*. Analysis by Speedy, using a large number of glasses prepared by different methods, shows that a kinetic glass transition occurs at $\phi_c \sim 0.57$ when the root-mean-square (rms) displacements the spheres becomes is approximately the same as their diameters. The ideal glass transition, however, occurs at a higher fraction, and for a single component fluid it is located near $\phi_c \sim 0.586$. By inspecting the dynamic and thermodynamic properties of polydisperse repulsive spheres, and a generalized VFT law, Berthier and coworkers have demonstrated a critical volume fraction $\phi_0 \sim 0.635$ that signifies a divergence of equilibrium or structural relaxation time [160]. Interestingly, the compressibility Z is finite at ϕ_0 and is approximately equal to 34.4, which is at odds with the free volume theory which predicts that both Z and the relaxation time diverge together. Thus, a point "G" is introduced by Berthier and coworkers that denotes the critical volume fraction corresponding to the *dynamic* divergence in the relaxation time as temperature $T \rightarrow 0$ [144, 161]. According to this view, the jamming transition at ϕ^* occurs deep in the glassy state and it is physically different from that kinetic transition at Point G ($\phi_0 \sim 0.635$), the latter is closely related to the Kauzmann packing fraction ϕ_K, where the configurational entropy vanishes. Further jamming transitions take place over a range of packing fractions $\phi^* \in [0.642, 0.664]$, implying a continuous range of densities where hard sphere jamming can occur – this state corresponds to an infinite pressure [144] with the average coordination number increasing from zero to around 6 at ϕ^*, or more precisely at the "glass close packed" (GCP) transition ϕ_{GCP}. The lower bound for GCP is given by $\phi_{GCP} > 0.664$, which is very close to $\phi_{OB}^* \sim 0.669$ that is given by the semi-empirical relationship of Odriozola and Berthier [136]. Interestingly, the only theory that predicts a finite compressibility is RFOT that predicts an ideal glass transition [144].

Although Speedy and Berthier/coworkers agree on the distinguishability of kinetic and jamming transitions, Speedy regards the jamming transition as reproducible and confers a thermodynamic basis to it while Berthier/coworkers treat the jamming transition as dependent on the numerical protocol for generating the jammed states. Ergodicity is lost at ϕ_0 or at ϕ_K which corresponds to the ideal glass transition, according to Berthier/coworkers, and a jamming transition occurs when the pressure diverges near ϕ^*. In an opposing view [162], ergodicity is lost at ϕ^* with diverging compressibility and relaxation time without any intervening ideal glass transition. Thus Point J controls jamming and the glass transition which occurs when $T/p \rightarrow 0$ or equivalently when $Z \rightarrow \infty$ as $\phi \rightarrow \phi^*$ [162].
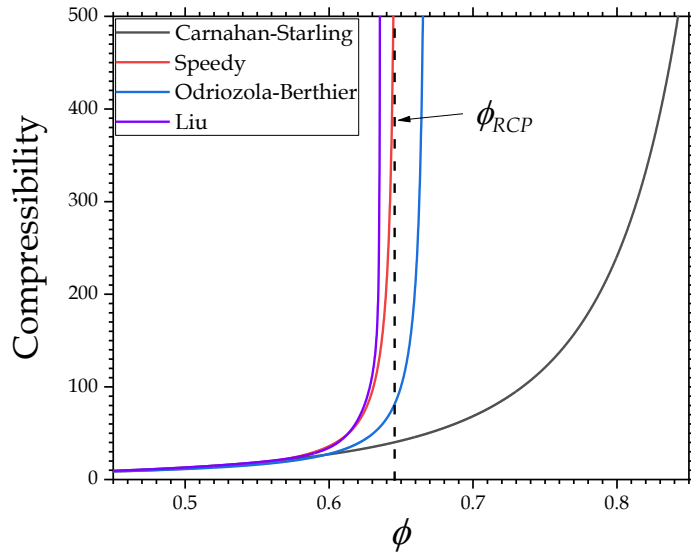
Figure 2-3:   Compressibility from four equations of state – Carnahan and Starling (CS) [163], Speedy [152], Odriozola and Berthier [136] and Liu [148, 164] considered in this work (only the metafluid branch is shown for Liu EoS [165]. The random close-packed value of $\phi_{RCP} \sim 0.64$ is denoted by a dashed line.

Another equation of state of interest, developed by Liu [164] very accurately encompasses both the low-density liquid and metastable fluid branches of the hard sphere phase diagram [165]. Liu's equation is given by

$$Z_{Liu}(\hat{\phi}) = Z_V + \frac{A\hat{\phi}}{1 - B\hat{\phi}} + C\hat{\phi}^{40} - D\hat{\phi}^{42} + E\hat{\phi}^{44}$$

$$Z_V(\hat{\phi}) = 1 + \left(\frac{V_1\hat{\phi}}{1 - V_2\hat{\phi} + V_3\hat{\phi}^2 - V_4\hat{\phi}^3 - V_5\hat{\phi}^4} \right)$$

(2.2.13)

The coefficients for Liu's equation [165] are provided in Table 2-2.

Table 2-2:   Parameters of Liu's equation of state [164], [165].

Parameter	Value	Parameter	Value
V_1	3.68584	A	0.31416
V_2	2.5848	B	1.573357
V_3	1.9499	C	4.1637×10^{10}
V_4	0.172284	D	2.3452×10^{11}
V_5	0.16012	E	3.6684×10^{11}

Although the functional form of Liu's EoS is significantly more cumbersome than the other equations, it remarkably describes the dense isotropic fluid branch of the phase diagram as well as the solid state by cleverly introducing a pole near the RCP packing limit. A plot of Liu's equation, as well as the three other equations of state, is shown in Figure 2-3.

Table 2-3 shows a comparison of the average absolute deviations for each of the three equations of state as compared to simulation data for the normal fluid and metastable fluid branches of the hard sphere phase diagram [164]. Liu's equation has by far the smallest average absolute deviation (AAD) relative to numerical hard sphere compressibility values in both the low-density and metastable fluid regimes. Speedy's equation improves upon the CS equation significantly in the metastable fluid branch. Since the Odriozola-Berthier equation is very similar to the Speedy equation, it is expected to produce a similar AAD value.

We have outlined here the fundamentals of describing the thermodynamic and jamming behavior of hard spheres in terms of their packing fraction ϕ. The application of hard sphere theory to our purposes – describing the dynamical processes of supercooled liquids and glass formers from the standpoint of jamming – is part of a larger story that will be made clear in the following chapters. In the next chapters, a theoretical framework that quantifies the extent of

"thermal" jamming is described, and the use of these accurate hard sphere equations of state will be linked to the understanding of jammed dynamics in supercooled liquids – the central focus of this work.

Table 2-3:   A comparison of the average absolute percent deviations (AAD) of the Carnahan-Starling, Speedy, and Liu equations of state compared to hard sphere compressibility data from simulations. All values are obtained from reference [165] except for the AAD of the CS equation in the metastable branch, which comes from [153].

Equation	Low-Density Fluid (% AAD)	Metastable Fluid (% AAD)
Carnahan-Starling (CS)	0.196	34.4
Speedy	-	4.70
Liu	0.0841	0.98

Chapter 3:   Quasi-Universality and the Hard Sphere Paradigm

Static jamming in systems of rigid objects, as evidenced by hard spheres, only depends upon the density. If boundaries of the atoms or other constituents of the system may be firmly established, the static packing fraction may be computed without ambiguity, independent of the motion of the constituents of the system. In molecular supercooled liquids where atomic boundaries are not unambiguously defined, as the temperature is lowered or the pressure is increased, the atoms begin to slow down as indicated by the pronounced "caging" period of the mean-squared displacement and the attendant prolonged structural relaxation time. The dramatic slowdown in the dynamics of model supercooled liquids can be described, under some conditions, through the 'thermal free volume', which is created by thermal energy working against pressure [132, 166]. Relaxing the small pressure limit and insignificant overlap between the atoms, the dynamics can be characterized by using an effective hard sphere packing fraction at finite temperatures [166]. In the thermal free volume conceptualization, the atoms may be thought of as becoming "thermally jammed" as temperature decreases. The jamming hypothesis is untested, as discussed in Chapter 2. There are two ways of conceptualizing the glass transition in supercooled liquids, as shown in Figure 3-1.

We adopt the point of view that thermal excitations create a thermal free volume which will decrease with decreasing temperature. Unlike the approaches before, it is posited that *only a subset* of the constituent atoms, modeled as hard spheres, in a supercooled liquid or glass forming liquid (GFL), will show the features of jammed conditions. ***Thus, the dynamic slowdown arises from the attrition of the thermally excited hard spheres with decreasing temperature – we refer to this effect as thermal jamming***. This thesis will seek to examine and apply this conceptualization of segregated or inhomogeneous dynamics in molecular glass forming systems, right up to the glass transition. The road to formulating the thermal jamming framework begins with an understanding of hard sphere theory, which was covered in Chapter 2, and two key concepts – static/dynamic equivalence [37, 166-168] and quasi-universality and the hard sphere paradigm observed in simple liquids [128, 131, 133, 134].
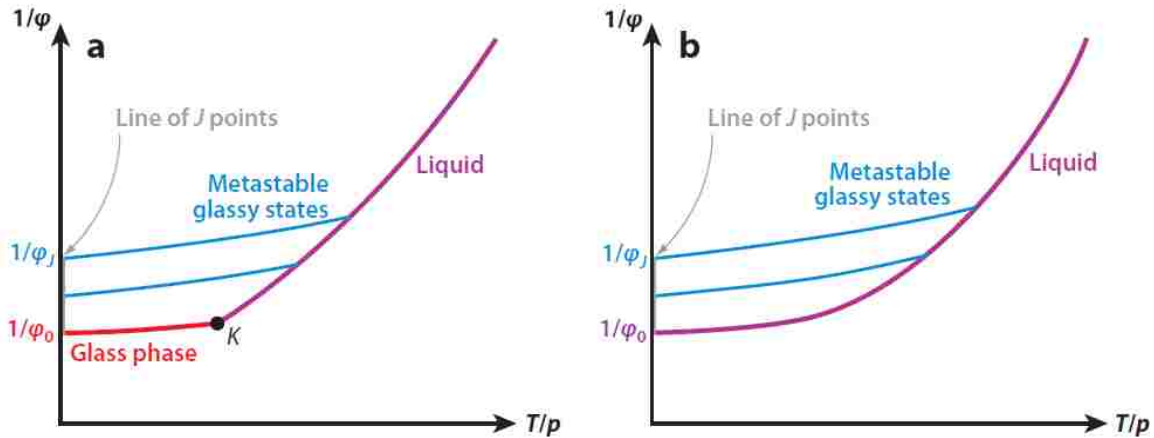
Figure 3-1: Two possible interpretations of glass transition in supercooled liquids (Reproduced from [162]). In the scenario shown by the left panel, a system, compressed at finite rates, becomes non-ergodic and undergoes glass transition well before the critical (static) packing fraction ϕ_J at the infinite pressure limit [169]. In the slow limit of infinite compression, a complete loss of configurational entropy occurs at the characteristic temperature/pressure state point (K) with the attendant divergence of the structural relaxation time. In this view point, jamming, more precisely, static jamming that is brought about by chains of forces associated with actual contacts, has no relevance to the phenomenon of glass transition [169]. In the mechanism shown by the right panel, the thermodynamic (ideal) glass transition, where configurational entropy vanishes, occurs only as $T/p \rightarrow 0$, and the jamming transition coincides along the line of J points.

Section 3.1 Static and Dynamic Equivalence

The idea of using hard spheres as surrogates to capture the properties of realistic gases and fluid systems dates back to the work of Van der Waals. It has long been accepted that fluid properties are dominated by repulsive forces, and hard spheres represent the idealization of severe repulsion [37]. Using equilibrium statistical mechanics, Andersen, Weeks and Chandler (AWC) developed a generalized cluster expansion that connects structural/thermodynamic properties of a soft sphere system to an equivalent hard sphere system [170]. By choosing an *effective* hard sphere diameter, the Helmholtz free energy and the following function $y(r) = e^{\beta u(r)}g(r)$, where $u(r)$ and $g(r)$ are the soft-sphere (SS) potential and radial distribution function, respectively, and $\beta = 1/(k_B T)$, can be made nearly identical to those of the SS system with the same number density. To derive the equivalent hard sphere diameter, the pressure and free

energy are set to equal those of the equivalent hard sphere system, and the following volume integral is minimized:

$$\int 4\pi r^2 y_{HS}(r)\left[e^{-\beta U(r)} - e^{-\beta U_{HS}(r)}\right]dr \equiv \int 4\pi r^2 B(r)dr = 0 \qquad (3.1.1)$$

The function $B(r) = y_{HS}(r)\left[e^{-\beta U(r)} - e^{-\beta U_{HS}(r)}\right]$ is called the "blip function" [170], and $y_{HS}(r) = e^{\beta U_{HS}(r)}g_{HS}(r)$. Using this approach, the static and thermodynamic properties of realistic fluid system, modeled by a SS system, can be mapped to an equivalent hard sphere system.

The dynamic equivalence between realistic soft sphere and hard sphere systems has been established more recently [167, 168] and it is developed in the context of seeking a possible universality between the *density-driven* colloidal glass transition and the *thermally-driven* molecular glass transition [168]. In addition to static structure, dynamic metrics are also involved in demonstrating the equivalence. For instance, the following equations show the static equivalence and dynamic equivalence involving the reduced diffusivity [168]:

$$g(r;\rho,T) \approx g_{HS}(r/\sigma_{HS};\phi_{HS}) \qquad (3.1.2)$$

$$D^*(\rho,T) \approx D_{HS}^*[\phi_{HS}] \qquad (3.1.3)$$

In the above set of expressions, $\phi_{HS} = \phi_{HS}(\rho,T)$, the reduced density $D^*(\rho,T) \equiv D(\rho,T)/D_0$, where D_0 is the short-time diffusion constant, and $D(\rho,T)$ is the long-time diffusion constant. Similarly, the equivalence for structural relaxation time can also be stated. The thermodynamic state equivalence is shown using an appropriate equation of state. The CS EoS is usually the equation of choice, and the scaling can be written as

$$Z(\rho,T) \approx Z_{HS}[\phi_{HS}] \equiv 1 + 4\phi_{HS}g_{HS}(\sigma^+;\phi_{HS}) \qquad (3.1.4)$$

As explained in the previous chapter, the CS EoS is reliable for lower densities, and more-accurate equations of state (which are empirically derived) are available for the jammed states of hard spheres. Using the condition that the height of the main peak of the structure factor of the SS system is coincident with that of the HS, Ramírez-González *et al.* [168] generated an impressive mapping to an equivalent hard sphere system. Fig. 3-2 shows the collapse of the inverse of

reduced diffusivity, both experimental and simulated, with the effective packing fraction ϕ_{HS} [168]. As evident from Figure 3-2, the underpinning of the SS-HS mapping rests on the self-consistent generalized Langevin equation (SCGLE) from which universal isodynamical surfaces can be generated. Interestingly, the mapping does not work very well for systems with weak or ultra-soft repulsive interactions and possibly for attractive interactions as well. It is also worth pointing out that there are several methods to generate the equivalence between the SS and hard sphere systems. The non-uniqueness indicates a lack of firm theoretical grounds for the mapping concept.
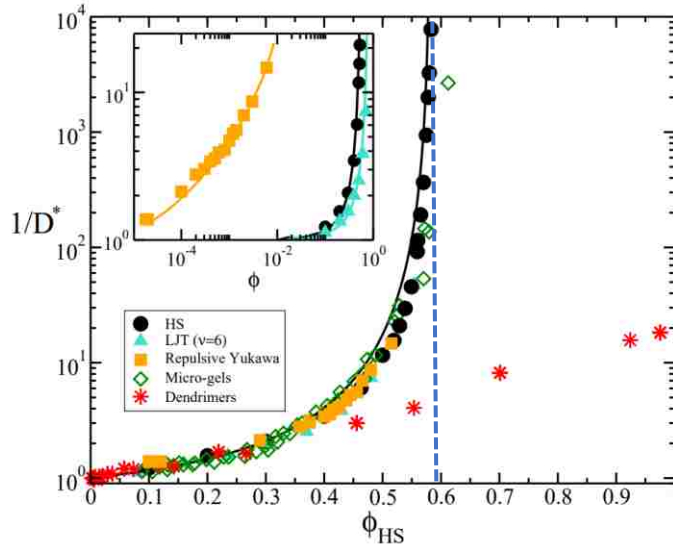
Figure 3-2:   Scaling of inverse of reduced diffusivity of experimental and simulated systems with the effective hard sphere packing fraction derived using the principle of dynamic and static equivalence. The line denotes prediction from the self-consistent generalized Langevin equation (SCGLE). The outlier corresponds to dendrimer solutions that have ultra-soft repulsive interactions. The vertical broken line suggests a limiting effective HS packing fraction near $\phi_{HS} \sim 0.58$, which is typically regarded as the packing fraction at colloidal glass transition [171]. The figure is reproduced from [168].

Investigations by Xu *et al.* [132], demonstrated the equivalence of glass transitions in molecular systems and colloidal glass transition in the hard sphere limit by showing [166]

$$\lim_{p\sigma^3/\varepsilon \to 0} \tau \sqrt{\frac{p\sigma}{m}} = f_{HS}\left(\frac{T}{p\sigma^3}\right) \tag{3.1.5}$$

The equivalence, which is strictly true in the limit of zero pressure or equivalently when the particles do not overlap, shows that the reduced relaxation time τ falls onto a single master curve with T/p. When this condition is relaxed, i.e., when the particles can overlap, it is observed that the hard sphere system equivalence can be demonstrated with an effective smaller hard sphere diameter; the equivalence is shown by using the same approximation used by AWC described previously. For several state points, the relaxation time with SS systems can be predicted with an equivalent hard sphere system of smaller diameter using the above mapping method and CS EoS [166].

Section 3.2   Surrogate Hard Sphere Glass Transition with Colloidal Systems

Colloidal systems such as suspensions and emulsions are often well-approximated by hard spheres [171, 172]. Upon compression, colloidal systems with polydispersity typically undergo a change in phase as shown in Figure 3-3. Similar to non-Arrhenius variation with temperature, the viscosity of a colloid exhibits fragility with respect to the packing fraction. The viscosity range, which spans only four orders of magnitude, however, is not as broad as in molecular systems. The "supercooled region" of colloidal phase starts around the freezing packing fraction ϕ_f and it is widely accepted that a "colloidal glass transition" occurs at around $\phi_g \sim 0.58$. which is close to the limiting effective hard sphere packing fraction shown in Figure 3-3.

There is no exact one-to-one correspondence between molecular, HS, and colloidal systems, but there are significant similarities and some notable differences [171]. The colloidal glass transition is driven by changes in density, while the glass transition in molecular GFLs is temperature (or pressure) driven (density changes in molecular GFLs under supercooling are typically small). There is a unique control parameter, which is the packing fraction in colloidal systems even though it is difficult to make measurements at high volume fractions. Although density driven, neither the mechanism of glass transition nor the corresponding volume fraction is known without ambiguity. The change in viscosity can be fitted to the Doolittle equation as $\frac{\eta}{\eta_0} = C \exp\left(\frac{D}{\phi_m - \phi}\right)$, where $\phi_m \sim 0.64$, which is close to ϕ_{RCP} [173]. As its functional form is identical to the VFT equation, the Doolittle equation predicts a divergence of structural relaxation

time at $\phi_m \sim 0.64$ and the corresponding vanishing of the configurational entropy. Therefore, the glass transition can be identified at $\phi_g \sim 0.64$ from a kinetic perspective.
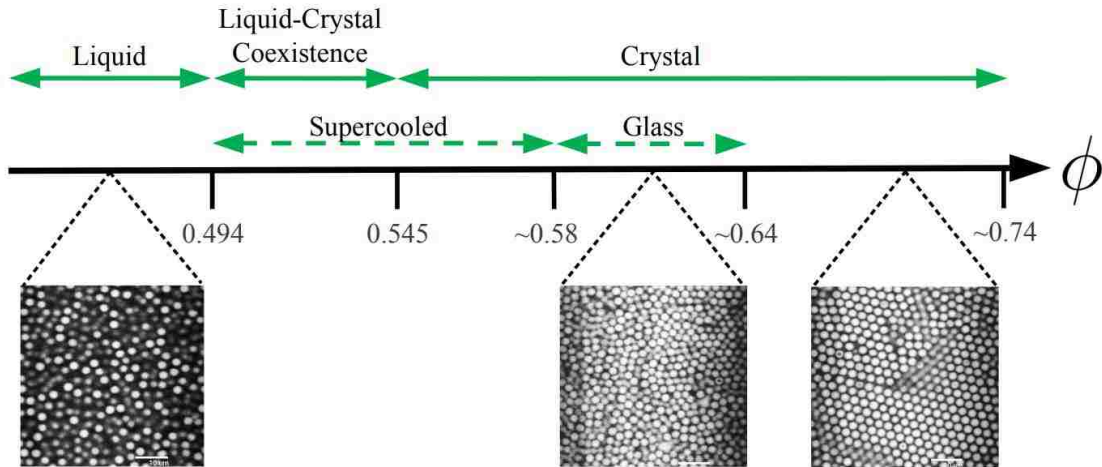
Figure 3-3:   Colloidal phases and the corresponding HS phase diagram, reproduced from [171]. A glass transition is thought to occur at a packing fraction $\phi_g \sim 0.58$, although there is some evidence to suggest that it may occur at the RCP value of $\sim$0.64. The MCT prediction suggests a critical packing fraction ϕ_c that varies from 0.51 to 0.58 [174, 175].

Other experimental and simulation evidence on polymer systems also suggest a diverging relaxation time at volume fractions between 0.62 and 0.64 [176]. As with molecular systems, the use of VFT-like form is also criticized [171, 177]; several non-diverging functional forms are equally capable of capturing the viscosity trend [65]. The early MCT investigations have predicted MCT $\phi_c \sim 0.51$, close to the freezing packing fraction, and it was then revised to $\phi_c \sim 0.58$, closer to the accepted fraction for glass transition [174]; recent work indicates that it can occur at lower fractions near $\phi_c \sim 0.53$ [175]. There is thus no broad consensus on the various packing fraction "crossovers", but the most commonly accepted value for the colloidal glass transition is $\phi_g \sim 0.58$, as shown by the lower limit in Fig. 3-3. As is seen in molecular GFLs, it is also unclear whether the structural relaxation time truly vanishes at or near the colloidal glass transition. The unpleasant hazard of extrapolation exists in both the experimental or numerical studies that are needed to establish a genuine divergence in relaxation time at finite volume fractions or temperatures.
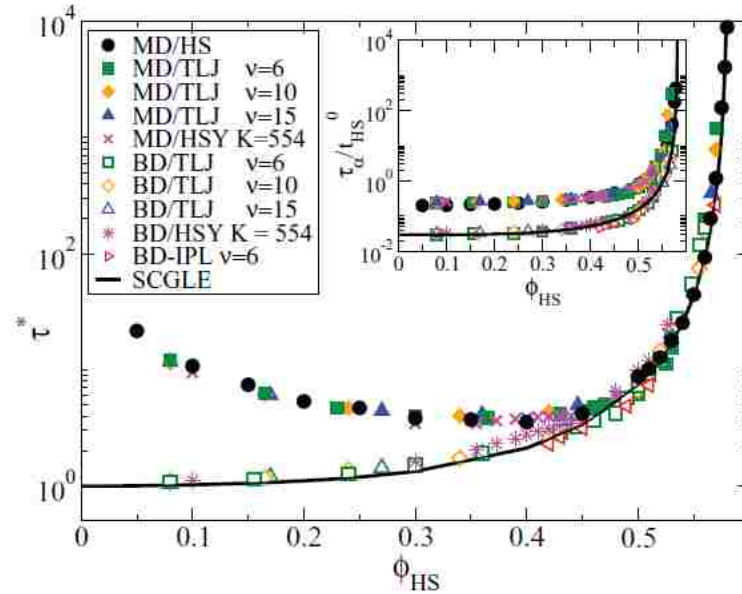
Figure 3-4: Mapping of reduced relaxation time of soft spheres to effective hard spheres using Newtonian dynamics and Langevin (Brownian dynamics) [178]. The collapse of Newtonian and Brownian at longer times show their equivalence above a critical packing fraction $\phi \sim 0.49$, roughly at the density when the HS fluid becomes metastable. The relaxation time appears to diverge at a packing fraction $\phi \sim 0.58$.

Regardless of the ambiguity in the transitions, recent theoretical work and numerical simulations show a class of universal equivalence between atomic and colloidal systems through an effective packing fraction [178]. Unlike molecular systems, the colloidal systems are influenced through hydrodynamic interactions. While the former can be simulated by model systems through Newtonian dynamics (ND), the dynamics of the latter can be captured through Brownian dynamics (BD); thus, the short time dynamics in colloids is diffusive, and ballistic in GFLs. Quite remarkably, the more interesting long-time dynamics is captured by both ND and BD, which indicates that microscopic solvent dynamics are relatively unimportant for colloids. This similarly and the near-equivalent collapse of diffusivity and structural relaxation time data to an effective hard sphere packing fraction has led to the concept of a dynamic universality class [178]. The key idea is that hard spheres with an effective diameter can capture the structure and long-time dynamics of soft spheres with *both* Newtonian and Brownian dynamics. This equivalence is shown by the collapse of data of soft spheres with Newtonian dynamics and with Langevin (Brownian) dynamics in Figure 3-4.

Section 3.3   Quasi-Universality: Hard Sphere Paradigm and Excess Entropy Scaling

The previous sections outlined methods of mapping molecular liquids and colloids to hard sphere (HS) systems, and the approximate collapse of structural and dynamic variables of different systems or states on to a master curve represents a quasi-universality in a broad class of liquids. The hard sphere model thus provides a theoretical underpinning or paradigm for drawing out the similarities, or sometime equivalences, in liquid structure and dynamics. The hard sphere paradigm itself is rooted on the seminal work of Van der Waals, who hypothesized that the strongly repulsive forces in liquids are responsible for determining the dynamics of the system, while long range attractive forces among the liquid's atoms give rise to the system's cohesive energy but has a negligible effect on the liquid's dynamics or structure. But the lack of a strict one-to-one correspondence between molecular liquids and the hard sphere system, or colloids and the hard sphere system, means that the hard sphere paradigm is only an expression of a quasi-universal description of liquid dynamics, and that the hard sphere description is only qualitatively correct for describing simple liquid dynamics but shows exceptions to true universality from a quantitative standpoint. Various exceptions, revealed both experimentally and computationally, have precluded the hard sphere paradigm from constituting a true universal description of liquids.

As described previously, Dyre and coworkers [133, 134] reversed the conventional relationship between hard spheres and quasi-universality by asserting that the hard sphere similarities are a *consequence* of quasi-universality. To this end, Dyre and coworkers developed a family of exponentially repulsive (EXP) pair potentials that portray quasi-universal behavior. Pair potentials that are typically used to probe glassy dynamics are included in this EXP quasi-universality class. Interestingly, the HS potential is *not* a member of EXP family but nevertheless is a member of the EXP quasi-universality class. The general claim, although untested, is that the EXP family of potentials can be regarded as a cardinal reference system from which quasi-universality can be derived. Thus quasi-universality is conjectured to be apposite only for certain potentials that belongs to the family of EXP potentials [133, 134]. This perspective can rationalize – but not prove – why certain interatomic potentials show quasi-universality while others do not.

In defining quasi-universality, a set of reduced units arises from scaling which are experimentally assessable. These reduced units are dependent on the thermodynamic state point; according to the isomorph theory of Dyre and coworkers [128, 129], the potential energy landscapes of isomorphic state points, which are expressed in terms of reduced units, are identical, meaning that reduced units allow for the unification of dynamical behavior among different regions of the phase diagram. The reduced units are obtained by taking some variable and using dimensional analysis to reduce it to a dimensionless quantity that is experimentally accessible. For diffusion coefficient, which has the units of distance squared per time, the scaling involves the temperature T and density ρ that define the state point, and the mass of the material under study. The use of reduced units allows for a meaningful comparison to be made among structural and dynamical properties at different points or curves along the phase diagram, either for one material or among different materials. It may be noted here that the reduced units which are typically employed in atomistic simulations are state-independent and not experimentally accessible [134]; the reduced units for quasi-universality scaling does not need a prior knowledge of the system Hamiltonian. The scaling for reduced quantities for energy, length, time, the diffusion coefficient, and the viscosity coefficient, is shown in Table 3-1 [134].

Table 3-1:   Physical quantities and scaling for reduced units [134].

Physical Quantity	Scaling for Reduced Units
Energy	$k_B T$
Length	$\rho^{-1/3}$
Time	$\left(\dfrac{m}{k_B T}\right)^{1/2} \rho^{-1/3}$
Diffusion Coefficient	$\rho^{1/3} \left(\dfrac{m}{k_B T}\right)^{1/2}$
Viscosity	$\dfrac{1}{\rho^{2/3}(m k_B T)^{1/2}}$

The early work of Yaakov Rosenfeld [179] demonstrated that a Lennard-Jones fluid's dynamical properties are strongly predicted by its excess entropy, and that there is a scaling relationship observed between dynamical properties and excess entropy that takes an exponential form. Rosenfeld (exponential) scaling is based on the Van der Waals description of liquids, in which a description of so-called "simple liquids" is formulated in terms of a reference hard sphere system. Simple liquids consist of point particles that interact by means of radially-symmetric pair potentials, such as the Lennard-Jones, Weeks-Chandler-Andersen, and harmonic sphere (HARM) model systems studied in this work [37]. Dyre and coworkers have recently illuminated this concept by further showing that all simple liquids have strong correlations between virial and potential energy fluctuations in a canonical ensemble [128]. As many liquids in nature exhibit characteristics that do not fit this classification, Rosenfeld scaling should in principle only present a quasi-universal description of a relatively small subset of liquids.

The excess entropy of a liquid may be computed in a variety of ways. In strict theoretical terms, the excess entropy S^{ex} is defined as the difference between the entropy of a hard sphere system and the entropy of an ideal gas at the same temperature and density [180]:

$$S^{ex}(\rho,T) = S_{liq}(\rho,T) - S_{IG}(\rho,T) \tag{3.3.1}$$

The following relation holds; it relates the temperature to the total potential energy U, which corresponds to the configurational component of the energy and the excess entropy:

$$\frac{1}{T} = \left(\frac{\partial S^{ex}}{\partial T} \right)_{\rho} \tag{3.3.2}$$

Other thermodynamic properties such as the Helmholtz and Gibbs free energies may also be broken into ideal gas and excess terms. For example, the excess entropy can be computed from the excess Helmholtz energy as

$$S^{ex} = -\left(\frac{\partial F^{ex}}{\partial T} \right)_{\rho} \tag{3.3.3}$$

The excess entropy can be expanded in terms of different levels of atomic interactions. A commonly used approximation is based on two-atom interaction which allows for the calculation of the approximate excess entropy S_2 as

$$S_2 = -2\pi\rho N \int_0^\infty \left(g(r)\ln\left[g(r)\right] - \left[g(r) - 1\right]\right) r^2 dr \tag{3.3.4}$$

This is particularly useful for application in molecular dynamics simulations where $g(r)$ may be easily obtained.

Note that the excess entropy S^{ex} is different from S_{ex} that was defined in the context of configuration entropy (see Section 1.1 B). The excess entropy S^{ex} is defined as the difference between the entropies of the liquid state and the ideal gas at the same thermodynamic state, while the S_{ex} is defined as the difference between the liquid state entropy and the entropy of the underlying crystal at the same state. While S^{ex} is always negative, S_{ex} as defined is always positive. These relationships are shown below:

$$S^{ex} = S_{liq} - S_{IG} ; \qquad S_{ex} = S_{liq} - S_{cryst} \tag{3.3.5}$$

Rosenfeld [179] and Dzugutov [181], with the two-body approximation of the excess entropy S_2, have established relatively simple scaling laws that predict dynamical properties in terms of the excess entropy. Both have obtained reasonable fits to data for liquids that showed an exponential scaling with excess entropy. Interestingly Rosenfeld, applying hard sphere theory and incorporating the Carnahan-Starling equation of state, establishes an "entropy" packing fraction as

$$\phi = \frac{S^{ex} + 2}{S^{ex} + 3}\left[1 - \left(1 - \frac{S^{ex}(S^{ex} + 3)}{(S^{ex} + 2)^2}\right)^{1/2}\right] \tag{3.3.6}$$

This is an intriguing result as it shows that there is a one-to-one correspondence between the packing fractions and the excess entropy S^{ex}. Therefore, if properties show a scaling behavior with excess entropy, they will also show the same behavior with the packing fraction.

Dyre [180] expands upon the scaling established by Rosenfeld and Dzugutov, in which dynamical properties of a liquid show exponential scaling with the system's excess entropy. This is generalized by Dyre to the more general concept of Excess Entropy Scaling (EES), in which the scaling of dynamical properties obeys relationships other than exponential scaling. In this definition, Rosenfeld scaling is a special case of EES, and any liquid is said to obey EES if its reduced dynamical properties are uniquely determined by its excess entropy. EES has been

demonstrated in a wide variety of materials; in confirmation of the theory, EES has been observed in atomistic simulations of simple Lennard-Jones and repulsive fluids [179], in the Kob-Andersen model at various densities and temperatures [111], liquid metals [182], and molecular liquids [183]. In these cases, a remarkably distinct collapse of dynamical properties is seen both among distinct materials, and within a given material at a wide range of phase points, indicating a universality of the scaling. However, various cases have also been uncovered where EES does not apply; for instance, in a Hertzian sphere system [184], silicon modeled by the Stillinger-Weber (S-W) potential [185], and the Fermi-Jagla model glass-former [186]. Dyre notes that liquids that exhibit anomalous dynamical behavior, such as diffusion coefficients that increase upon isothermal compression (i.e. water and silica), typically do not exhibit EES [180]. Figure 3-5 shows violation of EES for the Stillinger-Weber potential.
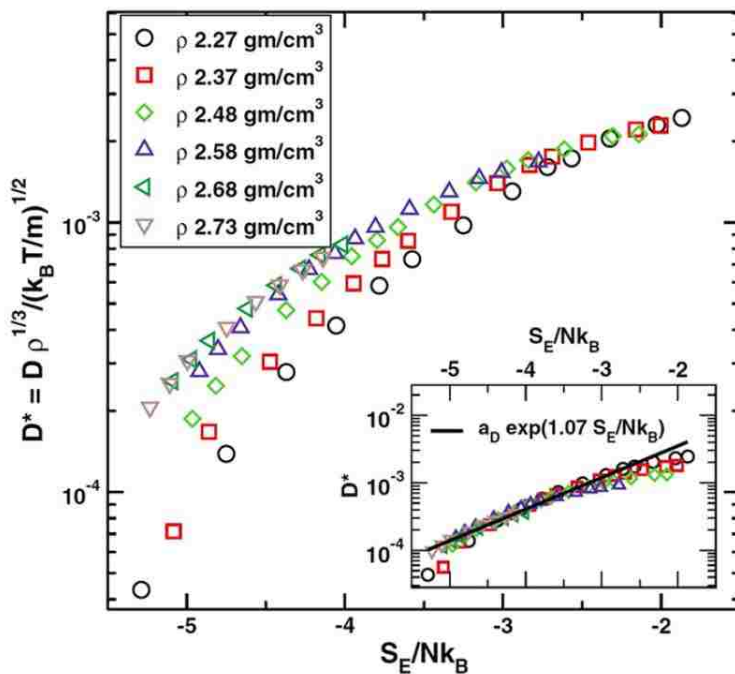
Figure 3-5:   Violation of EES for the Stillinger-Weber potential, which is precluded from being classified as a simple liquid given its three-body potential energy function. The inset shows limited Rosenfeld scaling with density-dependent empirical scaling. Figure is reproduced from [180].

While entropy is a measure of the phase space, the excess entropy is a measure of available volume in the phase space. EES is a demonstration of the strong relationship between

thermodynamics and dynamics in liquids. The scaling indicates that dynamic properties such as the diffusion coefficient and viscosity are determined by the liquid's excess entropy. In his original work, Rosenfeld [179] associated the quasi-universal entropy scaling to the one-to-one correspondence between excess entropy and the effective packing fraction. It has been later shown by Dyre and coworkers [180] that if two thermodynamic states have the same microscopic dynamics, they also possess the same excess entropy. This leads to the concept of hidden scale invariance (HSI), which indicates that the thermodynamic phase diagram becomes one dimensional in structure and dynamics. The isomorph theory, which is a consequence of HSI, forms the underpinning of excess entropy scaling [180]. The concept of universality is central to this work as it is in one form or another the goal of the various theories of the glass transition outlined in Chapter 1.

The motivation of this thesis is to explore ways to derive a description that shows true universality among different thermodynamic states and intermolecular interactions. The approach that is taken in this thesis differs from the path taken thus far – namely, to cast the structure and dynamics of the entire system comprising all the atoms/molecules into an equivalent system of hard spheres. Instead, a liquid system is portioned into a set of harmonic oscillators and a set of hard spheres. As shown in the next chapter, a true universality can be derived if only a subset of atoms/molecules in the liquid are considered to be hard spheres. While the partitioning concept itself is not new, this approach diverges from the conventional wisdom of considering a liquid to be dominated by repulsive forces.

Chapter 4:   Thermal Jamming Framework

A truly universal description of the wide range of liquid dynamics in terms of a single parameter has been viewed as a "holy grail" in the liquid physics community. As discussed in the previous chapter, various successful efforts of establishing quasi-universality among liquids using hard spheres and excess entropy representations evokes a suspicion that a universal description may not be entirely out of reach. As mentioned previously, the idea of using hard spheres as surrogates to capture the properties of realistic gases and liquids dates back to the seminal work of Van der Waals. It has long been accepted that fluid properties are dominated by repulsive forces and hard spheres provide the idealization of severe repulsion [37]. The quasi-universality that is brought out through hard sphere mapping and excess entropy scaling described in the previous chapter gives credence to this conjecture. Nevertheless, the observed scaling is not truly universal and significant exceptions are noted for a number of liquid systems [180].

In this chapter, we propose a method of establishing a true universal description of liquid dynamics by establishing separate partitions for the gas-like and solid-like behavior of liquids, which allows for the development of a description of the extent of thermal jamming in dense fluids such as supercooled liquids and glass forming liquids (GFLs). Unlike the traditional practice of considering the entire liquid state to be comprised of equivalent hard spheres, the current work posits that any liquid system can be regarded to be comprised of a set of hard spheres (HS) and a set of harmonic oscillators (HO). Thus, any property of the liquid system then becomes a weighted average of the contributions from hard spheres and harmonic oscillators. For properties such as diffusivity there is no contribution from harmonic oscillators by construction, while for extensive properties such as entropy there are contributions from both harmonic oscillators and hard spheres. With this partitioning, the attractive forces now have a contribution to the properties of the liquid state – a significant departure from the traditional viewpoint of dense liquids as approximated by a set of hard spheres.

The conceptualization treating a liquid as a superposition of two idealizations (HO and HS) is itself not new. The overarching challenge is to derive the weights for harmonic oscillators and hard spheres. We follow the Two Phase Thermodynamic (2PT) approach formulated by Lin,

Blanco, and Goddard (LBG) [187], and we adopt some of their terminology and notation in this work. To our knowledge LBG were the first to establish a quantitative method of partitioning a liquid into solid-like and gas-like components, and accurately predict the entropies and free energies of a number of liquids with very different atomic and molecular interactions [188-190]. However, the 2PT method was not formulated with the goal of demonstrating scaling of dynamical properties either within a single material nor among various materials, as the goal of LBG was to compute total absolute thermodynamic properties of liquids, and they did not dedicate effort to discerning the possible physical significance of the components of thermodynamic properties such as entropy that are associated with the hard sphere or harmonic oscillator partitions of the liquid. Here we reformulate the 2PT method to establish a framework for quantifying thermal jamming in glass-forming liquids.

Section 4.1   Partitioning Postulate

The central idea behind the establishment of this universal description of liquid dynamics, which allows for a demonstration of thermal jamming in supercooled liquids, is that a liquid state may be modeled as a superposition of a hard sphere and a harmonic oscillator. Depending on the thermodynamic or dynamic state of the liquid in question, it may be proportionally more solid-like than gas-like, or vice-versa. It stands to reason that a liquid very close to crystallization or the glass transition should have only a small contribution from the hard sphere component and its behavior will be predominately characterized by the harmonic oscillator partition.

Effuse gases can be very effectively modeled as hard spheres, as has been previously discussed. The thermodynamic and dynamic behavior of solids is also well-understood from a mathematical standpoint as a crystalline solid is well-modeled as a network of non-interacting quantum harmonic oscillators. We first establish the definition of the hard sphere partition of the liquid using a "partitioning metric" f, which is the ratio of atoms in the liquid that behave effectively as hard spheres (N_{HS}) to the total number of atoms in the liquid (N):

$$f \equiv \frac{N_{HS}}{N} \qquad (4.1.1)$$

In principle, there could be multiple ways to plausibly compute N_{HS} for a liquid. The calculation of the partitioning metric f is carried out by LBG in [187] somewhat heuristically by employing various relationships between the diffusion coefficient of the liquid and that of the hard sphere partition. In this work, the emphasis is placed on Equation 4.1.2 as the definition of f, which entails a general framework for computing f that need not rely on a diffusion-based approach at all – other transport coefficients such as viscosity or relaxation time could in principle be posited to derive an expression for f as well. We frame this discussion of partitioning a liquid by positing the following definition of the partitioning metric:

$$f \equiv \frac{1}{g(\sigma^+)} \qquad\qquad (4.1.2)$$

where $g(\sigma^+)$ is the value of the radial distribution function for a hard sphere system at the hard sphere diameter σ^{HS} approaching from the right. The numerical bounds of f are as follows: as $f \rightarrow 1$, the system is entirely fluidic, meaning that the system behavior is represented entirely by hard spheres (the system is an hard sphere gas); in the other limit, $f \rightarrow 0$ entails no partitioning and the hard sphere component represents none of the system's behavior (the system is a solid modeled as a set of harmonic oscillators).

The partitioning postulate is in fact a mathematical conclusion that arises from the assumptions used to derive f in the original 2PT method [187], but the explicit relationship between f and $g(\sigma^+)$ was seemingly missed by the authors. The postulate in Equation 4.1.2 is arbitrary but it can be rationalized in the following manner. The magnitude of $g(\sigma^+)$ is directly proportional to the coordination number of the hard spheres. In the limit $g(\sigma^+) \rightarrow \infty$, the coordination number of a random close-packed hard sphere system approaches a limiting value (of 6) [147], in which case the partitioning metric f approaches zero, meaning the system has no hard sphere (gas-like) component and has attained a solid state. As implied in [191], other functional forms may also be assumed but none is simpler than the relationship in Equation 4.1.2. From this cardinal assumption, the methodology used by LBG in the 2PT formulation, which involves hard sphere theory, Enskog theory and assumptions about the diffusivity of hard sphere systems in the limit of zero pressure, can be reproduced exactly.

With the partitioning approach, the liquid is deemed to have both solid-like (HO) and gas-like (HS) properties. Properties that depend on hopping across the potential energy basins such

as diffusivity and viscosity are exclusively dependent on the HS partitioning, while properties that rely solely on vibrations are attributed to the HO partition. Thermodynamic properties such as entropy and free energy that depend on both can then be written as a superposition of the HS and HO contributions.

One subset of atoms are considered mobile and thus the gas-like metrics can be normalized to the number of HS atoms (N_{HS}) or to the total number of atoms in the system (N). In this work, the normalized metrics with respect to the whole system are denoted with a "hat"; for example, number density of the HS partition, and the effective number density for the whole system are denoted by ρ and $\hat{\rho}$, respectively, with the functional relationship and $\hat{\rho} = f\rho$. Similarly, the volume fractions can be written as ϕ and $\hat{\phi}$, respectively, which satisfies $\hat{\phi} = f\phi$. More generally, all HS metrics follow this relationship; the effective system properties are the experimental observables, while the HS partition simply refers to an idealized subset of hard spheres. Therefore, the physical limits are satisfied by the effective system metrics. As an example, the upper limit of the effective volume fraction is bounded by the relation $\hat{\phi} \leq 1$ while ϕ itself is not, since the partitioning metric f is bounded by $0 < f \leq 1$. The key formulations of the 2PT Method which follow from the relation $f = g(\sigma^+)^{-1}$ are discussed below.

Section 4.2   Diffusion Relationships

The Enskog theory for dense gases relates the diffusion coefficient of a hard sphere system in the limit of zero pressure to its diffusion coefficient at nonzero pressure by the relationship [37]

$$D^{HS}(T,\rho) = \frac{D^{HS}_{P=0}(T,\rho)}{g(\sigma^+)} \tag{4.2.1}$$

Thus, the direct consequence of the assumption in Equation 4.1.2 is that the partitioning metric relates these diffusivities according to

$$D^{HS}(T,\rho) = fD^{HS}_{P=0}(T,\rho) \tag{4.2.2}$$

The original 2PT formulation by LBG listed the above relationship as a postulate [187]. With the fundamental relationship provided in Equations 4.1.2, and the Enskog result, the partition metric f can be written as

$$f = \frac{D^{HS}(T, f\rho)}{D_0^{HS}(T, f\rho)} = \frac{D^{HS}(T, \rho)}{D_0^{HS}(T, \rho)}$$

(4.2.5)

Above, the subscript refers to the zero pressure condition ($P = 0$). Note that the partition metric connects two diffusivities at the same states (ρ or $f\rho$). The Chapman and Enskog solution gives a theoretical expression for zero pressure diffusivity, which can be stated as [85]

$$D_0^{HS}(T, \rho) = \frac{3}{8} \frac{1}{\rho \sigma_{HS}^2} \left(\frac{k_B T}{\pi m} \right)^{\frac{1}{2}}$$

$$D_0^{HS}(T, f\rho) = \frac{3}{8} \frac{1}{(f\rho) \sigma_{HS}^2} \left(\frac{k_B T}{\pi m} \right)^{\frac{1}{2}}$$

(4.2.6)

where m is the mass of the system. Now the partition metric can be connected to the same diffusivity but at two different states as

$$f = \frac{D_0^{HS}(T, \rho)}{D_0^{HS}(T, f\rho)}$$

(4.2.7)

Implicit in the above relation is the assumption that the HS diameter σ_{HS} is invariant to changes in density. It will be shown later that this is indeed a reasonable assumption. Substituting the above equation in Equation 4.2.5, the following expression can be derived

$$D^{HS}(T, f\rho) = D_0^{HS}(T, \rho)$$

(4.2.8)

The above is an example of thermodynamic scaling relationship; it states that the HS diffusivity at a density of $f\rho$ (finite pressure) is exactly equal to the zero-pressure HS diffusivity at another density ρ (scale factor is unity). Note that $D^{HS}(T, \rho)$ is identically equal to the diffusivity of the system $D(T, \rho)$ by construct since there is no diffusion contribution from the HP partition. Thus the following relationships are also true by construct.

$$f = \frac{D(T, \rho)}{D_0^{HS}(T, \rho)} = \frac{D(T, \rho)}{D^{HS}(T, f\rho)}$$

(4.2.9)

The system diffusivity can be non-dimensionalized from the kinetic theory.

61

$$\Delta = \left(\frac{8}{3}\right)\left(\frac{\pi m}{k_B T}\right)^{\frac{1}{2}} \rho^{\frac{1}{3}}\left(\frac{6}{\pi}\right)^{\frac{2}{3}} D(T,\rho) \tag{4.2.10}$$

Although not noted by LBG in their original work [187], the above form, except for the constants, is virtually identical to the form that of the scaling relationship that is required for probing universal scaling behavior. The system diffusivity is also expressible in terms of zero-time vibrational density of states $G(0)$. The functional form is given by

$$G(0) = \frac{12mN}{k_B T} D(T,\rho) \tag{4.2.11}$$

Now the non-dimensional diffusivity can be recast in terms of the number of atoms N

$$\Delta = \frac{2G(0)}{9N}\left(\frac{\pi k_B T}{m}\right)^{\frac{1}{2}} \rho^{\frac{1}{3}}\left(\frac{6}{\pi}\right)^{\frac{2}{3}} \tag{4.2.12}$$

One advantage of the above form is that the system diffusivity $D(T,\rho)$ (and the non-dimensional diffusivity Δ) can be evaluated from atomistic simulations. It can either be computed using the mean-square-displacement or through the Fourier transform of the velocity autocorrelation function that gives the zero-frequency density of states [85]. Equation 4.2.10 allows a further reduction to connect Δ and the partitioning function. First Δ can be written as

$$\Delta = \left(\frac{6}{\pi}\right)^{\frac{2}{3}} \rho^{\frac{-2}{3}} \frac{1}{\sigma_{HS}^2}\left(\frac{\pi m}{k_B T}\right)^{\frac{1}{2}} \frac{D(T,\rho)}{D_0^{HS}(T,\rho)} \tag{4.2.13}$$

$$\Delta = \left(\frac{6}{\pi}\right)^{\frac{2}{3}} \rho^{\frac{-2}{3}} \frac{1}{\sigma_{HS}^2}\left(\frac{\pi m}{k_B T}\right)^{\frac{1}{2}} f \tag{4.2.14}$$

The above equation connects the non-dimensional diffusivity and the partitioning metric. Noting the definition for the effective packing fraction , $\hat{\phi} \equiv f\phi = \frac{N_{HS}\phi}{N} = \left(\frac{\pi}{6}\right)(f\rho)\sigma_{HS}^3$, Equation 4.2.14 now reduces to a simple relationship given by

$$f = \Delta^{3/5}\hat{\phi}^{2/5} \tag{4.2.15}$$

For a given system, the reduced diffusivity is determined by $D(T,\rho)$ and the material properties that are known. The above equation indicates that for a given state, there is a one-to-one

correspondence between the effective packing fraction and the partitioning metric f. Both the effective packing fraction $\hat{\phi}$ and f are unknowns at this stage.

Section 4.3 Incorporation of Hard Sphere Equations of State

As discussed in Chapter 2, the compressibility $Z(\hat{\phi})$ can also be related to the radial distribution function at contact $g(\sigma^+)$; it is given by [85]

$$Z(\hat{\phi}) = 1 + 4\hat{\phi}g(\sigma^+) \tag{4.3.16}$$

Note that the effective volume fraction $f\phi = N_{HS}\phi/N$ is denoted by $\hat{\phi}$. Rearranging this expression and using the definition of f as exactly equal to $g^{-1}(\sigma^+)$, the following relationship is then obtained:

$$f = \frac{4\hat{\phi}}{Z(\hat{\phi}) - 1} \tag{4.3.17}$$

An accurate equation of state is now needed to proceed. The Carnahan and Starling (CS) [149] equation of state is accurate for the stable fluid branch as noted in Chapter 2; the radial distribution function at contact and compressibility are expressed as

$$g(\sigma^+) = \frac{1 - \dfrac{\hat{\phi}}{2}}{(1 - \hat{\phi})^3} \tag{4.3.18}$$

$$Z(\hat{\phi}) = \frac{1 + \hat{\phi} + \hat{\phi}^2 - \hat{\phi}^3}{(1 - \hat{\phi})^3} \tag{4.3.19}$$

Using the CS equation of state the following relationship can be established.

$$\frac{2\left(1 - \hat{\phi}\right)^3}{2 - \hat{\phi}} - f = 0 \tag{4.3.20}$$

The above equation together with $f = \Delta^{\frac{3}{5}}\hat{\phi}^{\frac{2}{5}}$ can now be solved iteratively for $\hat{\phi}$ and the partition metric f. Thus, the HS partition can be uniquely determined using the partition postulate, the

Enskog expression for diffusivity, and an appropriate equation of state along with the non-dimensional diffusivity. Note that the original equations derived by LBG [187] are completely equivalent to the results shown here.

The inadequacies of the Carnahan-Starling EoS for dense hard spheres, as described in Chapter 2, makes it unsuitable for use in the dense GFLs studied in this work. As discussed earlier, the equations of state proposed by Speedy [151, 152], Odriozola-Berthier (O-B) [136], and Liu [165] are more apposite for GFLs since they are accurate in the metastable fluid branch. The semi-empirical equation of state developed by Speedy [151, 152] accurately predicts the compressibility in the metastable fluid branch of the hard sphere phase diagram [153]. A drawback of the Speedy equation is that it breaks down for the lower-density, isotropic liquid branch of hard spheres for which the CS equation is accurate. Another equation of state developed by Odriozola and Berthier [136] has the same mathematical form as Speedy's equation with parameters that differ slightly to reflect its basis on arguments from free-volume theory. As noted below, the two equations of state have the same mathematical structure; the Speedy and O-B equations are given by

$$Z_{S,O-B}(\hat{\phi}) = \frac{d}{1 - \dfrac{\hat{\phi}}{\phi_c}} \tag{4.3.21}$$

For the Speedy equation, $d = 2.67$ and $\phi_c = 0.6448088$. For the Berthier equation, $d = 2.82$ and $\phi_c = 0.669$. These parameters are also provided in Table 4-0-1. Note that for both equations $\phi_c \sim \phi_{RCP} \sim 0.64$. Since neither equation predicts valid compressibility values for low density hard spheres, the Carnahan-Starling equation is used in this work to compute $\hat{\phi}$ for effective packing fractions $\hat{\phi} < 0.30$. As noted earlier, the Liu EoS agrees with the numerical hard sphere compressibility data in the densest limit [165] more closely than both the Speedy and Odriozola-Berthier equations. Additionally, Liu's EoS is applicable along the stable fluid branch. These equations of states are chosen in this work as they are either functionally simple and reasonably accurate (Speedy, Odriozola-Berthier), or highly accurate (Liu). Using Equation 4.3.21 and the general expression $f = \Delta^{\frac{3}{5}}\hat{\phi}^{\frac{2}{5}}$ yields

$$\Delta^{\frac{3}{5}}\left[(d-1)\hat{\phi}^{\frac{2}{5}} + \frac{\hat{\phi}^{\frac{7}{5}}}{\phi_c}\right] - 4\left(\hat{\phi} + \frac{\hat{\phi}^2}{\phi_c}\right) = 0 \tag{4.3.22}$$

As before, this expression can be solved numerically to obtain $\hat{\phi}$ in terms of the dimensionless diffusivity for both Speedy and Odriozola-Berthier equations of state.

Table 4-0-1:   Parameters for the Speedy [151, 152] and Odriozola-Berthier [136] hard sphere equations of state.

Parameter	Speedy	Berthier
d	2.67	2.82
ϕ_c	0.648088	0.669

While mathematically more complex than the Speedy/O-B form, Liu's equation predicts the entire range of compressibilities in both the isotropic liquid and metastable fluid branches of the hard sphere phase diagram with high accuracy [164, 165]. Of special note is the pole introduced in Liu's equation at approximately $\phi_c = 0.63558$ that produces an additional asymptotic branch that encompasses the isotropic fluid branch leading to the stable packing configuration of the FCC lattice near the limit ϕ_{FCC}. Liu's equation is given by

$$Z_{Liu}(\hat{\phi}) = Z_V + \frac{A\hat{\phi}}{1-B\hat{\phi}} + C\hat{\phi}^{40} - D\hat{\phi}^{42} + E\hat{\phi}^{44}$$

$$Z_V(\hat{\phi}) = 1 + \left(\frac{V_1\hat{\phi}}{1-V_2\hat{\phi} + V_3\hat{\phi}^2 - V_4\hat{\phi}^3 - V_5\hat{\phi}^4}\right) \tag{4.3.23}$$

The coefficients for Liu's equation are provided in Table 2-2.

In this work, the solutions of the packing fraction $\hat{\phi}$ are limited to values less than $\phi_c = 0.63558$ with Liu's equation of state. Proceeding in the same way as was done for the Speedy form, the packing fraction can be solved for using the expression.

$$0 = \Delta^{\frac{3}{5}}\left[\frac{V_1\hat{\phi}^{\frac{2}{5}}}{1-V_2\hat{\phi}+V_3\hat{\phi}^2 - V_4\phi^3 - V_5\hat{\phi}^4} + \frac{A\hat{\phi}^{\frac{2}{5}}}{1-B\hat{\phi}} + C\hat{\phi}^{39.4} - D\hat{\phi}^{41.4} + E\hat{\phi}^{43.4}\right] - 4 \tag{4.3.24}$$

The three significant parameters involved in the Hard Sphere Partitioning method, the dimensionless diffusivity Δ, the partitioning metric f, and the effective packing fraction of the hard sphere partition $\hat{\phi}$, are all mathematically related; that is, there is a one-to-one correspondence between Δ, f, and $\hat{\phi}$. This relationship is depicted in Figure 4-1 for the Speedy, Odriozola-Berthier, and Liu equations of state.
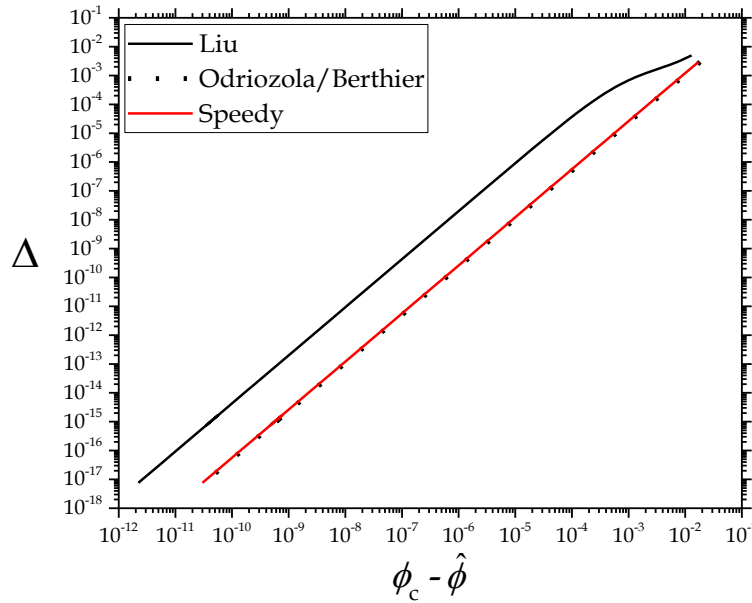
Figure 4-1: The power-law variation of the dimensionless diffusivity with $\phi_c - \hat{\phi}$ obtained using the Speedy [151, 152], Odriozola-Berthier [136], and Liu EoS [164, 165]. Standard reduced units are used for this calculation. At large Δ, Liu's EoS approaches the other two EoS, and exhibits a different power-law exponent at smaller Δ. Above approximately $\Delta = 10^{-1}$, the Speedy and Odriozola/Berthier EoS cannot be solved; in this work, the Carnahan-Starling EoS is used for these larger values of Δ.

Interestingly, a strict power-law relationship is observed between the partitioning metric and dimensionless diffusivity as a function of $\phi_c - \hat{\phi}$ for a wide range of Δ for the Speedy and Odriozola-Berthier EoS. For the Liu EoS, power-law variation is observed except at larger values of $\hat{\phi}$. The Speedy and Odriozola-Berthier results are virtually identical, which is not surprising. Fits of a power law of the form $\Delta = A(\phi_c - \hat{\phi})^B$ gives $B_{Speedy} = 1.66503$ and $B_{Liu} = 1.66212$; the

exponent for Odriozola-Berthier EOS is virtually the same. These power-law exponents are intriguingly close to 5/3 for all the equations of state. Generally-speaking, power-law variation seen in physical processes indicates, among many possibilities, invariance of time or length scales, self-similarity, and self-organizing critical behavior [192].

The difference in these EoS revealed by this power-law variation with $\phi_c - \hat{\phi}$ is worth consideration in and of itself; the practitioners who devised these equations of state primarily had in mind an empirical agreement with available compressibility data for hard spheres. The Speedy and Odriozola-Berthier equations of state are based on the well-known free volume form, but Liu's EoS is more complicated and involves parameters of such extreme magnitude that it can only be reasonably viewed as a highly-detailed fitting function, although parts of it are based on previously-established functional forms for hard sphere EoS. The hard sphere compressibility data in the literature has not been obtained for values of ϕ nearly as close to ϕ_c as depicted in Figure 4-2. Likely no attention has been given to the behavior of these EoS so far along in their asymptotic approaches to ϕ_c. Through this analysis, the power law exponents are observed to be close to 5/3.

It is instructive to compare the accuracy of the equations of states. In Figure 4-2, the predictions of the partitioning metric $f = g(\sigma^+)^{-1}$ is compared to simulation data of hard spheres. As expected, the Speedy and Liu equations of state match the simulation data significantly better than the "workhorse" Carnahan-Starling equation of state, and the choice of these equations of state are appropriate for glass formers. This result does not show the validity of the Hard Sphere Partitioning approach, but it underscores the appropriateness of the equations of states for the metastable fluid branch. Therefore, with these equations of state the Hard Sphere Partitioning method is well-equipped for probing supercooled liquids and GFLs.
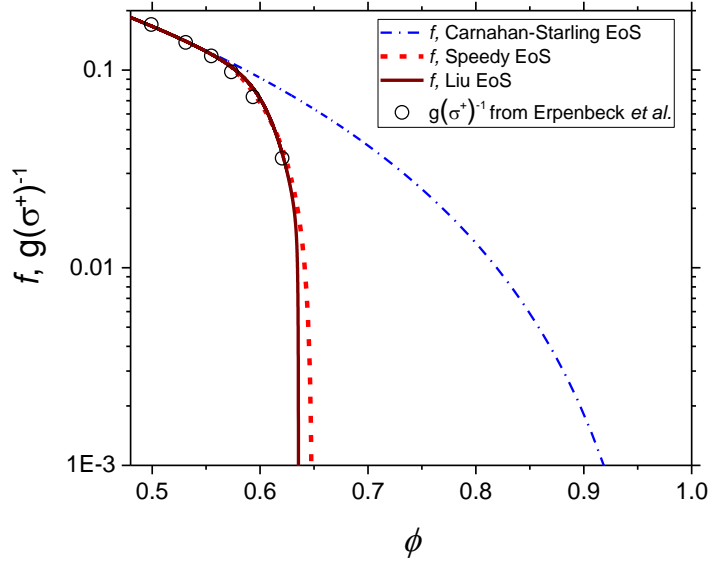
Figure 4-2:   The circles show data from Erpenbeck, *et al.*, representing $g(\sigma^+)^{-1}$ obtained from computer simulations of hard spheres [193] [164, 165]. Standard reduced units are used for this calculation. The Speedy and Liu equations of state bend towards $f = 0$ before the CS EoS and attain their maximal values near ϕ_c, and match very well with the numerical compressibility data.

Section 4.4   Entropy and Limiting Compressibility

With the HS and HO partition, the entropies and free energy can be calculated as a superposition of each component. Calculation of these properties is outlined in the original LBG reference [187]. In this work the property of interest is entropy, particularly the excess entropy relative to the ideal gas contribution; as outlined in the 2PT method, other properties such as total energy (which may include quantum corrections), free energy, and specific heat may be computed. As previously discussed, there excess entropy of relevance is given by

$$s^{ex} = s_{liq} - s_{IG} \tag{4.4.25}$$

Note the smaller case s denotes entropy per HS atom; the entropy normalized to the system is depicted by the larger case S, with the relationship $S = fs$. In the 2PT approach, the liquid entropy is given by

$$s_{liq} = s_{HS} + s_{HO} \tag{4.4.26}$$

Thus $s^{ex} = s_{HS} + s_{HO} - s_{IG}$. The 2PT method allows the calculation of the HO contribution to the entropy. This is possible when the Hamiltonian is known a priori. For experimental GFLs, the HO portion is not readily calculable. Hence, we define another measure for the excess entropy as the difference between the HS entropy and the ideal gas entropy. It is given by

$$s^{EXC} = s_{HS} - s_{IG} \tag{4.4.27}$$

The above measure is typically used in past work [146, 151, 152] and can be easily computed once the HS partition is known.

$$\frac{s^{EXC}}{k_B} = -\int_0^{\hat{\phi}} \left(\frac{Z(\phi') - 1}{\phi'} \right) d\phi' \tag{4.4.28}$$

where $\hat{\phi}$ is the effective packing fraction of the hard sphere partition and Z is the hard sphere compressibility. The excess entropy is thus dependent on the choice of the hard sphere equation of state (EoS). The excess entropy is of critical importance in this work as it can be directly related to the dimensionless diffusivity to demonstrate EES (or lack thereof). The ideal gas entropy s^{IG} is computed for the hard sphere partition containing N_{HS} hard sphere atoms at density $f\rho$:

$$\frac{s^{IG}}{k_B} = \frac{5}{2} + \ln \left[\left(\frac{2\pi m k_B T}{h^2} \right)^{\frac{3}{2}} \left(\frac{1}{f\rho} \right) \right] \tag{4.4.29}$$

The above expression has an important caveat in that the value of Planck's constant h in reduced units is not unique when applied to model liquids where explicit unit conversions to physical units are not applicable. A method of accounting for this difficulty for model GFLs is discussed in Chapter 7.

Like the entropy, the system compressibility can be expressed as fZ; an implicit assumption here is that the solid phase modeled as harmonic oscillators is incompressible. Interestingly, the system compressibility converges to a limiting value when f tends to zero. This can be easily verified by taking the following limit:

$$fZ(\hat{\phi})_{\lim f \to 0} = \left(f + 4\hat{\phi} \right)_{\lim f \to 0} = 4\hat{\phi}_c \tag{4.4.30}$$

Given that the effective packing fraction asymptotically converges to a $\phi_{RCP} \sim 0.64$, the limiting value of system compressibility is $\sim 4\phi_{RCP} = 2.56$.

Section 4.5   Thermal Jamming

The hard sphere partitioning (HSP) method is devised to provide an unambiguous jamming metric to liquids in the supercooled states. The HSP approach presumes jamming *a priori* and provides the jamming metrics as the liquid traverses into the deeply supercooled states. Since jamming progresses at finite temperatures, in contrast to static jamming, we call the jamming phenomenon in glass formers and supercooled liquids "thermal jamming."

The effective packing fraction $\hat{\phi}$ of the hard sphere partition of the liquid established by the HSP approach provides the extent of thermal jamming in the liquids in the supercooled states. When diffusivity of the liquid approaches zero, the partitioning metric $f \equiv N_{HS}/N$ also approaches zero and $\hat{\phi}$ approaches the critical packing fraction ϕ_c, which is close to the random-close-packed value ϕ_{RCP}. In general, the value depends on the choice of the hard sphere equation of state applied in the HSP approach. According to the Hard Sphere Paradigm, the dynamics of simple liquids is well-described by association with the reference hard sphere system, and according to one of the prevailing notions, the hard sphere fluid on the metastable branch undergoes a glass transition when the packing fraction approaches ϕ_{RCP}. In the HSP approach, we adopt this axiom but additionally incorporate an important caveat – only a subset of the atoms, as determined by the partitioning metric f, experiences the compressibility divergence. The partitioning metric, however, is expected to smoothly approach zero without exhibiting a discontinuity. Both the effective packing fraction and the partitioning metric are universally related for all glass forming liquids and supercooled liquids through the relation $f = \Delta^{\frac{3}{5}} \hat{\phi}^{\frac{2}{5}}$, where Δ is the non-dimensional diffusivity.

The HSP approach also provides a method of establishing a universal description of liquid dynamics that is capable of spanning the entire range of liquid dynamics. The form of the non-dimensional diffusivity, which is determined from the kinetic theory of gases, is most appropriate

for inquiry into any universal scaling relationships with effective packing fractions or excess entropy.

As will be shown in Chapter 7, the HSP analysis can be performed on real glass formers all the way to glass transition temperature and below. A divergence in the pressure or compressibility of the HS partition occurs as $\hat{\phi} \rightarrow \phi_c$. However, the divergence is not postulated to occur at a specific thermodynamic state. Thus, there is no unique glass transition temperature or pressure in this approach, by construct. However, as shown in Chapter 7, the analysis of eight glass formers shows that non-dimensional diffusivity, the partitioning metric, compressibility, and excess entropy all tend to converge to specific values at the traditional laboratory glass transition temperature.

In the HSP model, the dynamics becomes sluggish because the number of the participating diffusive (HS) atoms decreases precipitously on cooling. Relative to the existing theories, the HSP approach appears to be closest to the dynamic facilitation (DF) theory [117], although no formal correspondence is attempted in this work. No length scales are also identified in this approach although such metrics can possibly be constructed from the reduction of the HS atoms with decreasing temperature.

The HSP approach most importantly reveals an important attribute of liquids that seems to present a conflict with the seminal Van der Waals conception of liquids that are dominated by repulsive interactions among atoms. Numerous studies of simple liquids using the 2PT method, upon with the HSP approach is based, have indicated that the partitioning metric f for these liquids is not large, typically in the vicinity of 30-40%, meaning that 60-70% of the liquid's dynamics is better modeled by a system of harmonic oscillators than by hard spheres. For the molecular GFLs studied in this work, f is significantly smaller than what is observed for simple liquids (see results in Chapter 7). As harmonic oscillators are characterized by attractive interactions as opposed to repulsive interactions, the calculation of f suggests that liquid behavior is dominated by solid-like vibrational modes instead of gas-like diffusion. From at least a practical standpoint, the HSP approach predicts that liquid thermodynamics is better described by association of the liquid with solid-like vibrations in conjunction with HS gas-like diffusion.

Chapter 5: Atomistic Simulation of Supercooled Liquids

Atomistic simulations, or more generally, Molecular Dynamics (MD) simulations allows for the quantitative study of a wide range of materials at the atomic level. So-called *ab initio* MD simulations, which are often based on the Density Functional Theory (DFT), can give better interatomic forces because electronic interactions are explicitly modeled. Classical MD, however, uses empirical interatomic potentials; if finely tuned, these potentials are excellent surrogates for real-world interatomic interactions. Both *ab initio* MD and classical MD use Newton's laws to compute the atomic positions. The earliest attempts at direct simulation of atomistic motion were carried out by Rahman [194] and Alder and Wainwright [195] in the 1960s on the rudimentary computers that existed at the time. Today, the rapidly increasing access to computational resources has expanded the scope of problems that may be addressed by MD. The most significant shortcomings of MD – namely, that only relatively short times scales of hundreds of nanoseconds, and relatively short length scales on the order of hundreds of nanometers, may be accessed even with the fastest computational hardware – are unlikely to be addressed in the near future. Still, the success of MD in reproducing dynamical and thermodynamic characteristics of materials has kept MD in the forefront of research in statistical mechanics and the physics of liquids [196-198].

The ease or difficulty of simulating a given material by MD is dependent on several factors, such as the number of atomic species, the range and complexity of interatomic interactions, or the size of the system needed to accurately compute the desired data. Molecular interactions are modeled using interatomic potentials between atoms, for which the corresponding interatomic force may be computed. For each atom in the system, the sum of the forces exerted on it by its neighboring atoms is computed, which provides the net instantaneous acceleration on that atom [199]. Then, a numerical algorithm is used to integrate Newton's equations of motion to obtain the instantaneous velocity of each atom, and the system is finally evolved forward in time by a suitably small time step, chosen to minimize numeric error in the integration algorithm [199].

Monte Carlo methods are sometimes used in conjunction with MD simulations [200]. After an initial configuration of atoms is provided, MC randomly provide small displacements to

the atoms. Acceptance of the displacements evolves the system to the "inherent structures" or the local minima in the potential energy surface [82]. MC methods are used in the midst of an MD simulation if energy minimization is required. Other MD methods use coarse-graining where interactions are averaged over relatively large regions of the system [201, 202]. These methods allow for the study of systems of significantly larger sizes than with traditional MD, and can possibly serve as a good intermediary between the atomic scales of MD and those of the continuum simulations commonly performed in engineering and science.

Section 5.1   Fundamentals of Molecular Dynamics

For a many body system, Newton's equations of motion cannot be solved exactly and thus require solutions to be obtained using numeric integration methods. To proceed with the integration, the instantaneous acceleration $\mathbf{a}_i$ on an atom i is computed using the instantaneous force exerted on that atom by each neighboring atom j (assuming pairwise interaction) as shown below,

$$\mathbf{F}_i = \sum_{i \neq j} \mathbf{F}_{ij} \tag{5.1.1}$$

and dividing by the mass of atom i. The instantaneous force is computed from the system potential energy U as

$$\mathbf{F}_i = -\nabla_i U \equiv -\frac{\partial U}{\partial \mathbf{r}_i} \tag{5.1.2}$$

The interatomic potentials for the systems used in this work are described in the next section, and in Appendix A; only pairwise interactions are considered here. One of the most commonly-used integration algorithms is the leapfrog method [199], which is a second-order method that is computationally-cheap. It also belongs to the family of symplectic integrators that portray excellent long-time energy conservation. The leapfrog algorithm is typically formulated as a two-step process, where the velocity at a half step is computed, and then used to compute the position at the full step. The first half step is given by

$$\mathbf{v}_{j+\frac{1}{2}} = \mathbf{v}_j + \mathbf{a}_j \frac{\Delta t}{2} \qquad (5.1.3)$$

where Δt is a simulation time step chosen to be suitably small so that numeric error in the integration is negligible. The second step then involves the following.

$$\mathbf{x}_{j+1} = \mathbf{a}_j + \mathbf{v}_{j+\frac{1}{2}} \Delta t$$

$$\mathbf{v}_{j+1} = \mathbf{v}_{j+\frac{1}{2}} + \mathbf{a}_{j+1} \frac{\Delta t}{2} \qquad (5.1.4)$$

The above process is then repeated for all atoms in the system. After a sufficiently long equilibration period, the MD system can attain a state of thermodynamic equilibrium during which the pertinent thermodynamic properties can be computed. Various states of thermodynamic equilibrium are described using statistical ensembles. A given property A is computed as an average over all possible states in an ensemble. As an example, the property A in a canonical ensemble can be computed as

$$\langle A \rangle = \frac{\int A(\mathbf{r}_1 ... \mathbf{r}_N) e^{-U(\mathbf{r}_1 ... \mathbf{r}_N)/(k_B T)} d\mathbf{r}_1 ... d\mathbf{r}_N}{\int e^{-U(\mathbf{r}_1 ... \mathbf{r}_N)/(k_B T)} d\mathbf{r}_1 ... d\mathbf{r}_N} \qquad (5.1.5)$$

In this work two ensembles are used: the *micro-canonical* ensemble where the total energy, volume, and number of atoms are held constant (NVE), and the *canonical* ensemble where the temperature, volume, and number of atoms are held constant (NVT). In a MD simulation, the properties are time averaged rather than ensemble-averaged. The ergodic hypothesis, however, states that a given property computed over a large number of ensembles is equivalent to the average value over a number M of independent measurements that are temporally separated [199] as shown below.

$$\langle A \rangle_{Time} = \frac{1}{M} \sum_{x=1}^{M} A_x \qquad (5.1.6)$$

The direct integration of Newton's equations of motion in a system where periodic boundary conditions are used (as is the case with all simulations conducted in this work) naturally results in a system that exists in the microcanonical (NVE) ensemble – no atoms are added or removed, the volume of the system does not change and the total energy of the system remains sensibility

constant. For this reason, all thermodynamic properties are measured in the NVE ensemble in this work. The canonical (NVT) ensemble can be simulated by invoking a method of controlling the temperature, which is equivalent to coupling the system to a heat bath. For this work, the crude but effective method of velocity rescaling is used, wherein the velocities of all atoms in the system are periodically rescaled by a constant factor so that the desired temperature is achieved. The rescaling approach does not strictly generate a NVT ensemble but it is very effective for controlling the temperature. For the systems studied in this thesis, rescaling is employed only during the equilibration period during which it is ensured that the simulation has attained a sufficiently ergodic state at the desired thermodynamic state. After the equilibration period, velocity rescaling is turned off and all the equilibrium properties are measured in the NVE ensemble.

Another crucial characteristic of a MD simulation is the use of periodic boundary conditions (PBC) for mimicking an infinitely large system. Under PBC, the spatial limits of the system are defined (usually a parallelepiped box), and atoms that wander beyond the boundary limits are wrapped around to appear on the other side of the simulation boundary. For example, if the system boundary is a square box of side length L, with one corner beginning at the origin of the coordinate axis, and the box extending along the axes such that all x, y, and z coordinates are always positive, then an atom whose x-coordinate exceeds L at a certain time step will have its x-coordinate decreased by a linear shift of $-L$ before the potential is computed at the next time step. No linear modification is necessary for the other two directions if they do not exceed L. The use of PBC mimics the effect of a larger system than what is technically defined in the simulation boundary, as the force/potential energy calculation may be applied over the periodic boundaries where atoms interact with the "images" of atoms that are on the other side of the nearest boundary. It is not necessary to extend the interaction range to more than one periodic image; this is called the minimum-image convention [199]. Creative use of periodic boundaries can allow for interesting simulations, such as the study of surface effects by removing the periodicity in one spatial dimension.

Section 5.2   Model Supercooled Liquids

Realistic glass-forming liquids such as silica (SiO_2) have long been studied using MD, but the short time scales of MD mean that realistic cooling rates used in laboratory experiments, which may be as high as several tens of thousands of Kelvin per second, are in fact too slow to be simulated reasonably by MD. Thus, in MD simulations, extremely high cooling rates on the order of 10^{12} to 10^{15} K/s are sometimes used to keep the total simulation time within reason, which many have argued eliminates a significant amount of utility from simulations of realistic glass-formers. For this reason, practitioners in the glass community frequently use model systems to replicate glassy liquid behavior. These systems have advantages over realistic potentials such as those for silica in that they often have short interaction ranges, mathematically-simple expressions for their potentials that involve a smaller number of discrete calculations to evaluate, and model systems can even replicate glassy dynamics without the need for explicit supercooling. Model systems that don't require explicit quenching typically are multicomponent and have their interatomic potential parameters adjusted so that crystallization is geometrically difficult or impossible to achieve, even at low temperatures. Several model systems such as Kob-Andersen (KA) [111], Weeks-Chandler-Andersen (WCA) [203, 204], harmonic springs (HARM) [59] and Dzugutov [205, 206] are reported in the literature In this work, four model supercooled liquids are featured. The important crossover temperatures are listed in Table 5-1. In all simulations of the model systems, standard reduced units are used [199]. Note that the Dzugutov potential is only used for the string analysis in Chapter 6, and not for the HSP analysis in Chapter 7.

Table 5-1:   Crossover temperatures for the four model supercooled liquids [59].

Model System	T_c	T_S	T_O
Kob-Andersen (KA)	0.42-0.43	0.55-0.60	0.7 - 0.95
Weeks-Chandler-Andersen (WCA)	0.28	0.40 – 0.45	0.60 – 0.95
Harmonic Springs (HARM)	5.1 – 5.6	9.0 – 10.0	11.0 – 14.0
Dzugutov	0.42 - 0.43	0.7 - 0.8	1.0

Kob-Andersen (KA) [111]: this could perhaps be considered the workhorse potential for modeling supercooled liquid behavior. It is a binary system and it has been studied extensively for moe than two decades. The potential is given by the well-known "12-6" Lennard-Jones form

$$U_{\alpha\beta}^{KA}(r) = 4\varepsilon_{\alpha\beta}\left(\left(\frac{\sigma_{\alpha\beta}}{r}\right)^{12} - \left(\frac{\sigma_{\alpha\beta}}{r}\right)^{6}\right) \tag{5.2.1}$$

where α and β denote one of the two atomic species. The first term is repulsive for small values of r, and the second term is attractive. Values of the potential parameters $\epsilon_{\alpha\beta}$, which corresponds to the energy scale, and $\sigma_{\alpha\beta}$, which corresponds to approximately the ionic diameter and thus a pertinent length scale, are provided in Table 5-2. The KA system also features a disparity between the mole fraction of the two species, with 80% of the atoms being Type A and 20% being Type B. The skewed composition of the system and ionic diameters of the atoms act as inhibiting factors for crystallization.

Table 5-2:   Potential parameters of the Kob-Andersen potential [111].

Kob-Andersen Potential

σ_{AA}	1.0		ϵ_{AA}	1.0
σ_{BB}	0.88		ϵ_{BB}	0.5
σ_{AB}	0.8		ϵ_{AB}	1.5

Weeks-Chandler-Andersen (WCA) Potential [203, 204]: a potential predates the KA potential; it has the same form as the KA potential, except it is shifted upwards by a factor of $4\epsilon_{\alpha\beta}$ and truncated so that $U(r_{cutoff}) = 0$ which occurs at a distance of $2^{\frac{1}{6}}\sigma_{\alpha\beta}$. This turns the attractive-repulsive KA potential into a solely repulsive potential, also referred to as a soft sphere potential. Different variations of the WCA potential exist, using various potential parameters and masses for the atoms; we choose to use the same potential parameters as the KA system.

Table 5-3: Potential parameters of the Weeks-Chandler-Andersen potential [203].

Weeks-Chandler-Andersen Potential

σ_{AA}	1.0		ϵ_{AA}	1.0
σ_{BB}	0.88		ϵ_{BB}	0.5
σ_{AB}	0.8		ϵ_{AB}	1.5

Harmonic Sphere (HARM) Potential [59]: this is a computationally "cheap" potential that features a short interaction range and simple functional form, which is also a binary soft sphere potential. It is given by

$$U_{\alpha\beta}^{HARM}(r) = \frac{1}{2}\left(1 - \frac{r}{\sigma_{\alpha\beta}}\right)^2 \qquad (5.2.2)$$

Commonly, the HARM potential features a 50:50 ratio of atom species, with differing ionic diameters. Additionally, it has been found that finite size effects are not evident for system sizes as small as 1000 atoms [160]. Finite size effects refer to variations in properties such as potential energy, or variations in dynamical characteristics of atoms that occur when the length scales of the relevant physical processes exceed the width of the simulation cell.

Table 5-4: Potential parameters of the HARM potential [59].

HARM Potential

σ_{AA}	1.0		ϵ_{AA}	1.0
σ_{BB}	1.4		ϵ_{BB}	1.0
σ_{AB}	1.2		ϵ_{AB}	1.0

Dzugutov Potential [205, 206]: a monoatomic potential with a non-physical "hump" added in the potential function near the first nearest neighbor distance as indicated by the radial distribution function. The potential function is

$$
\begin{aligned}
V(r) &= V_1(t) + V_2(r) \\
V_1(r) &= A(r^{-m} - B)\exp\left(\frac{c}{r-a}\right) \quad && r < a \\
V_1(r) &= 0 \quad && r \geq a \\
V_2(r) &= B\exp\left(\frac{d}{r-b}\right) \quad && r < b \\
V_2(r) &= 0 \quad && r \geq a
\end{aligned}
\tag{5.2.3}
$$

This system does require explicit quenching to produce glassy behavior. A drawback of this system is its tendency to form quasicrystals, which are complex crystal structures that tend to exhibit their crystalline order in directions that are skewed from the normal Cartesian axes. This becomes evident in the simulations as the potential energy tends to drop in "steps", indicating that portions of the simulation cell are undergoing a quasi-crystalline transformation.

Table 5-5:   Potential parameters of the Dzugutov potential [205].

Dzugutov Potential

A	5.82		c	1.1
B	1.28		d	0.27
a	1.87		m	16
b	1.94			

The simulation of supercooled liquids can be more difficult in many respects than the simulation of low-density "well-behaved" liquids, or crystalline solids. They can be metastable because depending on the initial conditions of the simulation the liquid will attempt to explore a relatively large sample of configuration space, and time scales significantly longer than those allowed by current computer hardware may be necessary to achieve ergodicity of the system at low temperatures. Eventually, the divergence of dynamical quantities near the glass transition

becomes a stumbling block as relaxation time scales become so large that they may never be obtained via simulation, either due to system size or time constraints. To counteract the metastable nature of supercooled liquids, one generally tries to use larger simulation cells, often much larger than what is needed to merely avoid finite-size effects, in order to increase the range of the configuration space that the simulation samples. Results for thermodynamic and dynamic properties such as the specific heat, radial distribution function, mean-squared displacement, velocity autocorrelation function, and other time/space-dependent correlation functions, are typically computed as averages over results from several independent simulations run under identical conditions except for the initial velocities of the atoms. This increases the likelihood that an ergodic sample of the configuration space is obtained and that correlations between identical initial conditions are reduced. The metastability of supercooled liquids near the glass transition or mode-coupling temperatures frequently leads to some simulations whose properties differ significantly from run to run. Thus, in some cases the use of hundreds of independent simulations with different initial conditions may be necessitated.

Chapter 6: Stringlike Cooperative Motion in Supercooled Liquids

A number of studies (as described in Chapter 1) have found evidence of dynamical changes in supercooled liquids at the dynamic crossover temperature T_S [58, 59], [60]. In atomistic simulations, T_S has been identified as existing above the mode-coupling temperature and below the onset of super-Arrhenius behavior (see Figure 1-4) and has been most closely associated with the breakdown of the Stokes-Einstein relation. Since the dynamical processes are of key significance in supercooled liquids, a natural line of inquiry is stringlike cooperative motion, observed in molecular dynamics simulations of supercooled liquids in the 1990s, as well as in granular matter and other systems in both computer and laboratory experiments [13, 96, 97, 207]. Stringlike motion dramatically illustrates the rapidly increasing time and length scales associated with dynamical processes in supercooled liquids.

A simple yet powerful analogy from everyday life can provide a conceptual background for understanding why stringlike cooperative motion occurs in jammed systems. Think of a group of people attempting to cross a crowded thoroughfare. The group wants to move as effectively as possible through the crowd. It doesn't make sense for them to bunch up into a cluster and bludgeon through the crowd, but neither is it prudent for everyone in the group to split up as it would cause confusion and risk separation of the group. The natural way that people in groups move through crows is in a stringlike manner – one person forges a path, and the others follow behind as closely as possible – and the group doesn't need to confer on this matter. People move this way without giving it much thought. Atoms in supercooled liquids, it would seem, have the same intuition.

Now, imagine the crowd is less dense. The more space there is between people in the crowd, the less the group must rely on stringlike motion. In voids where there are no people, the group tends to cluster together and walk normally, only lining up again when it's necessary to pass between tightly bunched people in the crowd. This analogy serves to convey not just why stringlike motion is a natural mechanism for relaxation in jammed systems, but also why there is a relationship between the degree of stringlike motion and the density of the system. In this chapter, stringlike cooperative motion in supercooled liquids is described in detail, and evidence is presented of novel dynamical changes associated with stringlike cooperative motion that occur

at the dynamic crossover temperature T_S. This will serve to further corroborate results found in the literature, and results presented in the next chapter on the thermal jamming perspective applied to supercooled liquids.

Section 6.1   Quantifying Stringlike Motion

In MD simulations, strings are identified by examining a configuration, or "snapshot", of the system at some reference time, and comparing the positions of the atoms in the reference snapshot to subsequent snapshots separated by a time interval Δt. The following algorithm is applied to identify two-member strings or "cooperative pairs":

$$\min\left(\left|\mathbf{r}_i(t^*)-\mathbf{r}_j(0)\right|,\left|\mathbf{r}_i(0)-\mathbf{r}_j(t^*)\right|\right) < \delta \tag{6.1.1}$$

This algorithm compares the positions of two atoms in both snapshots, and it is applied to all atom pairs so that all cooperative motion between the snapshots is considered exhaustively. If atom i has moved to within a distance δ of atom j's position in the second frame, the algorithm's condition is satisfied and atoms i and j are said to constitute a cooperative pair. After all cooperative pairs have been identified, they are linked together into longer strings by joining together cooperative pairs that have common members. The parameter δ has been set in the literature to a value somewhat greater than the atomic radius when used to identify strings in the Kob-Andersen system [97]. However, others have found that the parameter used in the early literature for string analysis of the Kob-Andersen system was too large and resulted in "Y-like replacements," which occur when an atom moves precisely within the shell of size δ centered on the initial positions of two atoms [208]. In this case (illustrated in Figure 6-1), it can be said that the first atom has technically replaced two atoms and the identification of a cooperative pair becomes ambiguous. For this reason, in this work δ is set slightly larger than the radius of the smaller atom species in the system. For the KA and WCA systems studied in this work, $\delta_{KA} = \delta_{WCA} = 0.45$ ($\sigma_{BB} = 0.44\sigma_{AA}$), which has been demonstrated to eliminate Y-like replacements to less than 0.1%, while not qualitatively affecting the string analysis.

Overlap Region
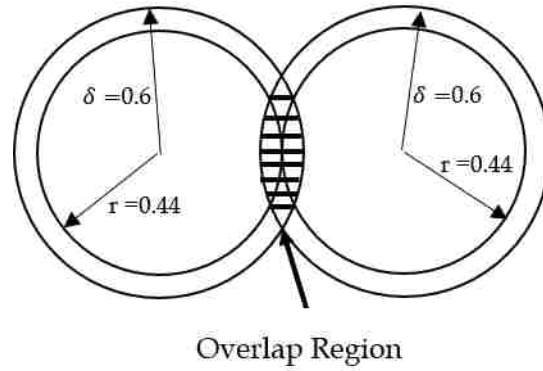
Figure 6-1:   A schematic of the string-finding algorithm's use of the overlap parameter δ for B particles in the KA/WCA systems.

Several key facts about strings in supercooled liquids should be noted:

1. For a given temperature, the average string length at a time interval Δt between snapshots, denoted $L(\Delta t)$, initially increases monotonically. At some time t_L it attains a maximum, after which $L(\Delta t)$ decreases monotonically to zero at long time intervals. The time Δt_L has been observed to scale nearly exactly with the time t^* that denotes the maximum value of the non-Gaussian parameter. This time is referred to in this work as the "peak string formation time" or "peak string population time."

2. For the Kob-Andersen system, strings are best quantified by considering only the 5% of the atoms in the system that have the highest mobility (the magnitude of the displacement vector of atoms between the two snapshots at Δt). In [207], the deviation of the extent of particle diffusion from Gaussian behavior in the KA system was quantified using the non-Gaussian parameter $\alpha_2(t) = 3\langle r^4(t)\rangle/5\langle r^2(t)\rangle^2 - 1$ and it was found that roughly 5% of the atoms diffused further than the expected Gaussian value. Therefore, the top 5% most-mobile ions/atoms has typically been used as a benchmark group of atoms used in studies of stringlike motion [16, 209], or in other works, an only slightly larger percentage has been used [208]. The examination of slightly larger or smaller percentages of mobile atoms does not *qualitatively* affect the nature of string behavior. In this work, the term "mobile" will be used to refer to atoms in the system that fall within this highest 5% group of fastest-moving atoms, and

slower-moving atoms outside this 5% group will be referred to as "immobile" (this is somewhat of a misnomer as these atoms are moving to some extent; rather, they are immobile with respect to their having a small impact on string formation).

3. For a given temperature, the probability of finding a string of length l in the system is approximately distributed according to an exponential function. It is possible to find strings with several tens of members with low probability. As temperature decreases, the average string length at the peak string participation time $L(\Delta t_L)$ increases, a result that may seem counterintuitive. As the system becomes more jammed, atoms are increasingly forced to follow the constrained pathways that necessitate relaxation by stringlike cooperative motion, according to the DF model [102]. The fraction of mobile atoms participating in strings at t_L increases as well, which also reflects the increases reliance on dynamically constrained pathways for relaxation. From a thermodynamic standpoint (c.f. RFOT theory), this increased participation of mobile atoms is reflected by an increase in the associated length scale.

4. A study by Gebremichael, et. al. [210] focused on the "coherence" of cooperative movements in the Dzugutov liquid. It was found that short strings of two or three members are most likely to jump in a coherent fashion – that is, the atoms in the string all tend to hop at approximately the same time. Longer strings move less coherently, meaning the hops of some or all of the atoms occur at different times.

The results from the simulations are discussed next. Figure 6-2 shows the fundamental characteristics of strings for the Kob-Andersen system. Panels A and B show the evolution of $L(\Delta t)$ for A atoms, and the number of A atoms that participate in the string, while panels C and D depict t_L, the time when the string length is maximum, and the probability of occurrence of a string with a particular length l. The peak string length and the atoms that participate in the string increase monotonically with decreasing temperature (panels A and B). As expected, the string length exhibits an exponential distribution with length (panel D).
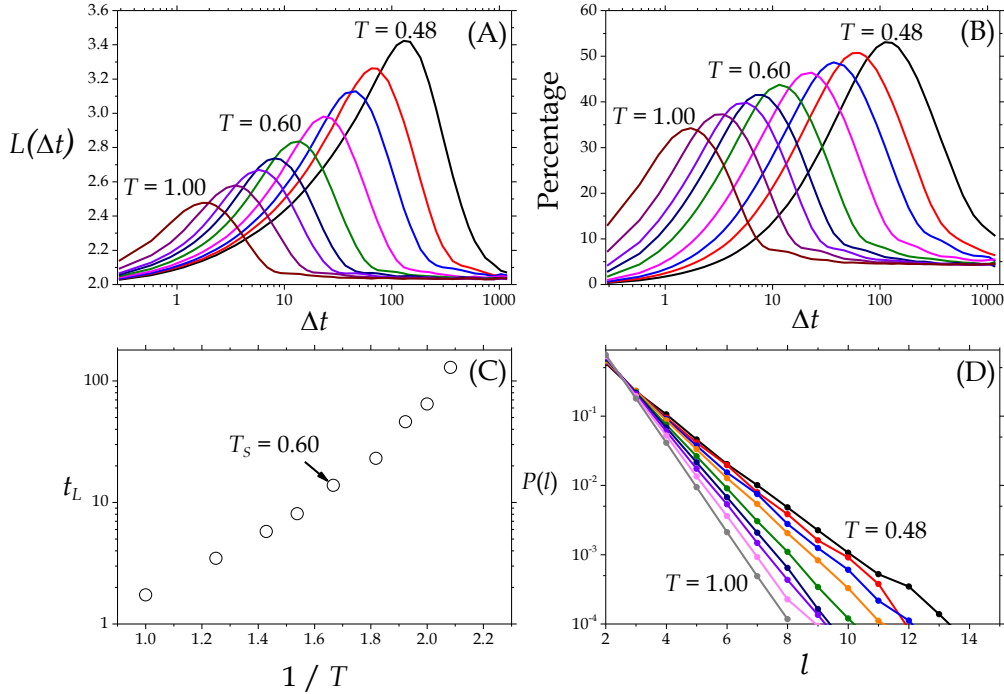
Figure 6-2:   Fundamental results for stringlike cooperative motion for the Kob-Andersen system: (A) the average string length $L(\Delta t)$. (B) The percentage of the 5% most-mobile atoms that are participating in stringlike motion. (C) The time t_L at which most strings are seen in the system, when $L(\Delta t)$ attains its maximum value. (D) The probability distribution of string lengths for a range of temperatures.

A slope change is evident in the Arrhenius plot of the peak string participation time for the Kob-Andersen system (Figure 6-2C) near the dynamic crossover temperature T_S, indicating a possible shift in the nature of string dynamics as governed by a different activation energy. This possibility was outlined by Kob and coworkers in their study of point-to-set correlations in supercooled liquids [60]. Since t_L has been shown to be proportional to the alpha-relaxation time τ_α and thus the diffusion coefficient, it is possible that string-like motion may drive the relaxation of atoms in supercooled liquids.

Short strings made of two or three members tend to form frequently even in normal liquids – perhaps the question is better framed as to determine the extent to which such

cooperative motions are merely correlated or imply causation as well. In line with the excitation model of Chandler and coworkers [102], correlated cooperative motion of atoms can occur but it may not be significant to the dynamic evolution of the system if the displacement of the atoms does not persist for a significant period of time. At lower temperatures near T_S and T_c, longer strings are found, and as temperature decreases the system increasingly visits the "landscape dominated" regime where configurational rearrangements involve the crossing of saddle points on the potential energy surface. At high temperatures it is not clear that a cooperative motion necessarily entails the crossing of a saddle point.
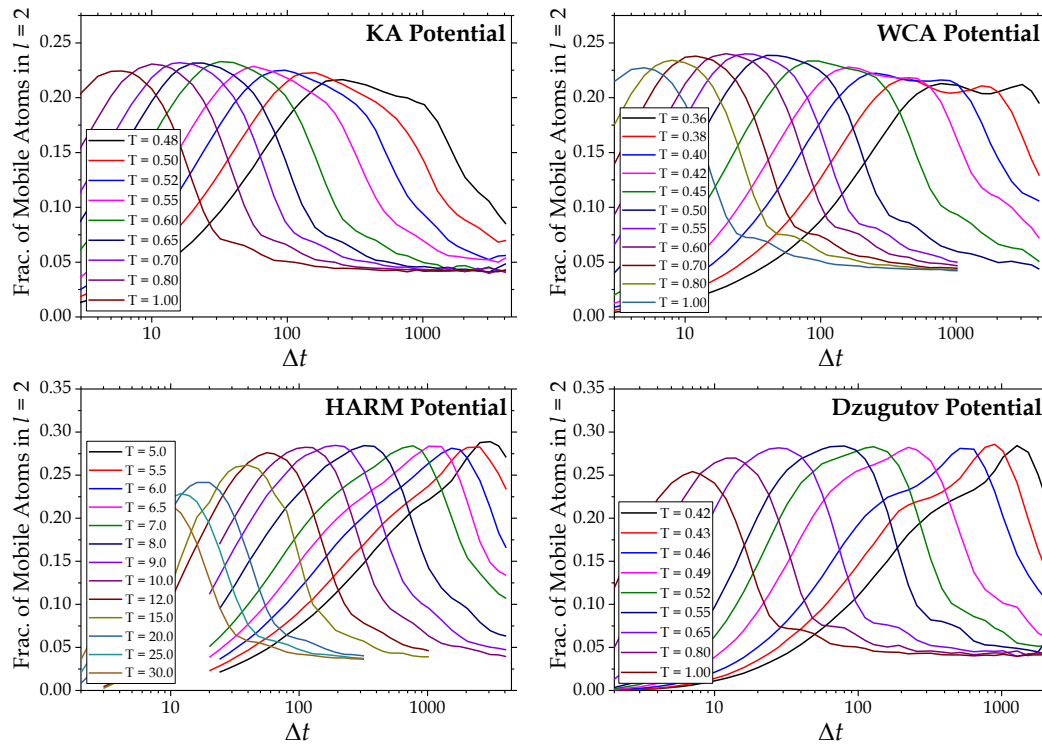
Figure 6-3:   Plots of the fraction of mobile atoms participating in cooperative pairs (l = 2 strings) for four model supercooled liquids.

The distinctions discussed in [210] by Gebremichael and others between the behavior of short microstrings and longer strings, as well as the above discussion about the significance of

cooperative pair formation with respect to activated processes, leads to a new type of study – instead of quantifying bulk characteristics of strings such as the average string length, one may instead compute the fraction of mobile atoms (here defined as the 5% most-mobile atoms) participating in strings of particular lengths. Obviously, there is no analog to the average string length when considering only discrete string lengths. This discrete string analysis requires barely any additional work – at each time interval Δt strings are identified as usual, and the numbers of atoms participating in strings of length $l = 0$ (immobile atoms), 1 (mobile, non-cooperative atoms), 2, 3, 4, etc. are simply tabulated. The results of this analysis are shown in Figure 6-4 for the four model supercooled liquids.

For each of the model systems interesting behavior is seen at low temperatures below T_S as T_c is approached. Hereafter this data will be referred to as the "participation curve" for cooperative pairs. The participation curves appear very nearly symmetric on a logarithmic time scale at higher temperatures, but beginning at approximately T_S the curves lose their symmetry and begin to exhibit depressions at approximately the peak string participation time t_L. At the lowest temperatures there are multiple inflection points, resulting in a splitting of the curves into two "peaks" for the KA and WCA systems.

Plotting the participation curves for different strings lengths at a given temperature reveals an interesting result as well. These plots are shown for the KA and WCA systems in Figure 6-4 and for the HARM and Dzugutov systems in Figure 6-5. One-member ($l = 1$) strings, which are atoms whose mobility is within the top 5% of the largest mobilities in the system but have not moved cooperatively, are also shown. The dotted lines on these plots show the time at which the population of individual, non-cooperatively moving atoms attains a minimum, which is typically very close to the time at which the populations of cooperative pairs, three-member microstrings, and longer strings attain their maximum values. This indicates that the time scales associated with individual atom hops represented by the $l = 1$ "strings", appears to drive the time scales of microstrings and longer strings.
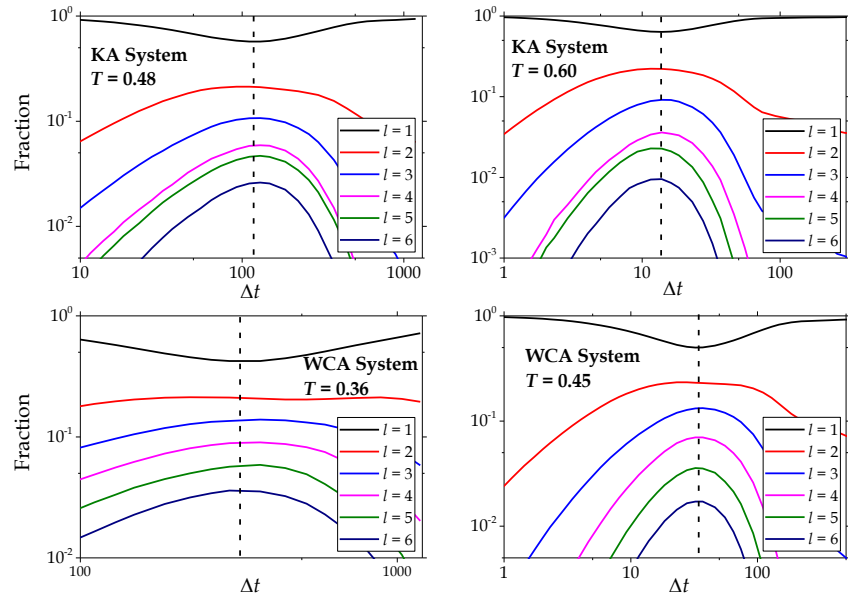
Figure 6-4: Plots of the participation curves for $l = 1 - 6$ strings for the KA and WCA systems, at the mode-coupling temperature T_C and the dynamic crossover temperature T_S.
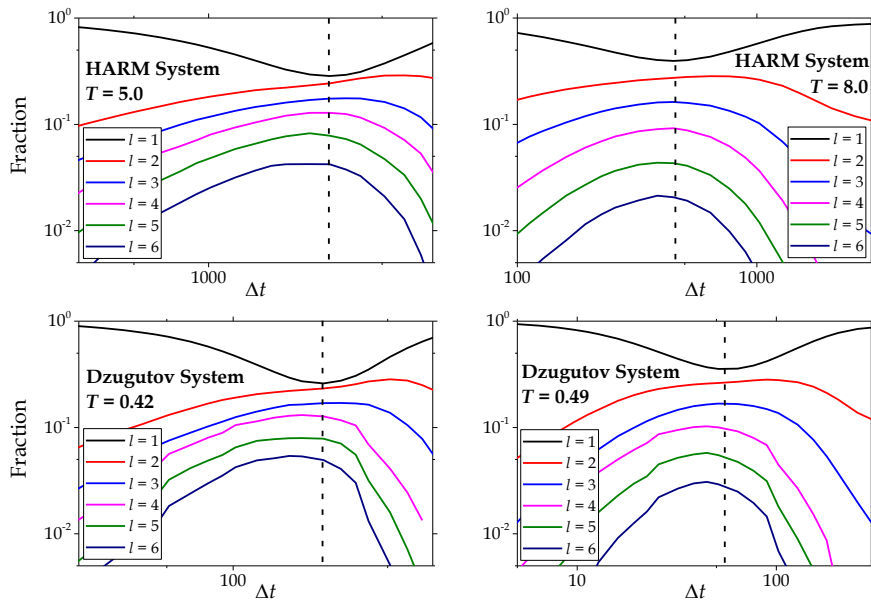
Figure 6-5: Plots of the participation curves for $l = 1 - 6$ strings for the HARM and Dzugutov systems, at the mode-coupling temperature T_C and the dynamic crossover temperature T_S.
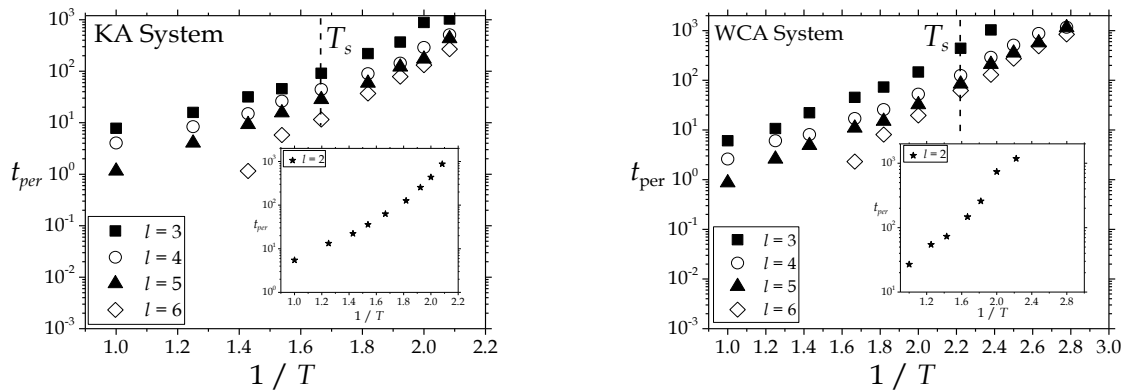
Figure 6-6: The persistence time t_{per} of strings of particular lengths l. For $l > 2$, t_{per} is taken to be the time interval at which these strings comprise at least 0.5% of the atoms participating in string-like motion. As cooperative pairs are found to always comprise a greater percentage of string-like atoms than longer strings, t_{per} is the time interval during which cooperative pairs comprise at least 5% of string-like atoms.

Further analysis of this intriguing result may be carried out by calculating a "persistence time" t_{per} for the groups of strings of length l that indicates the time scale for which strings of length l constitute a significant fraction of the atoms participating in string-like motion. The persistence time is calculated by noting the time at which strings of length l first attain a certain percentage of the string population, and the time at which they last attain at least that percentage, as indicated in the plots in Figure 6-4. For $l = 3$-6, we choose 0.5% of the total string population as the threshold for t_{per}; for $l = 2$ one is forced to choose a larger threshold of 5%, as cooperative pairs are always significantly more prevalent than the longer strings. Plots of t_{per} for the KA and WCA systems are shown in Figure 6-6. As expected given the results in Figure 6-4, t_{per} increases with decreasing temperature for a given string length l. At a given temperature, shorter strings have longer persistence times. A reasonable explanation for the closeness of the peak population time scales for various string lengths that may be drawn from these results is that longer string formation is facilitated by shorter string growth. On average, for a large enough sample of strings, strings of length l will typically not begin to form until there is a significant-enough population of [$l - 1$] strings. Since successively longer strings have shorter persistence times, strings of length l also typically break up before strings of length [$l - 1$]. The competition of these two factors may lead naturally to a centering of string population times around a central value controlled by the shortest strings in the system.
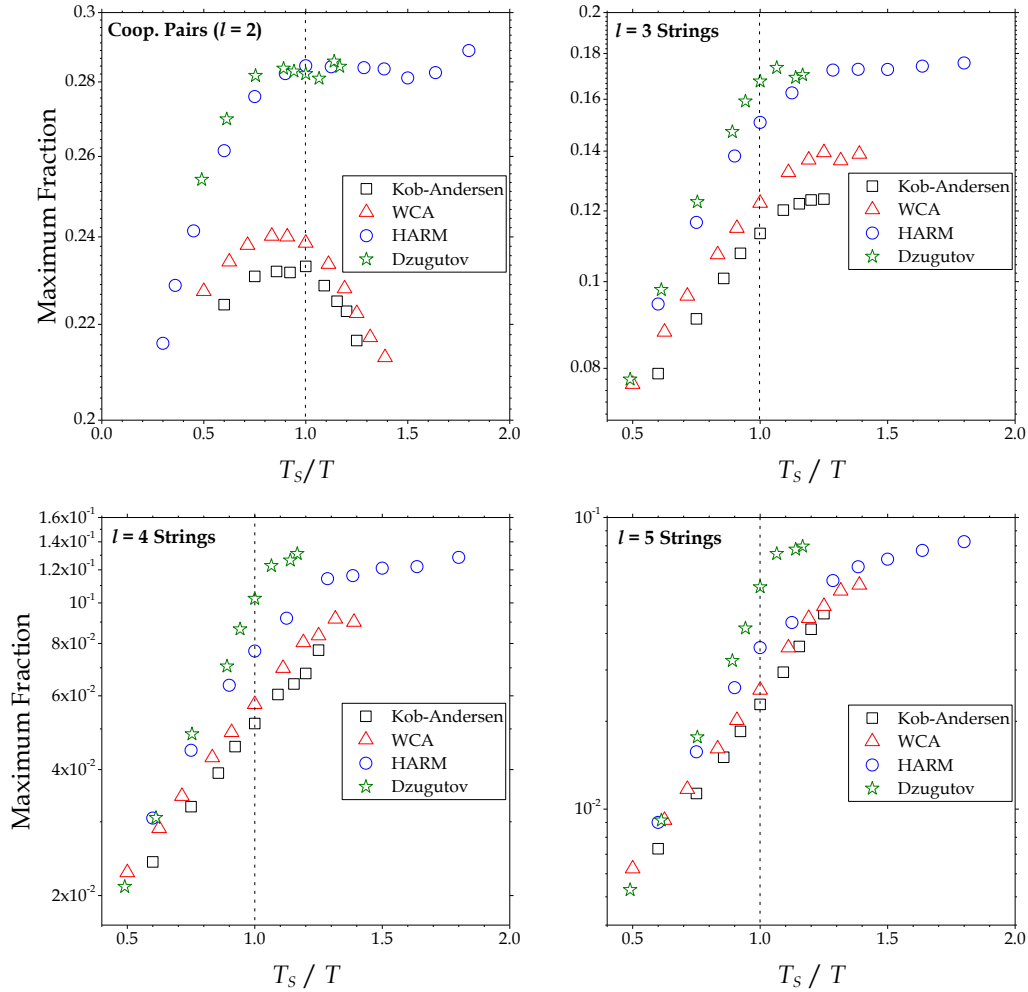
Figure 6-7:   Plots of the maximum fraction of mobile atoms participating in strings of length l = 2, 3, 4, and 5, for four model supercooled liquids. The temperature scale is normalized to the dynamic crossover temperature T_S for each system.

Of equal (or perhaps more) significance in the results shown in Figure 6-7 is the observation that the maximum values of the participation curves for cooperative pairs exhibit either *non-monotonic* variance in temperature, as seen in the KA and WCA systems, or an approximate leveling-off, as seen in the Dzugutov and HARM systems, and the maximum or leveling-off point occurs at the dynamic crossover temperature T_S. These maximum values for cooperative pairs are shown in

Figure 6-7 in Arrhenius plots, along with the corresponding maximum values extracted from the participation curves for l = 3, 4, and 5 strings, also plotted on Arrhenius scales with temperatures normalized to T_S. Three-member microstrings show nearly the same behavior as is seen for cooperative pairs, although the non-monotonic variance seen in the KA and WCA systems for cooperative pairs is not present. For the longer 4-5-member strings, shifts in the slope of the maximum fraction of participation are evident somewhat below T_S but still above the mode-coupling temperature.

This study of discrete string populations indicates the presence of shifts in the dynamical behavior of strings that are not as apparent in the analyses of bulk stringlike motion featured in the literature and in Figure 6-2. These results raise some important questions. First, it is not clear whether the peak values of the participation curves constitute length scales associated with string dynamics. If this is the case, then the non-Arrhenius variation of the maximum population of cooperative pairs suggests that in fact cooperative pair formation is *not* functioning according to activated dynamics at lower temperatures. Longer strings clearly show Arrhenius variance across the dynamic crossover temperature T_S. However, it is also not clear that the maximum population of strings of a particular length actually constitutes a viable length scale, and therefore caution must be exercised when attributing certain interpretations of these results in the context of activated dynamics.
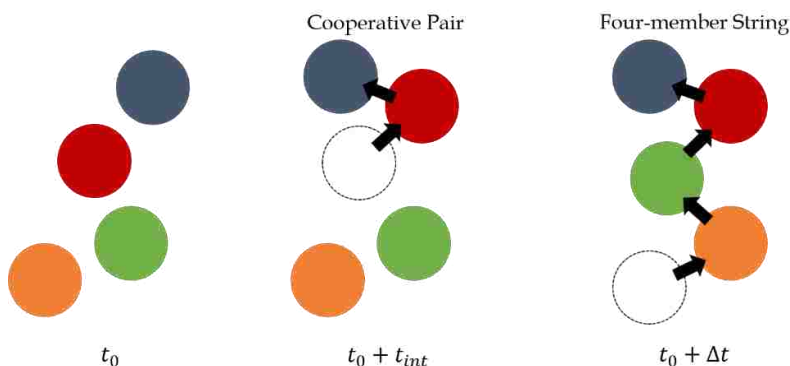
Figure 6-8:   Illustration of how the incoherent formation of a four-member string might cause the string-finding algorithm, which only compares snapshots at t_0 and $t_0 + \Delta t$, cannot account for the intermediate history of the string, where a cooperative pair forms at $t_0 + t_{int}$. In this scenario, two cooperative pairs are formed within the time interval but the string-finding algorithm identifies a four-member string.

Further consideration of the string-finding algorithm in the context of the coherency of string formation uncovered by Gebremichael, et. al. [210], illuminates a possible shortcoming in the discrete string population analysis. The method employed to link cooperative pairs into longer strings necessitates that strings are identified exhaustively – that is, cooperative pairs with common members are linked together until no other common members are found, and the resulting string excludes its constituent cooperative pairs from being included in the total count of cooperative pairs in the system. For example, a four-member string is found by linking together three cooperative pairs (see Figure 6-8). Within the time interval Δt between the two frames, the cooperative pair constituents of the four-member string likely moved at different times – the string-finding algorithm cannot say what occurs inside the time interval Δt. It is impossible to know whether a given string was formed coherently. Therefore, the plots in Figure 6-7, while interesting in their own right, may merely be a reflection that cooperative pairs are being assimilated into longer strings with increasing frequency, causing the population of cooperative pairs to drop off, and thus statements about the activated nature of string formation based on the participation curves are not necessarily valid. Furthermore, the origin of the depression needs to be uncovered, as an intuitive appraisal of the participation curves suggests that the formation of the depressions is what leads to the non-monotonicity in the peak values of the curves. If the origin of the depression is found, one might reasonably attribute the cause of the depressions to be the cause of the non-monotonicity as well.

There is no question that these results indicate a dynamical shift related to stringlike motion at T_S. To allay concerns that anomalies in the simulations or in the post-analysis are responsible for this result, we note that no parameters in the post-analysis were changed in the analysis for any system as the temperature was varied, and that the closeness of the results in this work to literature data (as indicated in Figure 6-2) shows the string-finding analysis was conducted correctly. For each system the distribution of string lengths $P(l)$ exhibits a very clear exponential decay as l increases, which matches results seen in the literature. This indicates that sufficiently good statistics were obtained from the simulations to cancel out any transient effects that may lead to erroneous results. The next task is to gain more insight into the precise nature of this dynamical shift, and why this shift might occur at T_S.

Section 6.2   String Tracking Analysis

A more in-depth analysis is needed to determine the true nature of the formation of cooperative pairs and their role in the formation of longer strings. In this situation, an analysis inspired by neutronics in nuclear reactors provides a possible answer. Just as the neutron population in a reactor may be computed by considering the "gain" and "loss" of neutrons by fission, scattering, and absorption [211], one may recreate the participation curves in Figure 6-3 by considering how strings of particular lengths are created and annihilated, quantifying all of these events, and summing them together again to obtain the total population of strings of a given length. For example, cooperative pairs may be formed by the confluence of individual atoms (either immobile or mobile) that, at one instant, are not moving cooperatively and then suddenly undergo a cooperative motion. Cooperative pairs may also be formed by the disintegration of longer strings, in which at one instant a long string of atoms is identified as moving cooperatively, and then in the next instant all but two members of the long string suddenly stop moving or move in different directions so that the motion of all the atoms in the string are no longer correlated, leaving only two atoms that continue to move together. By counting all instances of cooperative pairs being formed and breaking up, the difference of the two's sum is the *net population* of cooperative pairs. The goal is to determine whether the behavior of the participation curve for cooperative pairs entails one of the two following possibilities:

> Explanation 1: The depression in the curve is due to fewer cooperative pairs forming near the peak string population time t^*, and the Arrhenius growth of the population of longer strings is due to them forming coherently independent of cooperative pair formation.

> Explanation 2: Cooperative pairs are indeed being formed but their population merely appears to drop off because they are latching onto other strings to form long strings, which are mostly incoherent. The population drop-off is an artifact of the string-finding algorithm, which only compares strings between two configurations and cannot say anything about the history of the atoms between the configurations.

To perform this analysis, a reference time t_0 is chosen as is done normally when applying the string-finding algorithm. At *every* subsequent snapshot $t_1, t_2, t_3, \ldots, t_N$, where t_N is a sufficiently large time interval that the average string length $L(t_N)$ decays approximately to zero, the string algorithm is applied with respect to the reference frame at t_0. For each time t_i, the following information is tabulated for each atom:

1. Whether or not the atom is participating in a string's motion,
2. If the atom is in a string, the length of the string of which it is a member.

Then, each atom's membership at time t_i is compared to its membership at the previous time t_{i-1}. Thus, the history of every atom's participation in strings is recorded for the entire duration of t_N. One may see exactly when an atom transitions from, say, a cooperative pair to a six-member string, or when an atom is part of a ten-member string that breaks up, leaving it as a member of a shorter string.
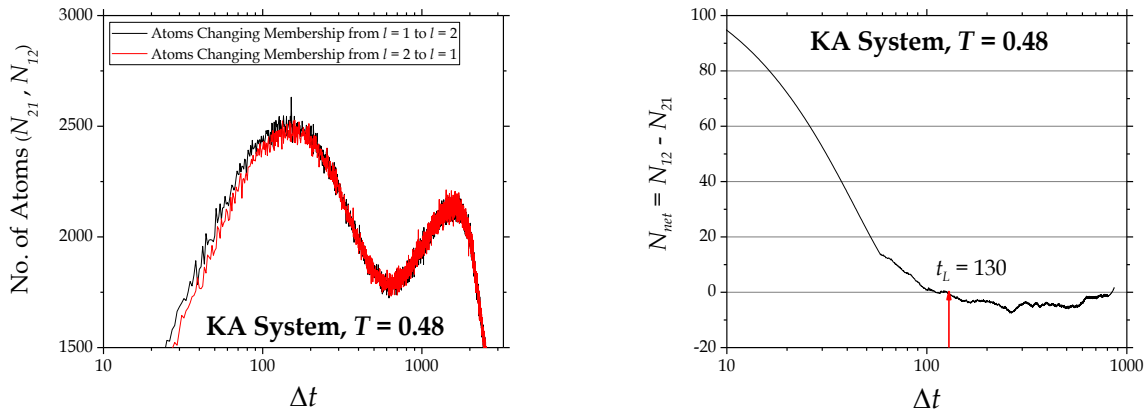
Figure 6-9: (left) A mirror transformation of mobile, non-cooperatively moving atoms ($l = 1$) and cooperative pairs ($l = 2$), for the KA system at a low temperature. The two rates are nearly identical, indicating that cooperative pairs break up into individual atoms nearly as often as they are formed by them. (right) The net rate obtained by taking the difference in the mirror transformation rates in the left figure. The net rate is positive before t_L and negative afterwards, indicating that more cooperative pairs are indeed formed from mobile atoms than break up into mobile atoms before t_L, where the opposite is true after t_L.

With this analysis, particular "transformations" or permutations of string formation and annihilation may considered. The number of atoms that transition from a string of length m to a string of length n at time t_i can be denoted $N_{mn}(t_i)$. For example, $N_{23}(t_i)$ is the number of atoms

that were members of cooperative pairs at time t_{i-1} and are now members of three-member strings at time t_i. If the spacing between all snapshots is equal (as is done with the data used in this work), this number can also be considered a rate $R_{mn}(t_I)$. The analysis computes R_{mn} at every time interval for $m, n = [0,10]$, with a zero-member "string" corresponding to a low-mobility, non-cooperative atom that is not within the top 5% most-mobile atoms, and a one-member "string" corresponding to a mobile, non-cooperative atom. Of special significance are so-called "mirror transformations," such as (R_{12}, R_{21}), that correspond to strings being created and annihilated by the same process. If mirror transformation rates are added together, they represent the net rate of strings of length m being created by strings of length n coming together, or annihilated by breaking up into strings of length n. A depiction of mirror transformation rates for the KA system at low temperature is shown in Figure 6-9. It is observed that for all mirror transformations – not just the one-to-two-member string transformations shown in Figure 6-9 – the creation rate is nearly identical to the annihilation rate, indicating that most strings break up shortly after they are formed. However, the creation rate is slightly larger than the annihilation rate prior to t_L, which is the expected result that must be true if strings are to be formed. The annihilation rate becomes larger after t_L. This reflects the monotonic increase before t_L, and subsequent decrease after t_L, seen in the bulk string population (Figure 6-2 and Figure 6-3). In the last step of the process, all rates corresponding to all permutations of n and m can be summed together for a particular string length and then integrated to obtain the total population of those strings as a function of time. For example, the sum of all rates R_{2m} and R_{n2} will give the net rate of cooperative pair formation, and the integral of $R_{net} = R_{2m} - R_{n2}$ should reproduce the string population curve for cooperative pairs depicted in Figure 6-3. The benefit of this complicated process is that one is now able to consider only some transformations, while neglecting others, to examine the impact of certain string transformations on the population of cooperative pairs. This is shown in Figure 6-11 below for cooperative pairs: by considering $R_{net} = R_{2m} - R_{n2}$ with $m, n <$ 2 provides the net rate of cooperative pairs that are formed only by the convergence of individual atoms, and annihilated only by breaking up into individual atoms.
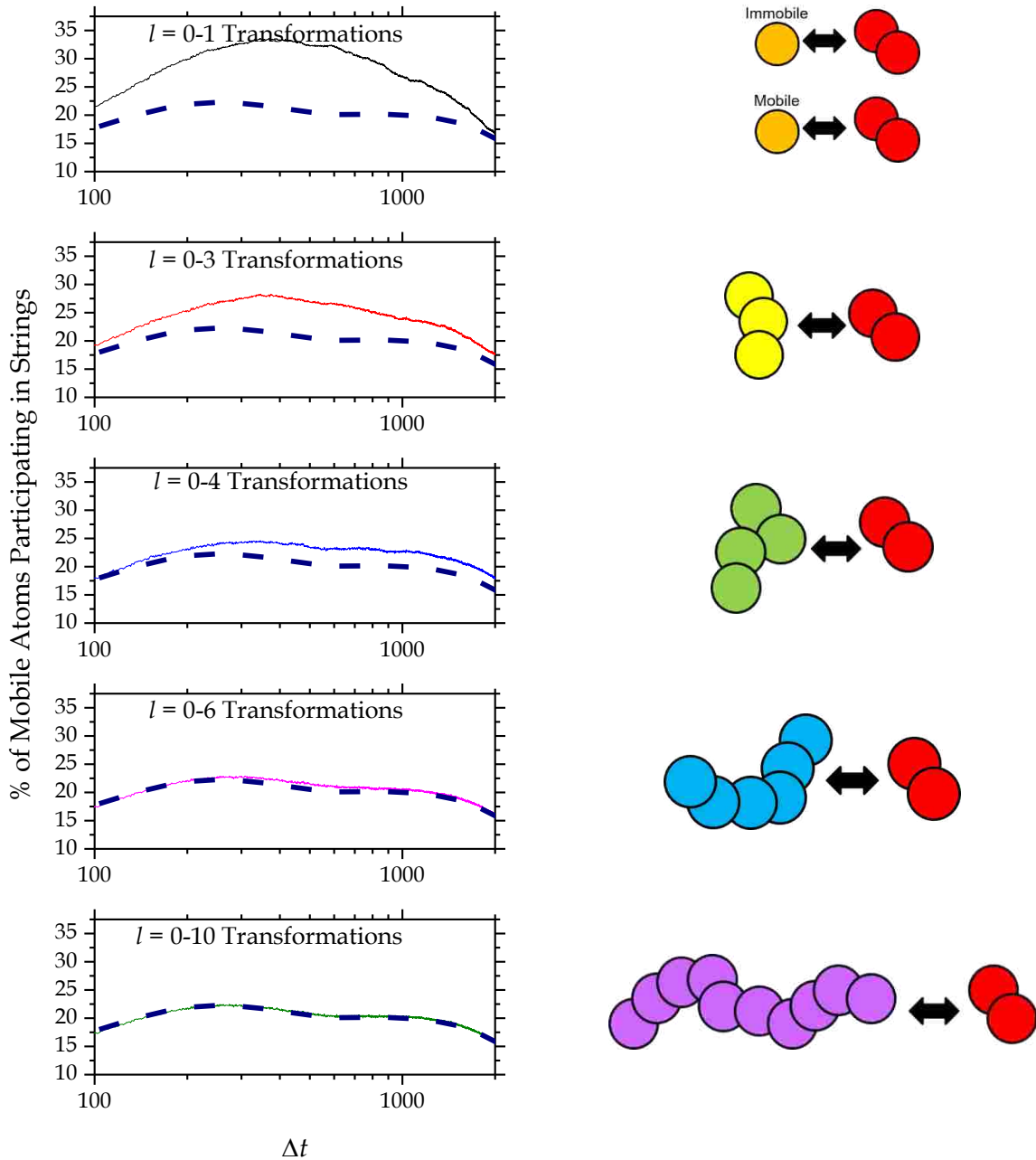
Figure 6-10: Evolution of the reconstruction curves for cooperative pairs in the KA system at $T = 0.48$ as successively longer string transformations are taken into account.

Note that strings longer than two members effectively do not exist in the system at all. For this scenario, the string population curve for cooperative pairs no longer exhibits non-

monotonic variance in temperature and is no longer asymmetric in time. Figure 6-11 (A) shows this scenario. As transformations between cooperative pairs and successively longer strings are considered (Figure 6-11 (B-D)), eventually the string population curve in Figure 6-3 is attained in Figure 6-11 (D). Note that the reconstructed curves are choppier than the original participation curves because the time-sampling is much more frequent in the reconstructed curves.
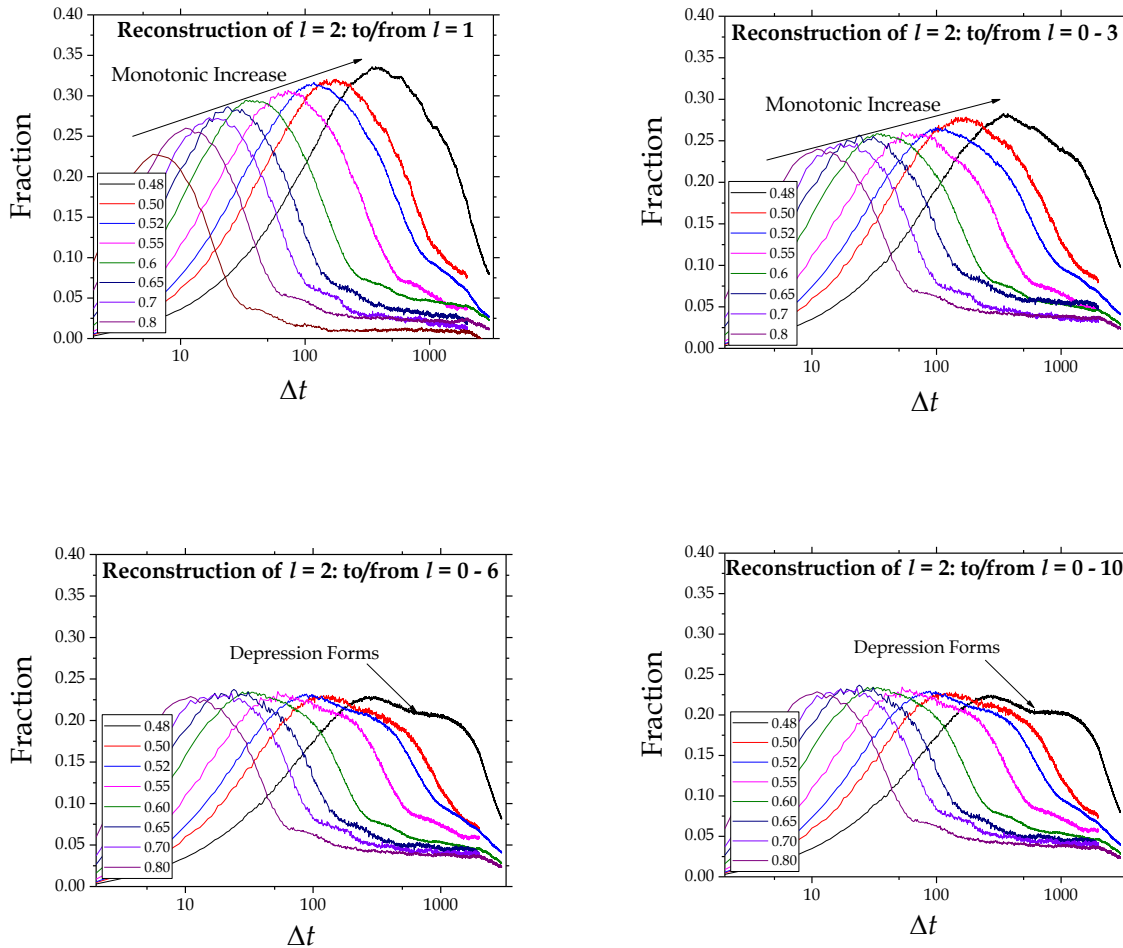
Figure 6-11: Plots of the discrete string population reconstruction curves for cooperative pairs in the Kob-Andersen system. As the interchange of cooperative pairs with only individual atoms ($l = 0, 1$) is considered, the peak values of the curves exhibit a monotonic increase in temperature. As the interchange of cooperative pairs with longer strings is considered, the non-monotonic behavior of the plot in Figure is obtained.

It is also important to note that the effect of adding longer string interchanges is less significant at higher temperatures, where long strings are rare. At the highest temperature $T = 1.0$ for the KA system, there is virtually no change at all among the four plots depicted in Figure 6-11. This indicates that $T = 1.0$ is the high-temperature limit in which virtually no long strings exist, and the consideration of strings longer than $l = 2$ is mostly unnecessary to reconstruct the participation curve. This analysis carries this exact same process to lower temperatures, where longer strings do exist, and where the act of excluding the interchange of cooperative pairs with longer strings produces dramatic results.

Section 6.3   Discussion

The relatively straightforward analysis of quantifying the population of strings of particular lengths (Figure 6-7) reveals a profound result at the dynamic crossover temperature that is not evident by an analysis that lumps all strings together. A broad view of the results presented in this chapter leaves no doubt that a change in string dynamics is occurring at the dynamic crossover temperature. The non-monotonic behavior of the curves for the KA and WCA systems indicates that this feature is not necessarily unique to one system (although the KA and WCA systems share the same binary Lennard-Jones form of their potential energy function), and although the HARM and Dzugutov systems don't exhibit non-monotonic variation of the cooperative pair population, a pronounced shift is evident at T_S for those systems too. That these changes are seen at this particular temperature for these distinct potentials renders extremely unlikely the possibility that these results represent a coincidence.

The string tracking analysis digs beneath the surface of the initial discrete string analysis and provides an explanation for the odd depressions in the participation curves for cooperative pairs. The fact that the participation curves for any discrete string length may be "reconstructed" using the tracking analysis considering *all* string interchanges indicates that an accurate bookkeeping of string transformations has been developed. The key part of the analysis presented here is represented by the stark difference between the top-left and bottom-right plots shown in Figure 6-11, which demonstrates how by excluding cooperative pairs that go on to form longer strings, or are formed by the breaking up of longer strings, one can pretend that the mechanism

for long string formation effectively doesn't exist, and it becomes apparent that cooperative pairs are indeed produced to an increasing extent as temperature is lowered. The other important take-away from this result is that the significance of long strings becomes *more important* as temperature decreases. The full participation curve at high temperatures may be reconstructed only using short string interchanges. This is partially due to the rarity of long strings at high temperatures. But the dearth of long strings also means that the participation curves don't exhibit the depression in the vicinity of the string formation time t_L.

An effect similar to that observed for cooperative pairs is also seen for three-member microstrings. They also act as the constituents of longer strings but to a lesser extent than the more-common cooperative pairs. Successively longer strings see a stronger Arrhenius growth as temperature decreases, and no decline in their population near t_L. The behavior uncovered by this analysis – that two- and three- member strings increasingly join together with other correlated atoms and string to form longer strings beginning at T_S – has possible implications for the dynamical facilitation model for string formation of Chandler and coworkers [102]. The microstrings identified in this analysis that are "annihilated" by absorption into longer strings persist in their displacements for an appreciable time.

The conclusion that should be emphasized the most from this chapter is how the discrete analysis, and the subsequent explanation of the non-monotonicity by the tracking analysis, emphasize the importance of the dynamic crossover temperature T_S. A clear change in string dynamics occurs at this temperature, particularly with shorter strings. This is evidence that a "jamming" threshold has been crossed, as a change in the nature of the dynamically-constrained pathways followed by the atoms has forced string relaxation to rely increasingly on incoherent motions. A fundamental observation in the literature has been that the average string length increases with decreasing temperature, meaning that the mobile atoms that are trying to explore the potential energy landscape are increasingly relying on activated dynamics to achieve relaxation. Since coherent motion of long strings is statistically improbable given the caging effect experienced by individual atoms, the conjoining of cooperative pairs or three-member microstrings is the only mechanism by which the long strings are generated.

As indicated by Figure 6-4 and Figure 6-5, extrema in the populations of individually-moving mobile atoms and all discrete string lengths occurs at approximately the same time scale,

while the persistence time decreases for successively longer strings at a given temperature. This situation is highlighted by the results of the tracking analysis, which shows (in conjunction with the analysis of Gebremichael and coworkers [210]) that the short strings are essential components of longer strings, and thus can be said to facilitate the formation of longer strings that form incoherently as a result of the conjunction of short, coherently-forming microstrings. As long strings are rare compared to microstrings, only a small fraction of cooperative pairs or three-member strings goes on to incoherently join other strings to form the long strings. The long string population "draws on" the population of short strings, and few long strings could exist without the prior formation of microstrings. If the time scales of the maximum populations of long strings differed from those of short strings, it would entail that the long strings are being formed coherently – meaning that potentially tens of atoms would hop at nearly the same time, which is extraordinarily unlikely.

Chapter 7:   Thermal Jamming in Supercooled Liquids

In this chapter a two-pronged thermodynamic and dynamic analysis of supercooled liquids is undertaken using the hard sphere partitioning (HSP) approach, from which the thermal jamming metrics are established for three model systems and eight real glass forming liquids (GFLs) using the assumptions within the methodology outlined in Chapter 4. Three model GFLs are featured in the first part of this analysis: the Kob-Andersen (KA) system [111], Weeks-Chandler-Andersen (WCA) system [203, 204], and the harmonic sphere (HARM) system [205, 206]. Details of the molecular dynamics (MD) simulations employed to study these systems is provided in Chapter 5 and Appendix A. These model systems have been extensively studied in their application to modeling the slowing-down behavior of supercooled liquids, and each can be classified as a simple liquid as they employ spherically symmetric pair potentials. Each system is studied from relatively high temperatures near the onset temperature T_O at which supercooled dynamics is first observed, across the dynamic crossover at T_s, and down to the vicinity of the mode-coupling temperature T_c; the important crossover temperatures for the model systems is listed in Table 5-1. This ensures that a range of glassy dynamics is incorporated in the results for the three systems. For the eight real GFLs, the analysis is performed to the experimental glass transition temperature T_g.

Prior to presenting the analysis, we provide confirmation of the validity of the simulations used in this work. Figure 7-1 shows a comparison of the (self) diffusion coefficients of the model GFLs computed by two methods – the slope of the mean-squared displacement (MSD), and the time integral of the velocity autocorrelation function [85]. Good agreement is seen between the two methods, which indicates that sufficiently long correlation time and configuration space sampling have been attained such that the integral of the VACF produces a reliable value of the self-diffusivity for all the systems. Some deviations are observed at lower temperatures where it becomes increasingly difficult to simulate the slow supercooled dynamics, but this error is relatively small and the VACF results match reasonably well with the diffusion coefficients obtained from the slope of the MSD. This check provides an important check for the density of states, the primary input of the partitioning (HSP) method. As shown in Equation 4.1.11, the zero-frequency mode of the density of states $G(\nu)$ is directly proportional to the self-diffusivity D.
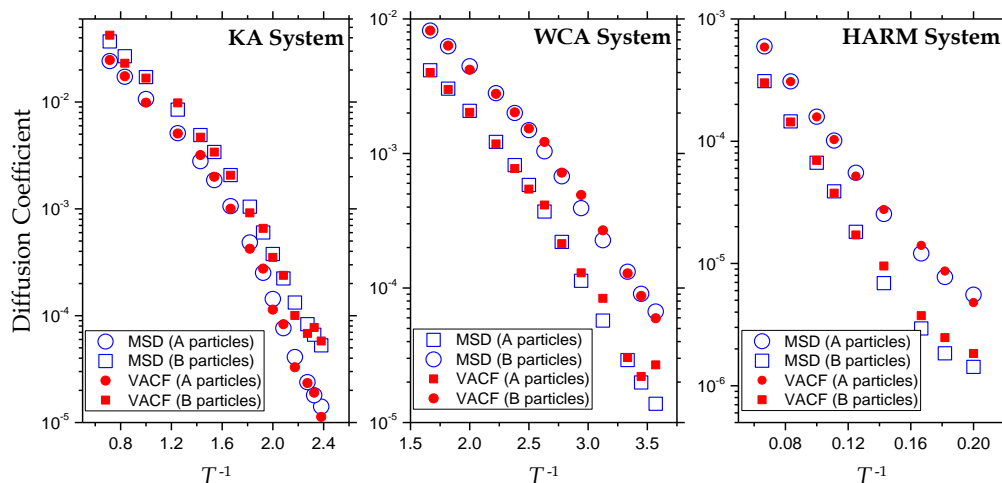
Figure 7-1:   A comparison of reduced (self) diffusion coefficients as a function of inverse temperature for the three model GFLs. The diffusivities are evaluated through the mean square displacement (MSD) and velocity autocorrelation function (VACF).

The density of states for the KA system is depicted for various temperatures in Figure 7-2. As evident the $G(\nu)$ converges to a constant value at small frequencies.
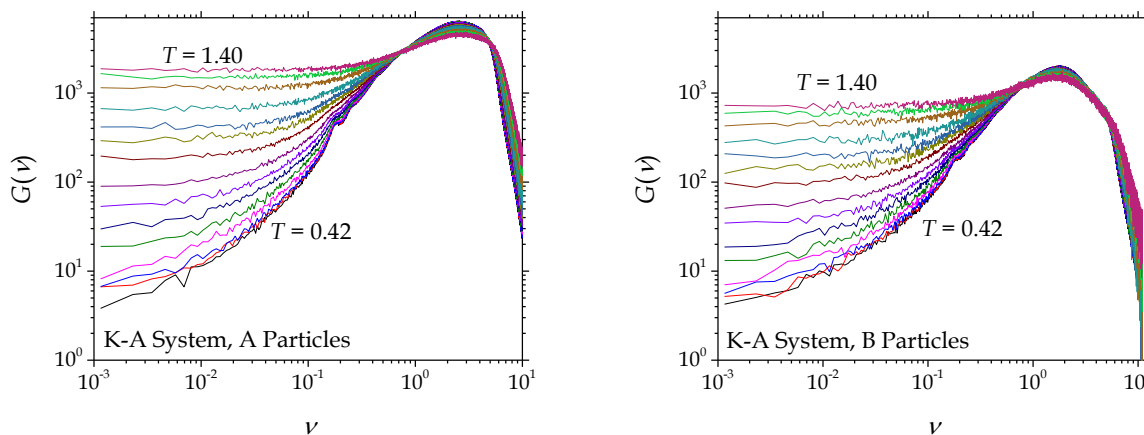
Figure 7-2:   The density of states $G(\nu)$ for the A atoms (left) and B atoms (right) in the Kob-Andersen system. Note that the plot features a log-log scale that exaggerates the height of $G(0)$. At low frequencies, $G(0)$ attains a nearly constant value.

Critical to the success of the HSP method is an accurate calculation of the diffusion coefficient from the VACF. The diffusion coefficient calculated from $G(0)$ should ideally be within

a few percent of the value computed from the time integral of the VACF – to observe a result to the contrary would indicate that a better-quality simulation is needed to reduce error in the diffusion coefficient. This could be remedied by 1) computing the VACF for a longer correlation time, and with a smaller time step, or 2) increasing the number of atoms in the simulation cell. For the supercooled liquids studied in this dissertation, it is also important to compute the VACF as an average of output from many (often hundreds) of independent simulations with different initial velocities. As ergodic sampling of the potential energy surface for these systems becomes increasingly time-consuming at low temperatures, a large number of independent runs ensures that a larger volume of the phase space is explored. With fewer independent runs or smaller system sizes, $G(v)$ becomes choppier and the resolution of $G(0) \propto D$ becomes more uncertain. Since the frequency interval dv is inversely proportional to the maximum correlation time used when computing the VACF, a sufficiently large t_{corr} was used such that a "flat" $G(v)$ is seen as v approaches zero. This flattening, coupled with the smoothing of $G(v)$ due to adequate sampling of the configuration space, provides confidence that $G(0)$ and the overall shape of the density of states is accurate for the model GFLs. The internal consistency of the HSP approach is verified through an error analysis as shown in Appendix B.

Section 7.1   Analysis of Model Glass-Formers

As discussed previously, this chapter features thermal jamming analyses of two systems – model supercooled liquids and experimental GFLs. We proceed in for each of the two systems with a discussion the excess entropy of the hard sphere partition and Excess Entropy Scaling (EES). For the model supercooled liquids, a verification of the total entropy is also performed using reference values for the entropy from the simulations obtained through the internal energy variation with temperature. This total entropy verification is important, as it provides a firm ground upon which the implications of the HSP method demonstrated in this work can rest.

7.1.A Dynamical Characteristics of the Hard Sphere Partition

Prior to calculating the entropy of the hard sphere partition and ultimately that of the entire liquid, the HSP method establishes a quantitative factor f that determines the extent of the hard sphere partition of the liquid. A plot of the partitioning metric for both particle species of the model GFLs is shown in Figure 7-3 in Arrhenius form.
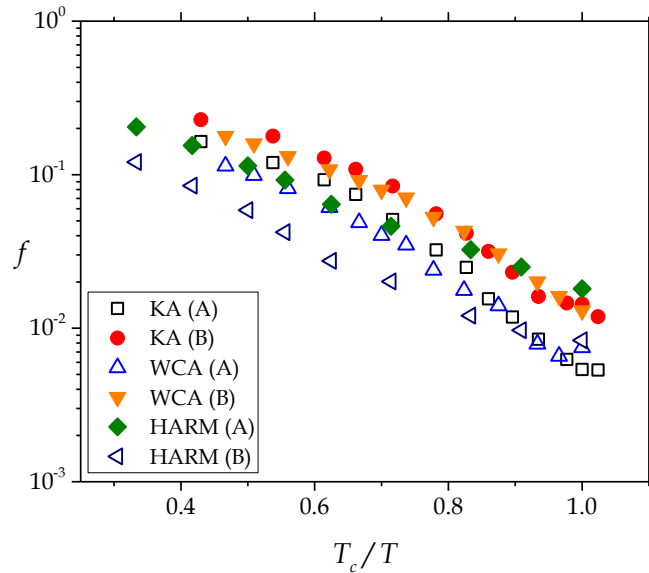
Figure 7-3:   The partitioning metric f as a function of T_c/T for the model GFLs.

The partitioning metric is ~0.3 at the onset temperature T_O, which is consistent with values typically obtained for normal liquids using the CS equation of state and the 2PT method [187, 188, 191] . Near the mode-coupling temperature T_c, f decreases significantly to values on the order of 10^{-2}. Keeping in mind the definition of f this observation means that as the temperature drops to T_c from T_O, the effective number of hard spheres reduces dramatically from ~30% to just ~2%. Thus near T_c, the diffusive dynamics is controlled only by a small number of HS atoms.

The partitioning metric for the model GFLs exhibits power law variation with $\phi_c - \hat{\phi}$, shown in Figure 7-4. At higher temperatures near T_O, which corresponds to larger $\phi_c - \hat{\phi}$, Liu's

EoS predicts values that approach the Speedy and Odriozola-Berthier equations of state; at lower temperatures, it deviates.
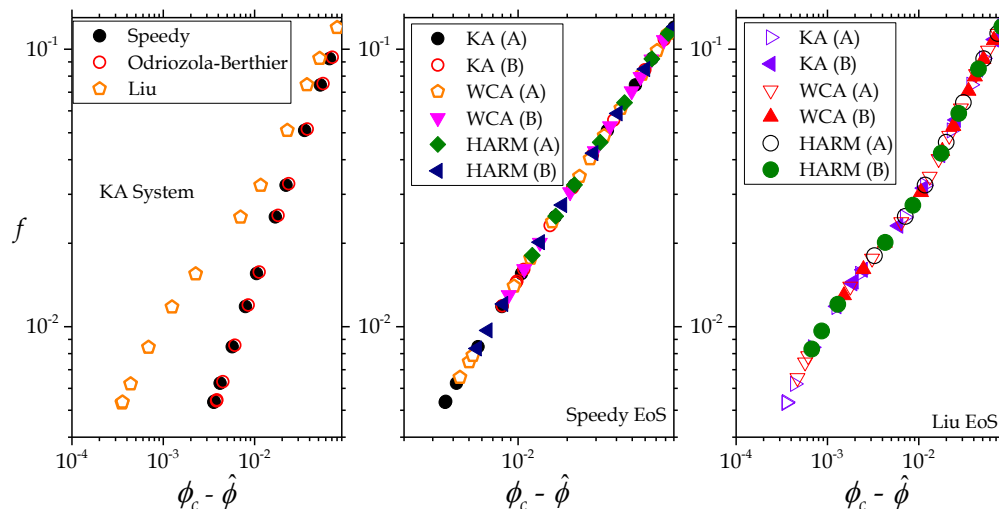
Figure 7-4: At left, the variation of the partitioning metric with $\phi_c - \hat{\phi}$ for the KA system, using the three equations of states. Speedy and Odriozola-Berthier (O-B) produce very similar results, while the Liu EoS predicts a closer approach to ϕ_c for the same f. The critical packing fraction ϕ_c for Speedy and O-B equations of state are 0.648088 and 0.669, respectively, while it is 0.63558 for the Liu EoS (see Chapter 4). The middle and right plots show the variation of f with $\phi_c - \hat{\phi}$ for the three model GFLs using the Speedy and Liu EoS, respectively.

The middle and right panels of Figure 7-4 shows f for all three systems using Speedy and Liu equations of state. All f values fall on the exact same curve, regardless of the choice of EoS or the supercooled system, due to the strict one-to-one correspondence between f and $\hat{\phi}$. The same analysis for the dimensionless diffusivity is shown in Figure 7-5. Since both parameters f and $\hat{\phi}$ have a one-to-one correspondence with Δ in the HSP approach, the same variation is observed between Δ and $\phi_c - \hat{\phi}$ as is observed between f and $\phi_c - \hat{\phi}$.

A power law variation is observed for both f and Δ with the Speedy EoS (and O-B). Small deviations are observed for Liu EoS. The origin of the "bend" observed for the Liu equation of state is not known; However, we note that power law variation of Liu equation of state is eventually recovered below the "bend" observed in Figure 7-5 (also see Chapter 4); this will be more apparent for the analysis of experimental data later in this chapter.
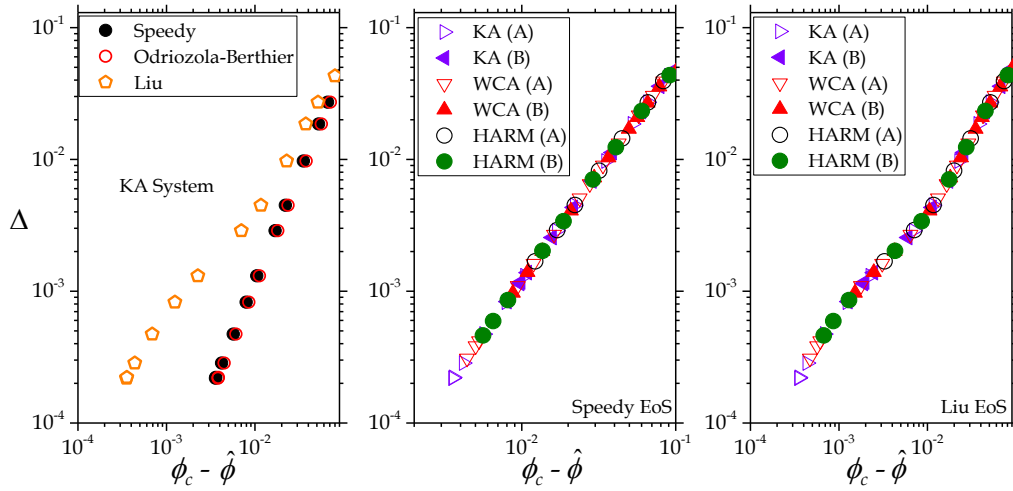
Figure 7-5: At left, the variation of the dimensionless diffusivity parameter with $\phi_c - \hat{\phi}$ for the KA system, using the three EoS. Speedy and Odriozola-Berthier produce very similar results. The middle and right plots show the variation of Δ with $\phi_c - \hat{\phi}$ for the three model GFLs using the Speedy and Liu EoS, respectively.
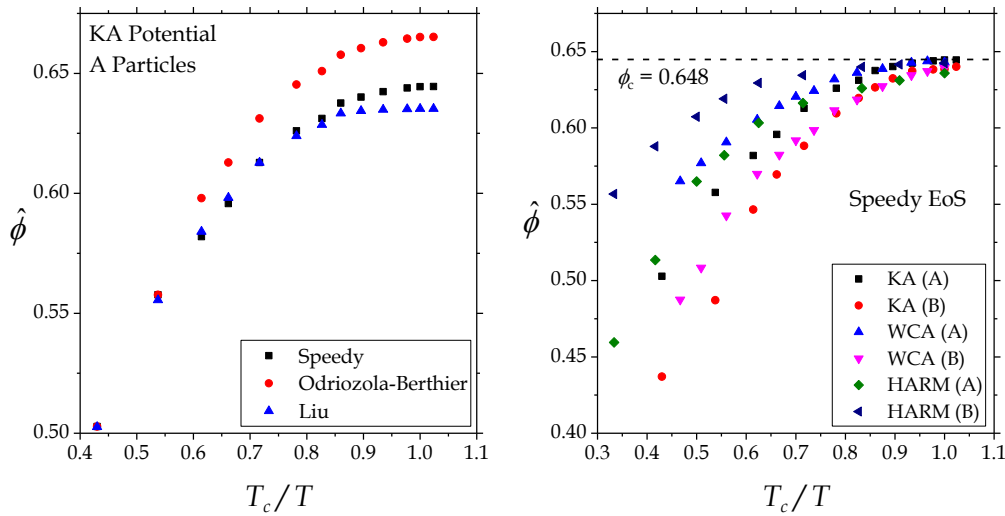
Figure 7-6: At left, the packing fraction $\hat{\phi}$ of the hard sphere partition, calculated for A particles in the Kob-Andersen potential using the Speedy, Odriozola-Berthier, and Liu equations of state. At right, $\hat{\phi}$ for both particle species of the three model GFLs using the Speedy EoS.

Figure 7-6 shows the predicted values of the effective packing fraction $\hat{\phi}$ associated with the hard sphere partition. The left panel shows how the three equations of state differ, which is mostly to say that the critical packing value $\hat{\phi}_c$ is different for each equation; all three demonstrate approximately the same behavior in approaching $\hat{\phi}_c$. The right panel shows results for the Speedy EoS for both particle species of all three model systems; note that rate at which the packing fraction approaches its maximal value differs among the systems and particle type. For all three systems, it is true that the smaller particle size (in terms of the ironic radius defined by the length scale of the potential energy function) exhibits a slower approach to $\hat{\phi}_c$ as temperature decreases; put another way, at a given temperature, the smaller particles in each system are said to be less jammed than the larger atoms as confirmed by the larger diffusivity od the B particles. In the context of thermal jamming, this is a critical piece of evidence, as it shows the method is able to qualitatively confirm a necessary requirement of characterizing the dynamical slowing down of atoms in GFLs.
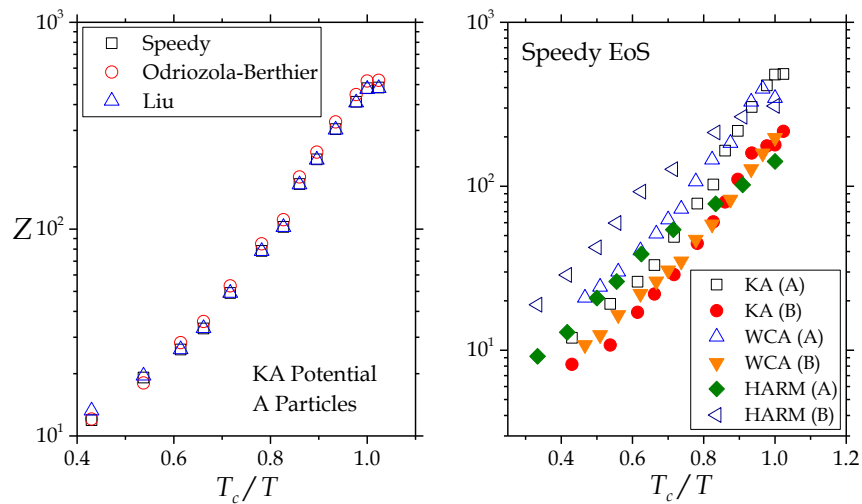
Figure 7-7:   The left panel shows the compressibility Z of the hard sphere partition for OTP using all three EoS. At right, the hard sphere compressibility for all eight liquids is plotted using the Speedy EoS.

The compressibility Z, depicted above in Figure 7-7 for the model GFLs, shows that it increases significantly as temperature decrease. It is not as clear that any particular value of Z is attained near T_c. The effective compressibility fZ may also be computed, as shown in Figure 7-8;

as discussed in Chapter 4, it saturates near a value of $4\hat{\phi}_c$ at the lowest temperatures. Further discussion of the implications of fZ with regards to thermal jamming is given at the end of this chapter. Given that $\hat{\phi}_c$ differs for each of the three EoS, the saturation levels out at slightly different values depending on the EoS used as can be seen in the left panel of Figure 7-8. For the Liu EoS, a small non-monotonicity is seen where fZ slightly exceeds $4\hat{\phi}_c$ before dropping to the expected asymptotic value (~2.54). It is likely this effect is a result of the mathematical complexity involved in Liu's EoS than a physical anomaly.
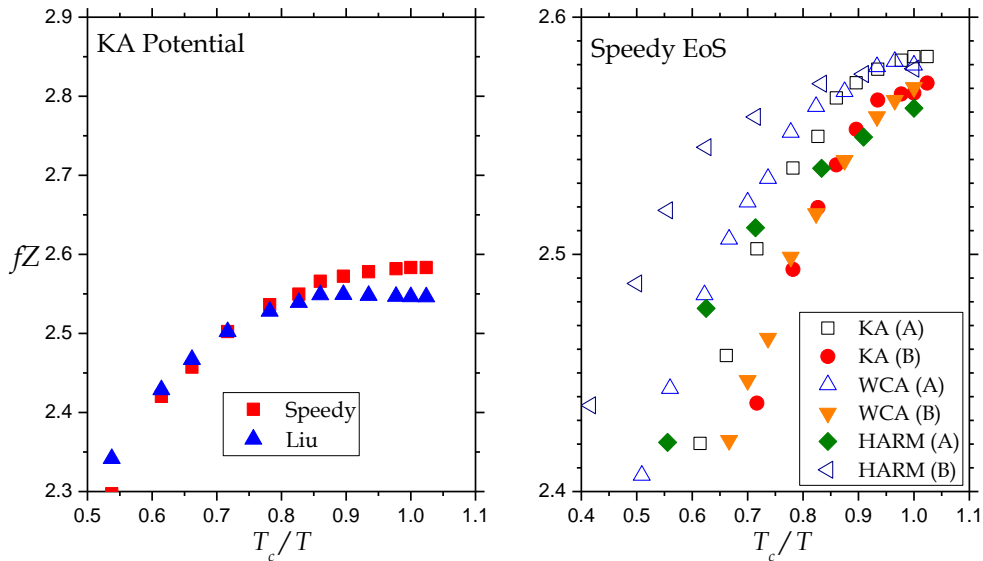
Figure 7-8:   At left, the effective compressibility fZ as a function of T_c/T for the KA system, using Speedy and Liu equations of states. For each EoS, the curves converge to nearly $4\phi_c$. The right panel shows the effective compressibility for three model liquids using the Speedy EoS.

7.1.B   Verification Using the Total Entropy Calculation

Since the HSP approach is based on the 2PT method, the framework of that method may be carried out to compute the total entropy for the model GFLs, which serves as an verification of the validity of the results subsequently presented in this chapter, and as a necessary but not sufficient condition for accepting the physical inferences from this analysis. However, the calculation of the total entropy for the model GFLs in this work present some additional

challenges that have not been previously addressed for the application of the 2PT method. This total entropy verification requires that the harmonic oscillator partition of the liquid be established in addition to the hard sphere partition; then, contributions from both partitions are summed to obtain the total entropy [187].

7.1.B.1   Ideal Gas Entropy and Planck's Constant

To compute the entropy contribution from the hard sphere partition of the liquid to the system total entropy, expressions for the ideal gas entropy and excess entropy for hard spheres are employed, so the total entropy of the hard sphere partition is $s^{HS} = s^{IG} + s^{EXC}$, where s^{EXC} is defined such that it is always negative (see Chapter 4). For application to the model GFLs, a problem is presented by the inclusion of Planck's constant in the expression for s^{IG} in this methodology (Equation 4.4.29). Interatomic potentials are usually designed so that within the MD code, a reduced system of units is used so that results are applicable to a family of real materials. When using realistic potentials that approximate the behavior of real materials, appropriate unit conversions between real (for example, S.I.) units and the reduced units used within the simulations are always defined so that reduced simulation output may be converted to the appropriate real units. Liquid Argon, for example, features a length conversion scale defined by $\sigma = 3.4$ Å and a temperature scale defined by $\epsilon/k_B = 120$ K, in addition to the mass conversion factor that is equal to the S.I. mass of Argon [199]. When results (thermodynamic properties, transport coefficients, etc.) are computed, the S.I. conversion factors are applied to transform the reduced results into physically realistic values.

The model supercooled liquids in this work were not necessarily intended to model realistic materials. For instance, the Kob-Andersen system is approximately based on a binary Lennard-Jones potential for amorphous $Ni_{80}P_{20}$ [111], but the potential parameters have been further adjusted (for the purpose of better avoiding crystallization) so that the KA system typically studied in the literature and in this work does not accurately describe that material. The WCA and HARM potentials only feature repulsive components; thus, none of these potentials can be associated with any realistic material. Consequently, the definition of unit conversion factors between reduced and real units is ambiguous. The lack of a clear heuristic for defining

109

realistic unit conversions for these model systems leads to some confusion as to the value of Planck's constant, h, which appears in the HSP/2PT Method in Equation 4.4.29. In this thesis, the reference material is taken to be Argon; there is precedent in the literature for studying Argon (monoatomic Lennard-Jones) that leads to $h^* = 0.185$ [212, 213], a value that is obtained by taking the energy and time unit conversions for Argon, $\epsilon = 1.67 \times 10^{-21}$J, $\tau = 2.14 \times 10^{-12}$ s. In reduced units, Planck's constant is then computed as follows:

$$h^* = \frac{h}{\epsilon\tau} = \frac{6.626 \times 10^{-34}\,\mathrm{J \cdot s}}{(1.67 \times 10^{-21}\,\mathrm{J})(2.14 \times 10^{-12}\,\mathrm{s})} = 0.185 \qquad (7.1.1)$$

We develop a method for choosing an appropriate value of h^* for a given model GFL as follows: both the magnitude and slope of the total entropy (computed as the sum of the hard sphere and harmonic oscillator contributions) changes depending on the value of h^*. An independent calculation of the total entropy can be obtained by integrating the heat capacity C_V. One begins by invoking the elementary thermodynamic relation,

$$dE = TdS - PdV \qquad (7.1.2)$$

Dividing both sides by the differential dT, and noting $dV/dT = 0$,

$$C_V = \frac{dE}{dT} = T\frac{dS}{dT} \qquad (7.1.3)$$

The total entropy is then obtained by integration,

$$S = \int \frac{C_V}{T} dT + S_{ref} \qquad (7.1.4)$$

The constant that results in the solution of the indefinite integral is a reference entropy, which can be taken to be zero and any other constant as appropriate. It is now posited that the most appropriate value of h^* for use in the HSP approach is the value that minimizes the root mean-squared error (RMSE) between the HSP total entropy and the total entropy obtained by integrating C_V. To achieve this, a set of entropy values are computed for temperatures between T_c and T_O for a range of h^* values, and all entropy data sets are scaled linearly so that the value at T_O is the same. Then, the RMSE is computed for all the HSP entropy data sets.

For the HARM system, a temperature scale $T^* = 10^{-4}T$ is used. This is a matter of convenience as the numeric values of the temperatures needed for the HARM system to achieve

glassy liquid dynamics are on the order of 10^{-4}. One may arbitrarily assume that the "real" temperature conversion is $T^* = 10^{-4}$ K. Using the S.I. value of k_B, the resulting energy scale is $\epsilon = 1.381 \times 10^{-19}$ J. Setting the time scale to a reasonable value of $\tau = 10^{-12}$ s results in

$$h^* = \frac{6.626 \times 10^{-34} \text{ J} \cdot \text{s}}{(1.381 \times 10^{-19} \text{ J})(10^{-12} \text{ s})} = 0.0048 \tag{7.1.5}$$

This value will serve as a starting value for our search of the correct value of h^* for the HARM system. Figure 7-9 shows how the total entropy varies for the three materials depending on the choice of h^*; the optimal choice of h^* is determined from Figure 7-10.
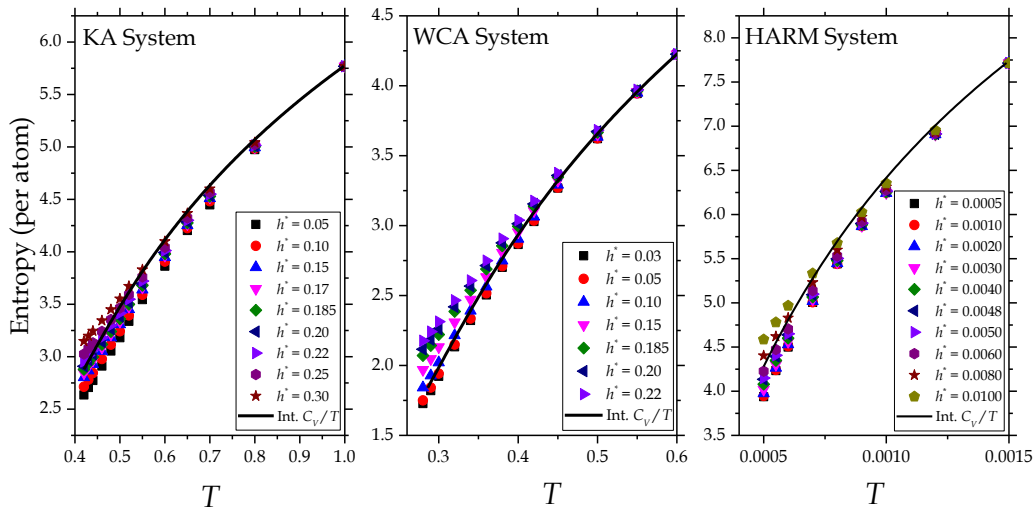
Figure 7-9: Entropy computed for the model GFLs using several values of h^* in the ideal gas entropy component.

Table 7-1: Optimal values of Planck's constant, in reduced units, for the three model GFLs.

Model System	Optimal Value of h^*
KA	0.22
WCA	0.10
HARM	0.008
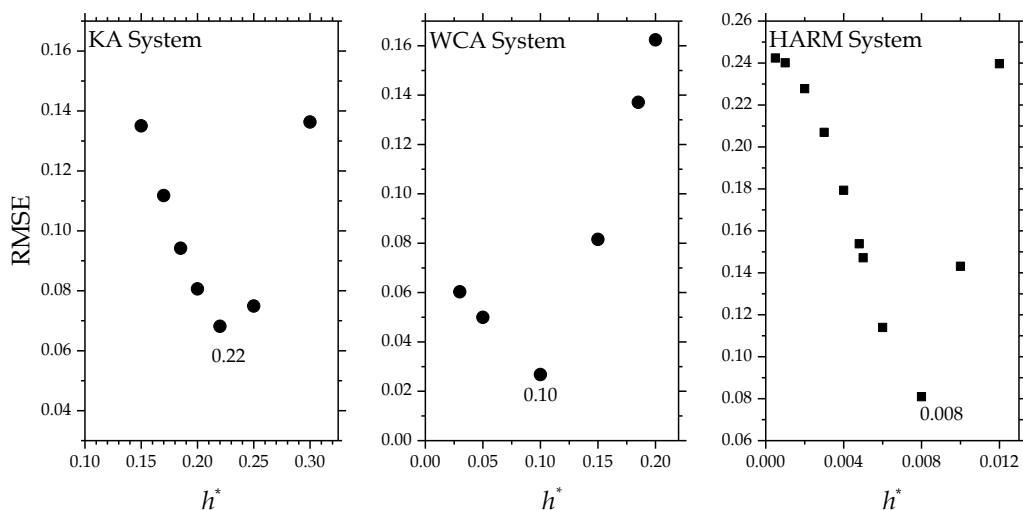
Figure 7-10:   For the KA, WCA, and HARM systems, the RMSE between the total entropy computed using the integral of C_V/T to the total entropy computed by the 2PT Method using a range of h^* values. Clear minima are observed for each system that determines the optimal value of Planck's constant.

With a solution to the unique problem of how to handle Planck's constant in the HSP approach for model GFLs in hand, the total entropy calculation can proceed. The ideal gas entropy of the hard sphere partition, s^{IG}, and the ideal gas contribution from the hard sphere partition to the total entropy, $S^{IG} = f s^{IG}$, is depicted for the model systems in Figure 7-11, where h^* has been set to the values in Table 7-1 for each of the model systems. The ideal gas entropy is computed at the density of the hard sphere partition, $f\rho$ – not the density ρ of the actual liquid system. This leads to the seemingly counterintuitive result in which s^{IG} increases with decreasing temperature. This is due to the corresponding decrease of the hard sphere component's density, which offsets the decrease in temperature by creating an increasingly effuse HS gas of higher entropy.

When s^{IG} is multiplied by f to obtain the ideal gas contribution from the hard sphere component to the total entropy, S^{IG} does show a decrease with decreasing temperature. By taking the product of f and s^{IG}, the ideal gas entropy now corresponds to the whole system.
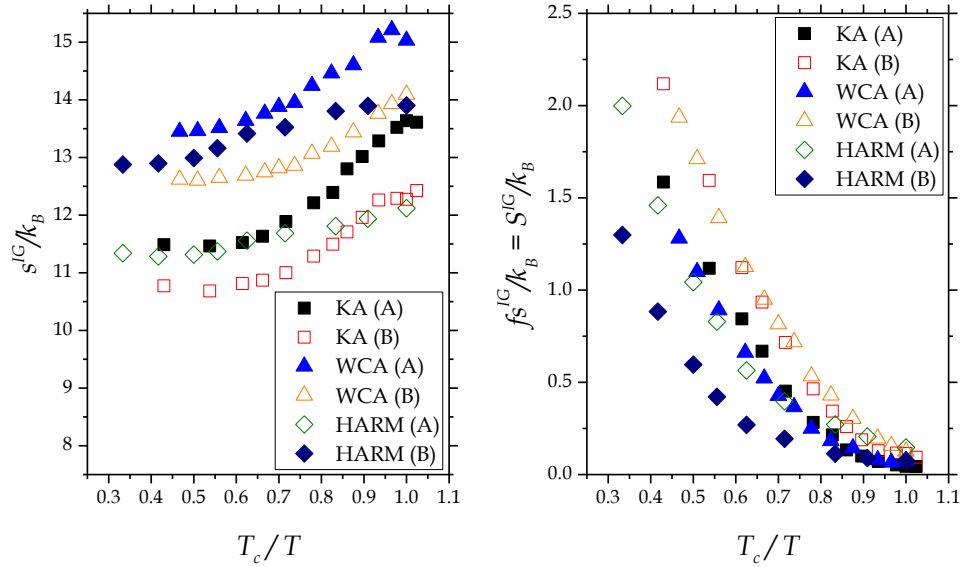
Figure 7-11: The left plot shows a comparison of the ideal gas entropy s^{IG}/k_B of the hard sphere partition (per atom) for the three model GFLs, for A and B particles separately. At right is the contribution of the hard sphere partition's ideal gas entropy to the total entropy, $S^{IG}/k_B = f s^{IG}/k_B$. For this data, the Speedy EoS is used; results with the Odriozola-Berthier and Liu EoS are similar.

7.1.B.2   Verification of Total Entropy

Given the appropriate consideration of Planck's constant in the ideal gas entropy calculation for the model GFLs, the total entropy analysis may be carried out. The following plots (Figure 7-12 and Figure 7-13) show comparisons of the total entropy computed using the HSP approach with the independent calculation of total entropy using the internal energy of the system, for the three model GFLs. For the time being, only the total entropy is presented; in the next section, a discussion of the various contributions to the total entropy is described.

For the KA system, the total entropy using $h^* = 0.22$ matches very well to independently-obtained results presented by Kob, Sciortino, and Tartaglia in the literature (Figure 7-12). This agreement holds from the onset temperature T_O down to the mode-coupling temperature $T_c = 0.43$. For the WCA and HARM systems, the total entropy computed with the HSP approach is compared against the self-consistent (integral of the) specific heat data from independent MD simulations in Figure 7-13.

113
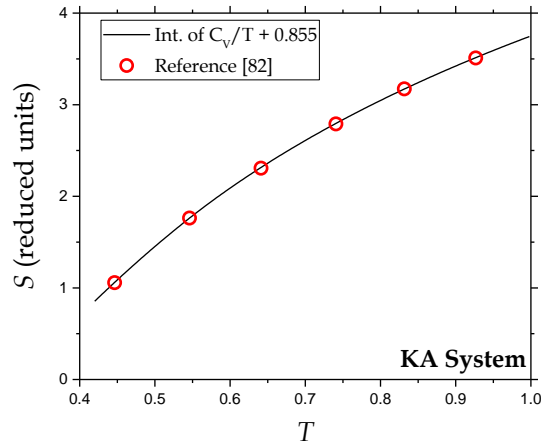
Figure 7-12: A comparison of the total entropy computed from MD simulations of the KA system computed by taking the integral of C_V/T (Equation (7.1.4)). Open circles represent the results from Sciortino, Kob and Tartaglia [82], and the solid line represents the result from this thesis. The total energy is computed at very fine temperature intervals of $\Delta T = 0.002$.

As can be seen in the preceding figures, the 2PT Method with the inclusion of more accurate hard sphere equations of state can accurately compute the total entropy of the model GFLs. A demonstration of this methodology's accuracy has previously not been established for dense fluids. It is possible that others had undertaken such analysis previously but were unsuccessful, as the Carnahan-Starling EoS used in the 2PT Method breaks down at high densities of the hard sphere partition, leading to non-physical results for fluids where f is small. The inclusion of hard sphere EoS (Speedy, Odriozola-Berthier, Liu) that are more accurate in the regime of dense hard spheres allows for this accurate calculation of the entropy. This development, on its own, serves as an important contribution to the field of liquid physics, as to our knowledge the 2PT approach in the literature has not been modified to incorporate EoS other than the Carnahan-Starling EoS. Other modifications have been made in the literature to the methodology that have modestly improved its accuracy for fluids in general [191, 214], but these modifications have only been demonstrated for less dense liquids. A consequence of this work, which primarily strives towards establishing thermal jamming in dense fluids, is a practical improvement of the 2PT Methodology for computing thermodynamic properties of glass-forming liquids.

114
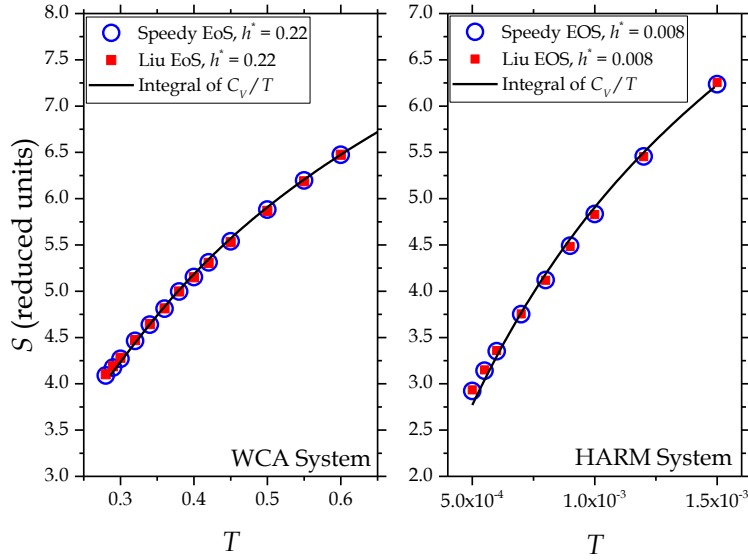
Figure 7-13:   (left panel) for the WCA system, comparison of the total entropy computed by the HSP approach using the Speedy (triangles) and Liu (circles) equations of state with $h^* = 0.22$ to the relative entropy computed by integration of the heat capacity obtained from MD simulations. (right pabel) The same data the HARM system with $h^* = 0.008$. For both systems, the entropy calculated by the HSP method has been shifted to match the value obtained from the heat capacity at the highest studied temperature.

As an analysis of thermal jamming in GFLs is the primary scope of this work, the total entropy calculation is not a goal in itself, but it is critical to demonstrate that this methodology is accurate via comparison to independently-obtained results, as the objective in the following sections is to attribute physical significance to the excess entropy of the hard sphere partition. The following section provides an analysis of the ideal gas and excess entropy as they contribute to the hard sphere partition's total entropy.

7.1.C   Excess Entropy of the HS Partition

As defined earlier, excess entropy that is considered in this thesis is the difference between the HS entropy and the ideal gas entropy $s^{EXC} = s^{HS} - s^{IG}$; as defined, s^{EXC} is always negative. The excess entropy of a hard sphere system at constant density is computed as

$$s^{EXC} = -\int_0^{\hat{\phi}} \frac{Z(\eta)-1}{\eta} d\eta \qquad (7.1.6)$$

Note that in the above expression, a dummy variable η is used, and the upper bound of the integral is evaluated at the hard sphere partition packing fraction $\hat{\phi}$. Analytic solutions to Equation 7.1.6 can be constructed for different equations of state; these were also verified through numerical means (results not shown).

Numerical values of s^{EXC} are delineated for the KA system (Figure 7-14), WCA system (Figure 7-15), and the HARM system (Figure 7-16) below, using the Speedy and Liu equations of state. The Odriozola-Berthier EoS produces results very similar to those computed using the Speedy EoS. This calculation of the excess entropy of the hard sphere component provides a basis for the examination of excess entropy scaling (EES) in model GFLs, but its application in this work differs from what has been previously undertaken in the literature as the excess entropy is only calculated for a subset (the hard sphere partition) of the liquid, as opposed to the whole liquid. Recall that the critical input to the HSP approach, is the diffusion coefficient of the liquid and the EoS, in addition to the liquid's temperature and density. The jamming metrics (f, $\hat{\phi}$) are computed entirely in terms of these inputs, and all the components of the hard sphere partition's entropy are computed in terms of these metrics.
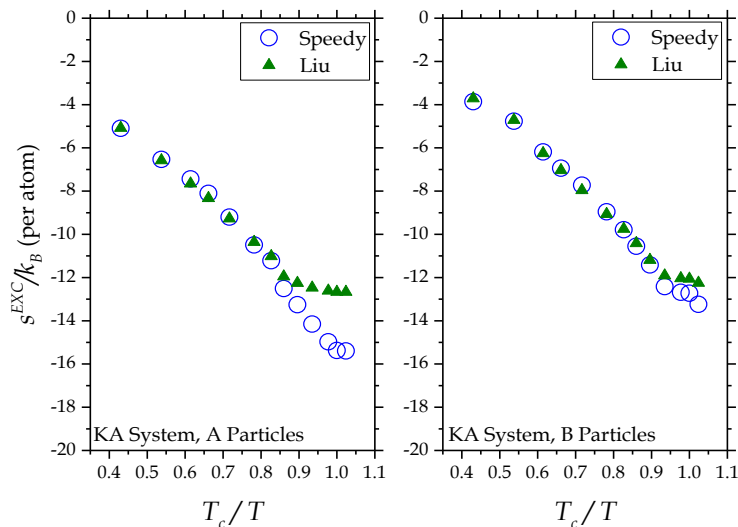
Figure 7-14: For the KA system, the excess entropy of the hard sphere component s^{EXC}. The left panel is for A particles and the right panel is for B particles.
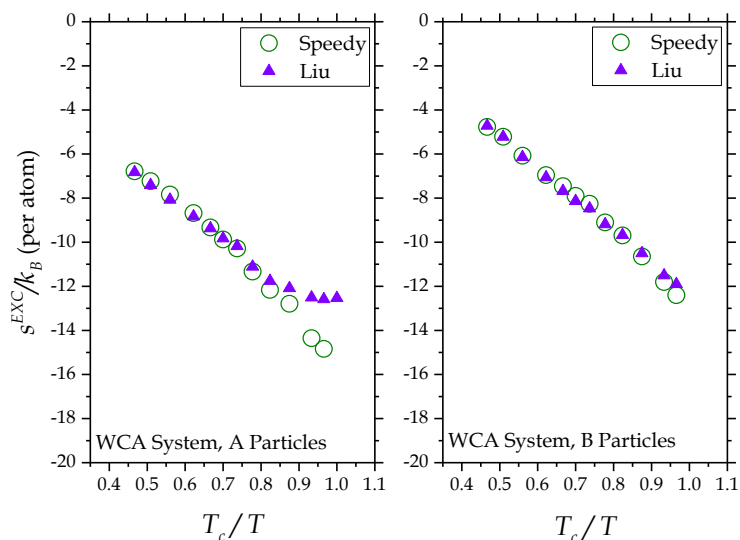
Figure 7-15: For the WCA system, the excess entropy of the hard sphere component s^{EXC}. The left panel is for A particles and the right panel is for B particles.
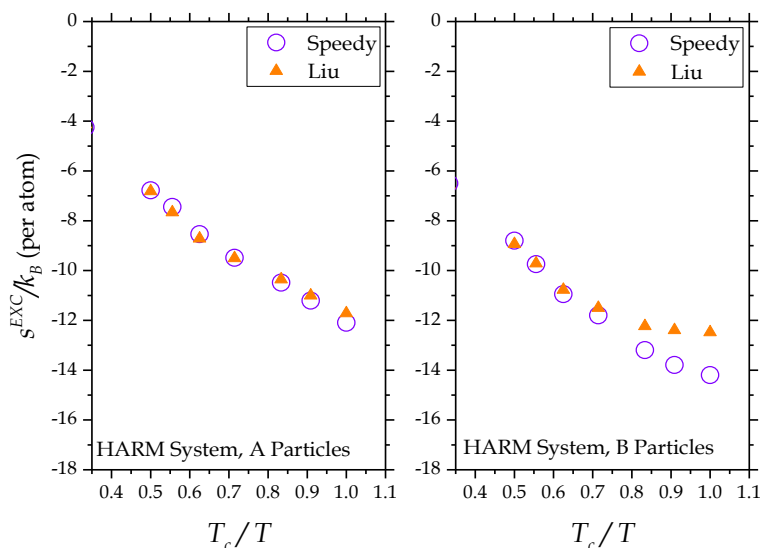
Figure 7-16: For the HARM system, the excess entropy of the hard sphere component s^{EXC}. The left panel is for A particles and the right panel is for B particles.

It is interesting to note the larger difference in the results for the excess entropy between the Speedy (which we consider effectively identical to that of Odriozola-Berthier) and Liu EoS,

evident in Figure 7-14 through Figure 7-16 at temperatures close to T_c. As mentioned earlier, the functional complexity and parameters of large magnitude involved in the Liu EoS may have resulted in a leveling-off of the excess entropy not seen using the Speedy form. This behavior's effect on the system-normalized entropy, however, is relatively miniscule, as will be demonstrated. This is mostly due to the diminishing contribution of the hard sphere component's entropy to the total entropy, relative to the harmonic oscillator partition's contribution.
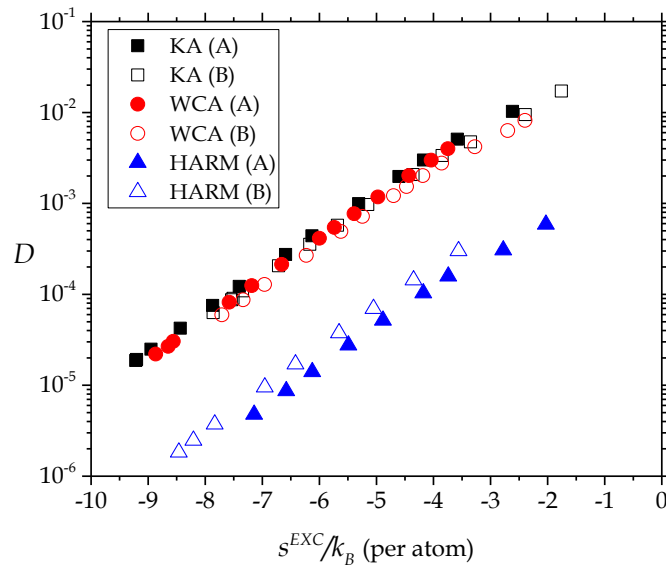
Figure 7-17:   The diffusion coefficient (A and B particles) of the model GFLs plotted as a function of the respective excess entropy per atom of the corresponding system. The KA and WCA systems exhibit similar diffusivities that both differ significantly from that of the HARM system. Note that D does not show a universal scaling behavior.

The temperature variation of the diffusion coefficients of the three model GFLs as a function of the hard sphere component's excess entropy s^{EXC} is shown in Figure 7-17. The KA and WCA systems, which share similar potential functions and parameters, cluster together, but the scale of the HARM system's potential parameters establishes distinctly smaller diffusion coefficients for that system compared to the other two. Note that there is no universal scaling behavior for the diffusion coefficient. However, the non-dimensional diffusivity Δ (see Chapter 4) does indeed portray a universal Rosenfeld (exponential) scaling behavior with excess entropy s^{EXC} as shown in Figure 7-18.
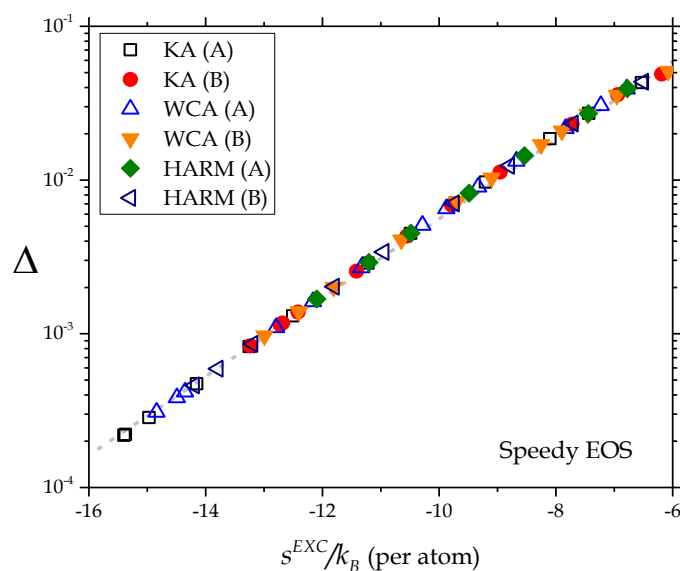
Figure 7-18: The dimensionless diffusivity for the model GFLs, with A and B particles plotted separately, as a function of the excess entropy per atom of the hard sphere component (computed using the Speedy EoS). A universal Rosenfeld (exponential) scaling behavior can be observed with s^{EXC} for all systems

Excess entropy scaling is thus observed for the hard sphere components of the model GFLs in a manner similar that that presented by Dyre [180], and critically, strict adherence to a single master curve is exhibited by all three systems for both particle species. Of worthy consideration is the fact that the values of the excess entropy for the hard sphere component of the model GFLs are of similar magnitude to those obtained in the literature for similar systems using different methodologies [180], but are of course computed in an entirely different fashion. We reiterate that the physical interpretation of the hard sphere component excess entropy is distinct from that which has been previously calculated for liquids by subtracting the ideal gas entropy of a liquid from its total entropy.
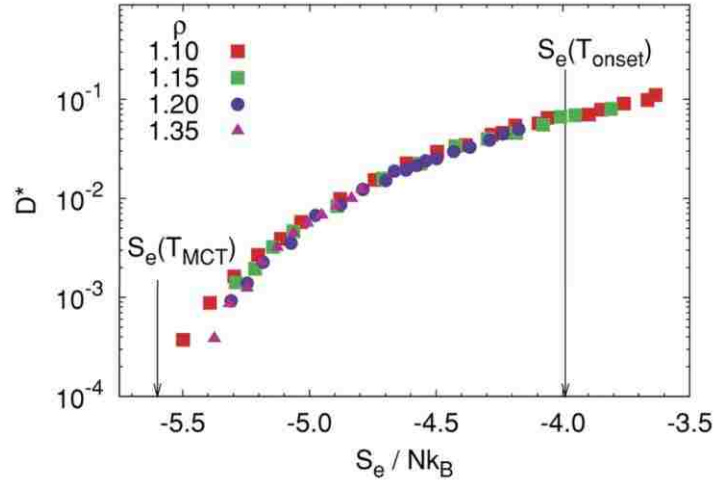
Figure 7-19:   Excess entropy scaling for the Kob-Andersen system; the figure is reproduced from [180]. Limited non-exponential scaling is observed among various densities until near the mode-coupling temperature $T_c = 0.43$.

Compared to data collected by Dyre for the Kob-Andersen system in Figure 7-19, the HSP method's s^{EXC} shows some notable differences; it shows strict expoential variation, or Rosenfeld scaling, while literature data for the same material exhibits limited non-exponential scaling with excess entropy with the scaling breaking down near T_c. In contrast, s^{EXC} computed by the HSP method shows strict scaling for the entire temperature range. Also, the magnitude of s^{EXC} is larger than what is observed in the literature. Note that the physical interpretation of these excess entropies is not the same, s^{EXC} applied only to a small subset of the atoms while the data in Figure 4-19 is for the whole system.

7.1.D   Excess Entropy Scaling with the System-Normalized Entropy S^{HS}

As noted previously, we have posited that the entropy associated with the hard sphere component may be converted to the appropriate corresponding variable for the whole system by multiplying by the partitioning metric f (see Chapter 4). Of concern in this section is the physical interpretation of the excess entropy of the hard sphere component as translated to apply to the whole system. By multiplying the hard sphere excess entropy by the partitioning metric f, the contribution of the hard sphere system's normalized excess entropy is established. This is not

equivalent to the excess system entropy that is generally computed for liquids [180], where the total entropy of the liquid is computed by taking the temperature integral of the $C_{V,P}/T$, and subtracting the entropy of the ideal gas computed at the same temperature and density. Strict universal behavior is also evident in S^{EXC} as shown in Figure 4-20; this follows from the fact that since s^{EXC} shows universal behavior, and s^{EXC} is computed in terms of the partitioning metric f, then $f s^{EXC} = S^{EXC}$ must show universal behavior as well.
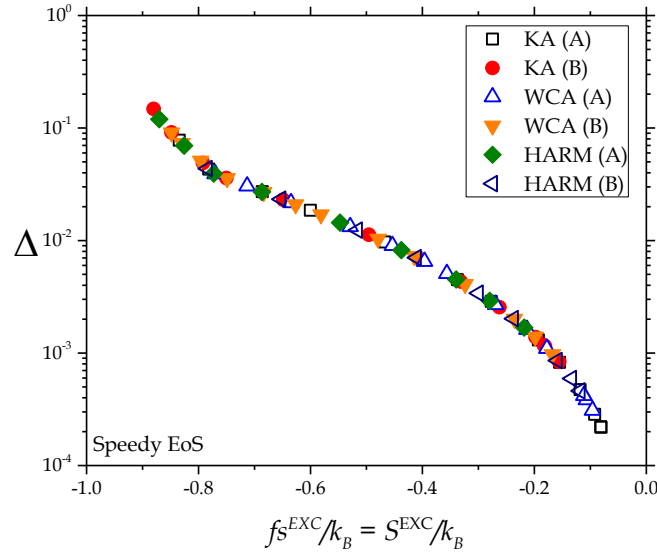
Figure 7-20:   The reduced diffusivity Δ plotted as a function of the system-normalized excess entropy $f s^{EXC}/k_B = S^{EXC}/k_B$. A and B particle species are plotted separately for the three model GFLs. The Speedy EoS is used to compute this data.

One may then proceed to analyze the entropy of the hard sphere partition computed as $S^{HS} = S^{IG} + S^{EXC}$, where $S^{IG} = f s^{IG}$ and $S^{EXC} = f s^{EXC}$. When the dimensionless diffusivity parameter Δ is plotted as a function of S^{HS}, entropy scaling is not observed (Figure 7-21). It does not show strict enough adherence to a single curve to indicate universal or quasi-universal behavior; this is acceptable as there is no known theoretical basis for claiming that scaling should be observed for anything other than the excess entropy. The ideal gas entropy s^{IG}, which is not computed strictly in terms of the partitioning metric like s^{EXC} and depends on the thermodynamic state of the liquid, is the source of the absence of scaling behavior in S^{HS} that is observed strictly for s^{EXC}.

121
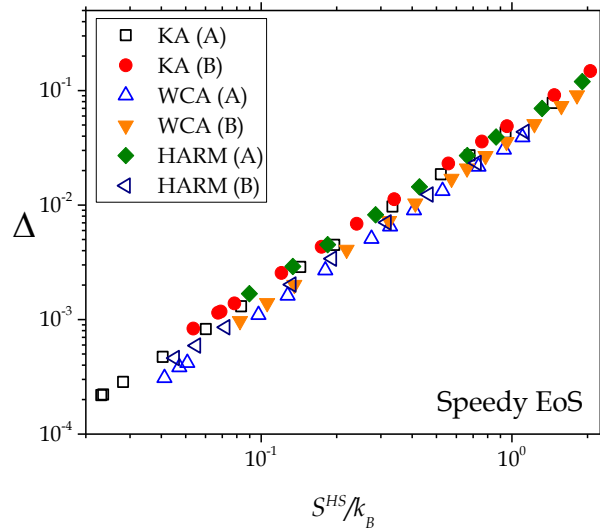
Figure 7-21:   The dimensionless diffusivity plotted as a function of the entropy of the hard sphere partition S^{HS}, for the model GFLs (A and B particles plotted separately). The Speedy EoS is used to calculate these values.

7.1.E   Components of Total Entropy

In the following sections we present the total entropy components of the whole system, which includes the HO and HS contributions. The HO contributions are evaluated as outlined by LBG in the original reference [187]. As is demonstrated in Figure 7-22 for the KA system, the total entropy is mostly dominated by the harmonic oscillator contribution at low temperatures near T_c – this holds for the other two model GFLs as well. We will briefly discuss how the entropy components may be related to the configurational entropy S_c. It would appear that S^{HS} component may be a measure of S_c but there is not clear evidence for either from a theoretical point of view or numerical results. Further verification beyond the scope of this work is needed to confirm or reject the possibility that the hard sphere entropy of the HSP method approximates the configurational entropy.
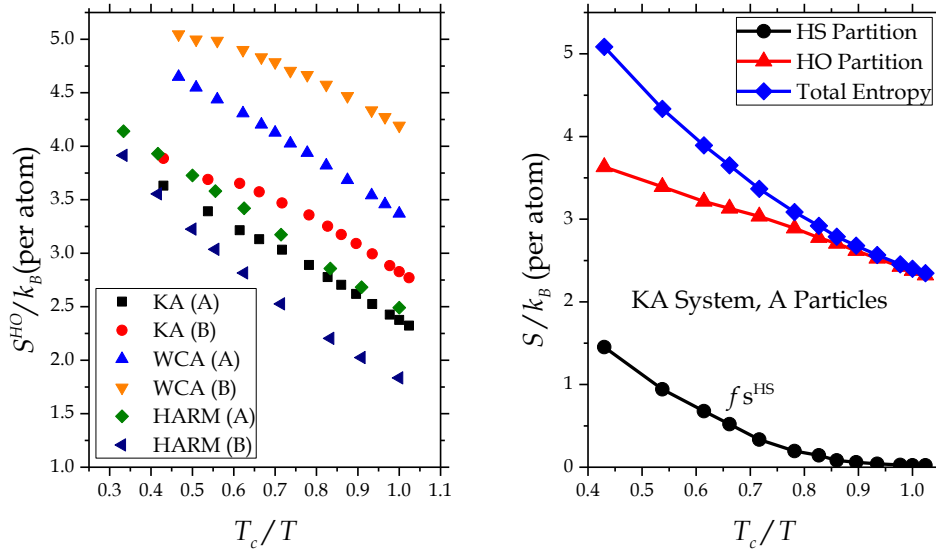
Figure 7-22: The left panel shows the entropy of the harmonic oscillator partition computed for the three model GFLs, with A and B particles plotted separately. The right panel shows the hard sphere, harmonic oscillator, and total entropy for A particles in the Kob-Andersen system down to the mode-coupling temperature $T_c = 0.43$.

The first-ever application of the HSP/2PT approach to model supercooled liquids in this work drives home the already dramatic conclusion – that the hard sphere partition becomes increasingly small as the dynamics of the liquid slows, and the harmonic oscillator partition dominates the total entropy of the liquid. The model supercooled liquids in this work exhibit partitioning that is significantly smaller than the already small values in the vicinity of 0.3 obtained for simple liquids such as molten KCl [188]. It bears repeating that the incorporation of more accurate hard sphere EoS in the metastable region of the hard sphere phase diagram makes the accurate analysis of these dense liquids possible, and no significant work has been previously published applying the 2PT Method to such liquids.

In terms of glass theories, the HSP approach is effectively silent on what happens at the significant temperatures associated with the onset of glassy dynamics, such as T_S and T_c. It is approximately true that the parameters of the liquid, such as $\hat{\phi}$ and f, generally level off in the vicinity of T_c, but as these parameters are tied to the diffusivity Δ of the system, no behavior would be revealed that could not have been seen in the temperature variation of D. The HSP approach does indicate that as model supercooled approach the mode-coupling temperature, the

thermodynamics is very well described by the harmonic oscillator partition and the significance of the hard sphere partition diminished, although it never disappears as long as the liquid has non-zero diffusivity. The small but non-zero diffusivity near T_c, which results in a correspondingly small contribution from the hard sphere partition to the total entropy which is dominated by the harmonic oscillator partition, serves as an illustration of the thermal jamming that occurs in supercooled liquids and GFLs, since the non-zero diffusivity indicates that atoms are still free to diffuse by increasingly rare cage-breaking while the system becomes increasingly dynamically-arrested.

There is a further application of the HSP approach that deviates from this application to molecular dynamics simulations and seeks to expand upon it. The HSP approach can be applied to materials where solely the diffusion coefficient and information about the liquid state are provided. One issue with this approach is that the lack of detailed dynamical history that would normally be provided by simulations precludes the calculation of the total entropy for such systems. On the other hand, we have at our disposal a trove of experimental data for GFLs in the literature for which transport coefficients have been measured across the whole temperature range of glassy dynamics, from the onset temperature T_O to below T_g. This analysis proceeds in the following section.

Section 7.2   Analysis of Experimental Data

Recall that for the HSP method, all that is needed to completely determine the extent of the hard sphere partition, as well as all characteristics of the hard sphere partition, is the dimensionless diffusivity parameter Δ, which may be computed in terms of the diffusion coefficient, temperature, and density of a liquid. Previously in this chapter, materials have been studied using input from molecular dynamics simulations, but the power of the partitioning method outlined in this work is that it need not be limited to computational studies, and provides a straightforward approach of studying liquids where only D and thermodynamic information is provided. In this section, the method is applied to data for real supercooled liquids whose transport properties have been reported in the literature.

This section employs literature data for eight GFLs: silica (SiO_2), glycerol ($C_3H_8O_3$), diopside ($MgCaSi_2O_6$), toluene (C_7H_8), o-terphenyl ($C_{18}H_{14}$), salol ($C_{13}H_{10}O_3$), boric oxide (B_2O_3), and n-Propanol (C_3H_8O). References to the literature data used for these materials are presented in Table 7-2. By using the diffusion coefficient, the dimensionless diffusivity Δ can be computed for each material, which allows for the subsequent calculation of f and $\hat{\phi}$. For computing the density (which is an input for computing Δ) for the experimental GFLs, the temperature-dependence of the density of the GFLs is calculated by the formula [215]

$$\rho(T) = \rho_g \left[1 - \alpha_l^0 (T - T_g) \right] \tag{7.2.1}$$

Here, ρ_g is the density of the liquid at T_g and α_l^0 is the thermal expansion coefficient of the liquid. The values used for the parameters in Equation (7.2.1) are provided in Table 7-2 and plots of $\rho(T)$ data are shown in Figure 7-23; given the values of α_l^0 obtained from the literature for these eight materials, the density changes only slightly throughout the range of temperatures studied. Note that the above equation allows to estimate the GFL density at any temperature; Figure 7-23 shows only the density data pertinent to the analysis.

Table 7-2: Input for the analysis with experimental GFLs. The references associated with each material in the leftmost column are where the viscosity data is obtained.

GFLs	T_g (K) [50]	T_c (K)	ρ_g (kg m^{-3})	R (nm)	α_l^0 (K^{-1})
Silica [215]	1480	1613	2200 [216]	0.174	0.0003 [217]
Glycerol [215]	188	249	1332 [216]	0.237	0.0005 [218]
Diopside [215]	995	1178	3220 [219]	0.235	0.000008 [219]
Toluene[215, 220]	117	160	857 [221]	0.258	0.000929 [215]
Salol [215, 222]	220	268	1268 [216]	0.311	0.0005 [223]
OTP [222]	240	290	1111 [216]	0.340	0.000605 [224]
Boric Oxide [225]	550	800	1792 [226]	0.186	0.0000135 [227]
Propanol [228]	96	138	800 [228]	0.219	0.000995 [229]

We compute the diffusion coefficient using literature data for the viscosity of the materials, obtained from [215, 220, 222], and a combination of the Stokes-Einstein relation (SER) and the fractional SER, which has been observed to hold for GFLs below T_c [50]. The fractional SER is given by

$$D = \frac{k_B T}{6\pi R \eta^\gamma} \tag{7.2.2}$$

where η is the viscosity and R is the average hydrodynamic or ionic radius. Setting the exponent $\gamma = 1$ yields the SER, and setting $\gamma = 0.85$ yields the fractional-SER. The values of the average ionic radius for the selected GFLs [215] and are listed in Table 7-2. Viscosity data is used instead of direct diffusion coefficient data as the experimental methods employed to measure viscosity typically allow for data to be obtained over a broader temperature range that comfortably encompasses both T_g and T_O. Plots of the viscosity for the GFLs are shown in Figure 7-24. In most cases, the temperature ranges of the experimental data ranges approximately from the mode-coupling temperature T_c to very close to T_g.
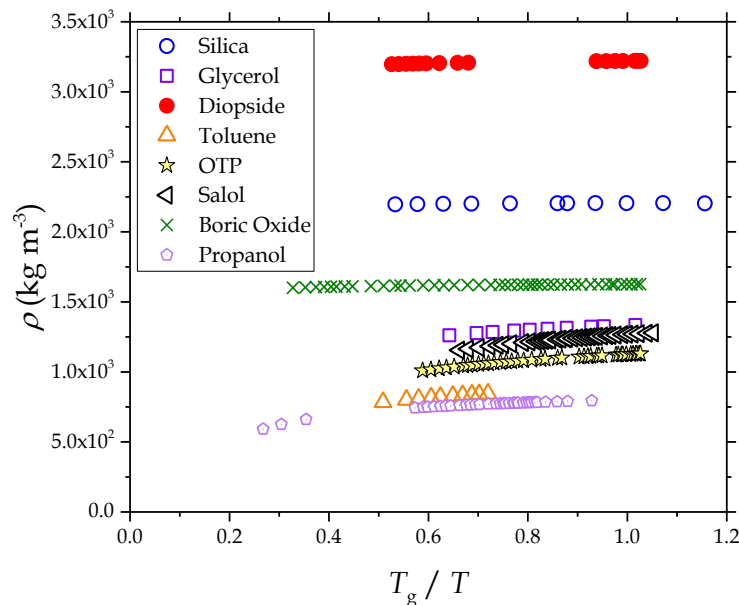
Figure 7-23:   The temperature-dependence of the density for the experimental GFLs. The chosen temperatures correspond to those where viscosity data is available.

Table 7-3: For the eight GFLs studied in [215], the chemical formula and bond type.

GFLs	Chemical Formula	Bond Type
Silica	SiO_2	Covalent
Glycerol	$C_3H_8O_3$	Hydrogen
Diopside	$MgCaSi_2O_6$	Covalent
Toluene	C_7H_8	Van der Waals
Salol	$C_{13}H_{10}O_3$	Hydrogen, Van der Waals
OTP	$C_{18}H_{14}$	Hydrogen, Van der Waals
n-Propanol	C_3H_8O	Hydrogen, Van der Waals
Boric Oxide	B_2O_3	Covalent

The eight experimental GFLs featured in this work exhibit the entire range of fragility (the viscosities of the materials are depicted in Figure 7-24) and feature molecules that interact with a variety of bond types (listed in Table 7-3).
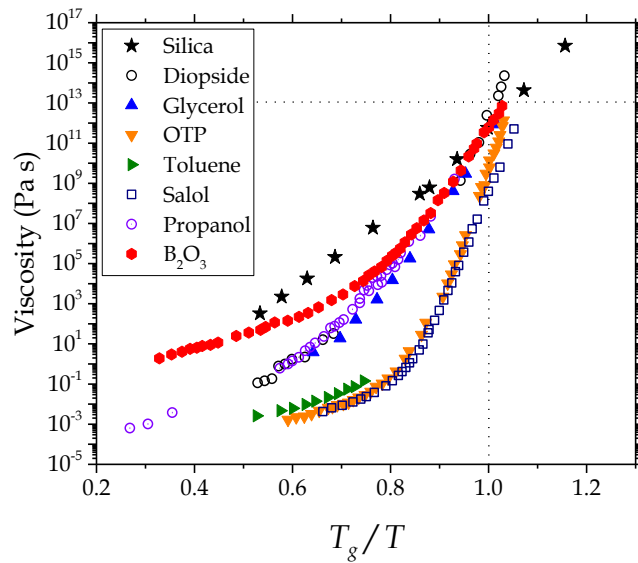
Figure 7-24: The viscosity of the experimental glass-forming liquids used in this thesis. The dotted vertical line indicates the experimental glass transition temperature T_g at which the GFLs attain a viscosity of $10^{13}\ Pa.s$.
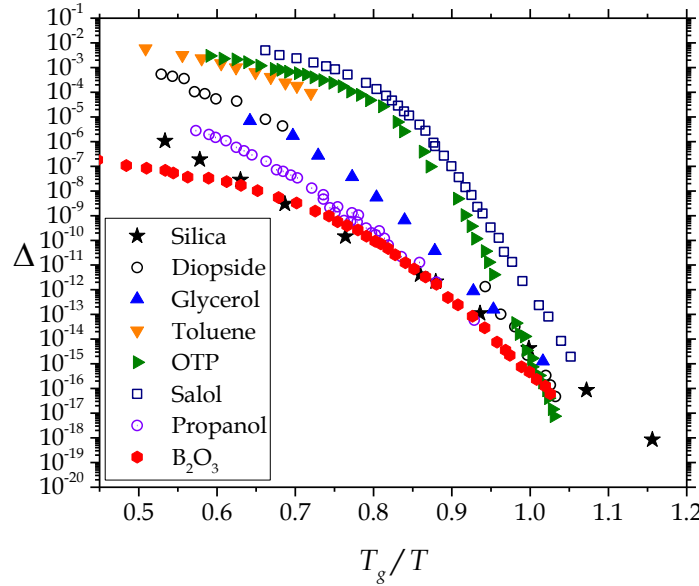
Figure 7-25: The dimensionless diffusivity Δ for the experimental data, computed using the viscosity in conjunction with the Stokes-Einstein relation. For temperatures above T_c, the regular Stokes-Einstein Relation is used, and the fractional SER = 0.85 is used below T_c. When available, the calculated diffusion coefficients are compared to independent literature data and sufficient agreement is found.

7.2.A Dynamical Characteristics of the Hard Sphere Partition

Figure 4-25 shows the non-dimensional diffusivity of the selected GFLs evaluated with the Stokes-Einstein relationship. Much of the analysis that was conducted for the simulations of model supercooled liquids may be readily repeated for the analysis of experimental GFLs. First, the variation of Δ and f with temperature is shown in Figure 7-26. At T_g, f for all the materials approaches approximately 10^{-10}; this was not achievable for the simulated GFLs, and allows the association of a particular partitioning value that is commensurate with the glass transition, much in the same way that T_g is arbitrarily defined by a viscosity value of $10^{12}\ Pa \cdot s$. Given that significantly lower temperatures are attainable using the experimental GFLs versus the model

GFLs studied by atomistic simulations, the partitioning metric is observed to attain correspondingly small values.
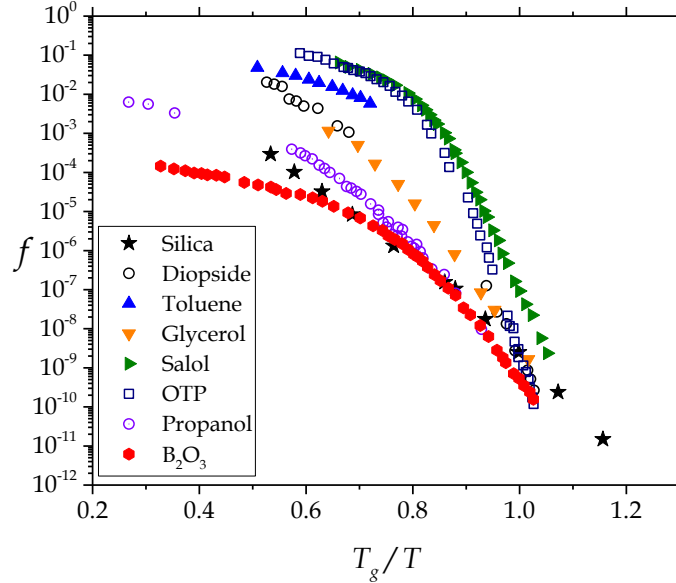
Figure 7-26: The partitioning metric f as a function of T_g/T for the experimental GFLs using the Speedy EoS.

The partitioning metric for the experimental GFLs exhibits power law variation with $\phi_c - \hat{\phi}$, shown in Figure 7-27. At higher temperatures near T_O, Liu's EoS predicts values that approach the Speedy and Odriozola-Berthier equations of state. These results show clearly how the slope of this variation for Liu's EoS also approaches that of the other two equations of state when plotted on a log-log scale. The functional form of the variation of f with $\phi_c - \hat{\phi}$, does not change relative to that which is observed for the model systems, but the lower temperature range accessible with the experimental data allows the analytic curve to proceed significantly further into the power-law regime for the Liu EoS – and far past the "bend" that corresponds with the low-temperature limit (near T_c) for the model GFLs - as depicted in Figure 7-27. The same analysis for the dimensionless diffusivity is shown in Figure 7-28. The universality of the dynamical properties of the hard sphere partition is therefore verified down to below the glass transition temperature.
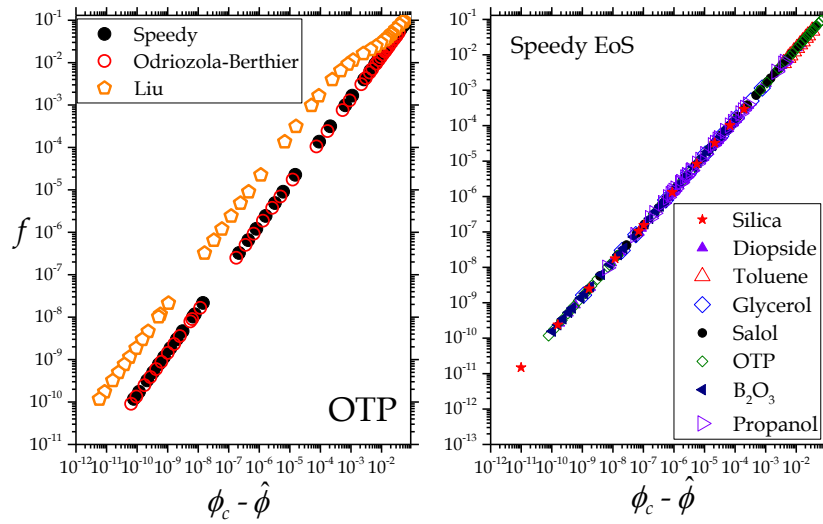
Figure 7-27: At left, the variation of the partitioning metric with $\phi_c - \hat{\phi}$, for OTP, using the three equations of states. Speedy and Odriozola-Berthier produce very similar results. At right, the variation of f with $\phi_c - \hat{\phi}$, for all experimental GFLs, using the Speedy EoS.
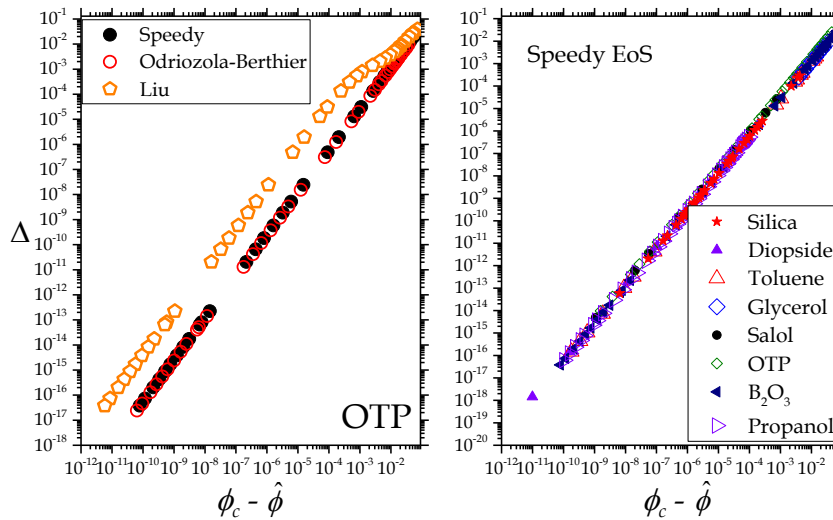
Figure 7-28: At left, the variation of the dimensionless diffusivity parameter with $\phi_c - \hat{\phi}$ for OTP, using the three EoS. Speedy and Odriozola-Berthier produce very similar results. At right, the variation of Δ with $\phi_c - \hat{\phi}$ for all experimental GFLs, using the Speedy EoS.
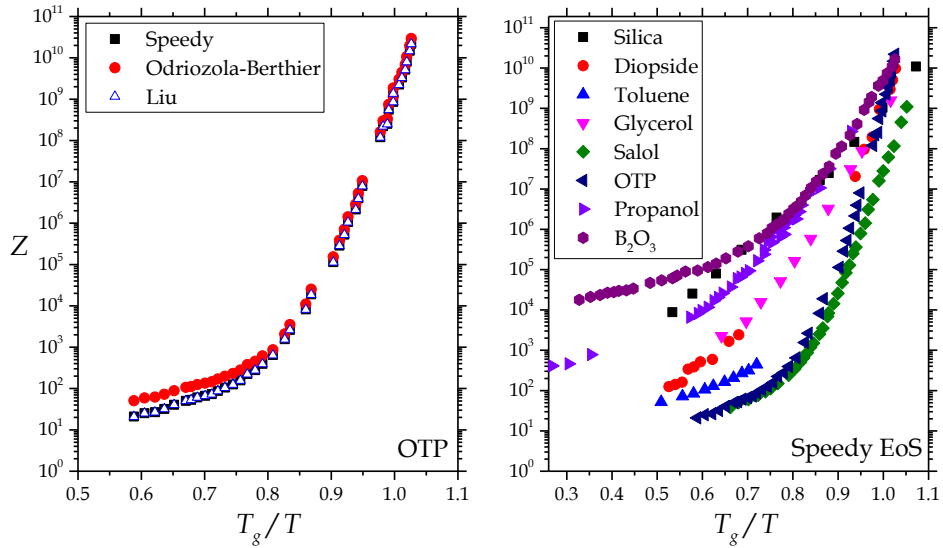
Figure 7-29:   The left plot shows the compressibility Z of the hard sphere partition for OTP using all three EoS. At right, the hard sphere compressibility for all eight liquids is plotted using the Speedy EoS.

Similar to the dynamical properties, the compressibility Z (shown in Figure 7-29) changes significantly as the GFLs approach the glass transition temperature. It appears Z attains a value of $\sim 10^{10}$ near T_g, which are significantly larger than the values observed by Berthier and Witten for hard spheres [144], although the interpretation of these results are not the same; the high Z values shown above are only a small number HS atoms that exist at temperatures close to T_g. The effective or system-normalized compressibility fZ which is shown in Figure 7-30 for the experimental GFLs saturates at a value of $\sim 4\phi_c$ at the lowest temperatures for all systems. For the more fragile GFLs, this saturation occurs approximately at the mode-coupling temperature, whereas for less fragile liquids (propanol and B_2O_3, in particular) this convergence occurs well above T_c.
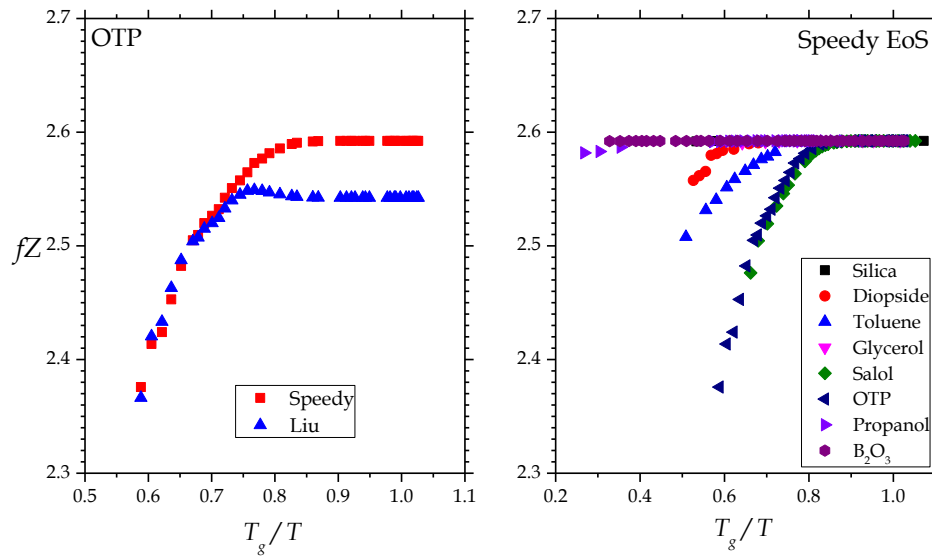
Figure 7-30:   At left, the hard sphere partition's effective compressibility fZ as a function of T_g/T for OTP, using the Speedy and Liu equations of state. For each EoS, the curves converge to ~$4\phi_c$. The right panel shows the effective compressibility for all eight liquids using the Speedy EoS. The liquids converge differently; some show saturation of fZ at the limit $4\phi_c$ relatively far above T_g; all liquids show convergence before attaining T_g.

What is remarkable is how firmly fZ saturates well above T_g, for all three EoS. Given that ϕ_c differs for each of the three EoS, the saturation levels out at slightly different values depending on the EoS used, as can be seen in the left plot of Figure 7-30. The system-normalized fZ with Speed EoS shows a smooth approach to the limiting value. A small non-monotonicity is, however, seen for the Liu EoS, where fZ slightly exceeds $4\phi_c$ before dropping to the expected asymptotic value, as was seen for the model GFLs; the lower temperatures accessible for the experimental GLFs demonstrates how the behavior of fZ proceeds below the limit achieved for the model GFLs. Interestingly, fZ saturates closer to T_g for fragile GFLs such as OTP and salol.
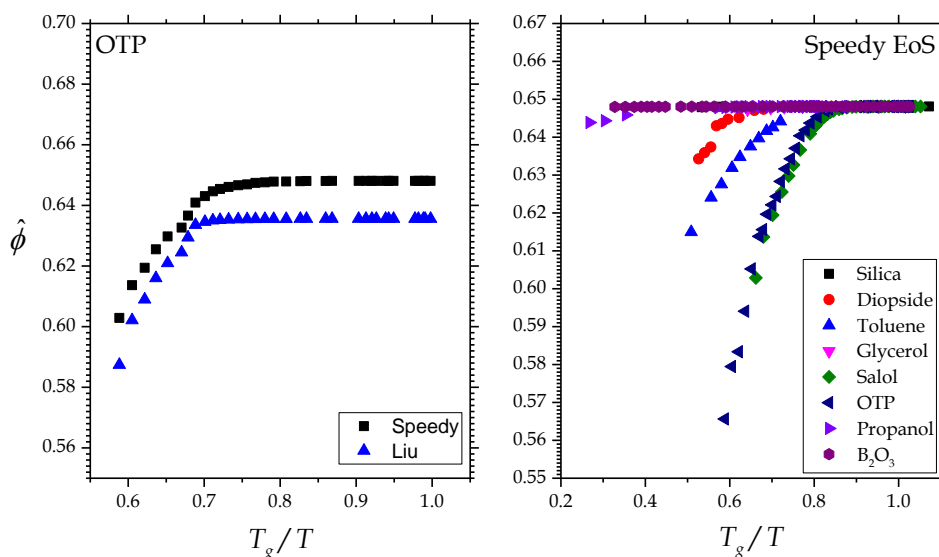
Figure 7-31: The HS packing fraction $\hat{\phi}$ for the experimental GFLs; the left plot shows $\hat{\phi}$ for OTP calculated using the Speedy and Liu EoS. The right plot features $\hat{\phi}$ for all eight liquids using the Speedy EoS.

Strong convergence of the effective packing fraction of the hard sphere component is observed for the experimental GFLs in Figure 7-31. Convergence to ϕ_c occurs at different "rates" for the various GFLs. Salol and OTP, which are the most fragile liquids of this group, only attain saturation in $\hat{\phi}$ relatively close to T_g, while less-fragile liquids like propanol and B_2O_3 saturate significantly above T_g. Note that the temperature range featured for most of the eight liquids extends from approximately the onset temperature T_O to at or below T_g. For the model GFLs, $\hat{\phi}$ in the vicinity of T_O is smaller (~0.5) than is exhibited for the experimental GFLs at T_O.

7.2.B   Excess Entropy of the Hard Sphere Component

As was done in the study of the model GFLs, the excess entropy can be computed for the experimental liquids, but for a wider temperature range, which allows for the verification of excess entropy scaling down to temperatures below T_g. Although the analysis cannot be as complete as that which was carried out for the model systems – the total entropy cannot be computed using experimental data – the effectiveness of the HSP method as verified with the

model systems lends weight to its broadened application to the experimental GFLs. The fundamental concept behind the HSP approach is that a one-parameter descriptor of the extent of thermal jamming in the hard sphere component of the liquid, which is "extracted" using the diffusion coefficient (or in principle, another transport coefficient such as viscosity) and assumptions from hard sphere theory; all of this information is available for these materials and in principle the same entropy scaling may be demonstrated for these experimentally-determined materials as was seen for the model systems. The missing piece is information about the corresponding harmonic oscillator (solid-like) component of these experimental GFLs, which cannot be determined without the information on the total density of states.
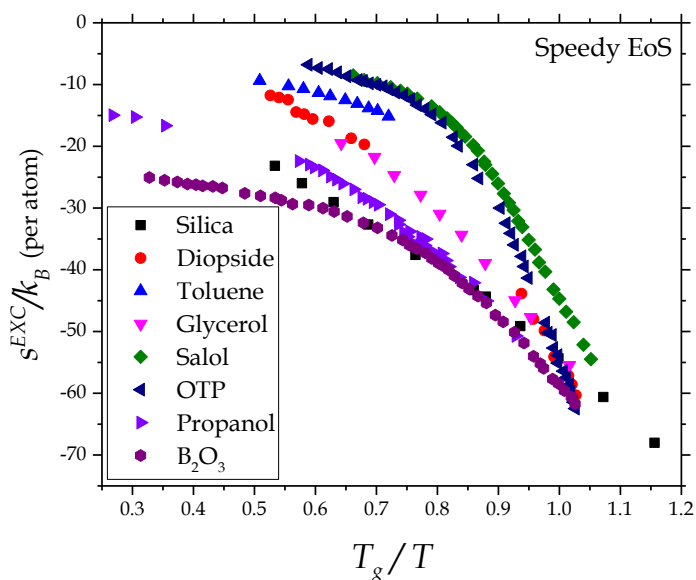
Figure 7-32:   The excess entropy s^{EXC}/k_B (per HS atom) for the experimental GFLs. Near T_g, a value of -$60/k_B N_A$ is attained for all materials. N_A represents the Avogadro number.

The normalized excess entropy (per HS atom) is depicted in Figure 7-32. Interestingly, the excess entropy of the hard sphere partition attains a value of approximately -$60/k_B N_A$ near the glass transition temperature. This value corresponds to the attainment of approximately 10^{-10} for the partitioning metric f at T_g (see Figure 7-26).
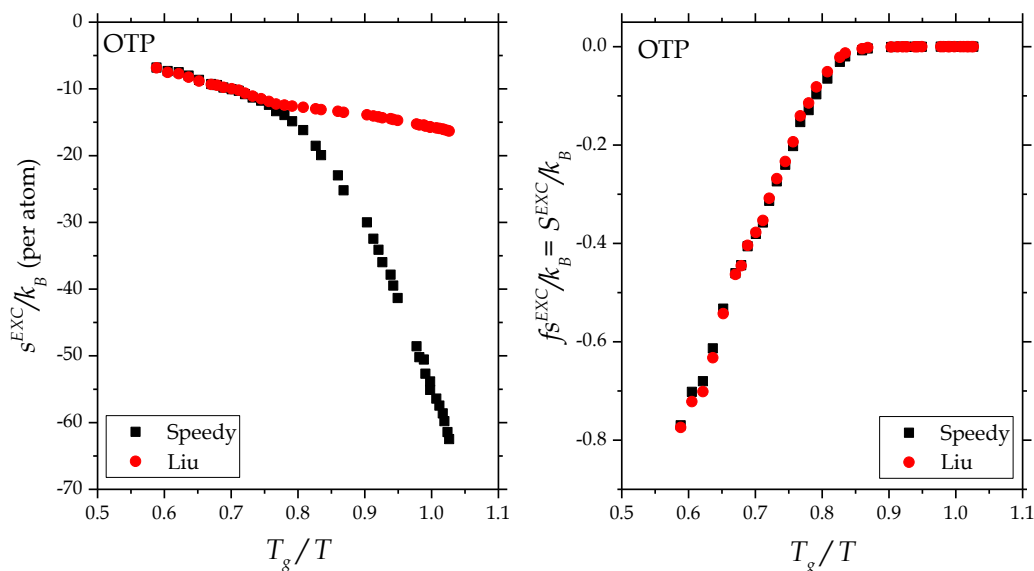
Figure 7-33:   A comparison of the excess entropy of the hard sphere partition (left panel) and its contribution to the system entropy (right panel) using the Speedy and Liu equations of states for OTP. At higher temperatures the equations of states agree predict similar excess entropy but show a dramatic divergence at lower temperatures for s^{EXC}. This divergence is less dramatic for S^{EXC}, as the inclusion of the partitioning metric offsets the divergence seen in s^{EXC}.

A noticeable difference may be observed between the Speedy and Liu EoS when computing the excess entropy, as shown in Figure 7-33 (left panel). When using the Liu EoS, s^{EXC}/k_B (per HS atom) does not trend as negative with decreasing temperature. The numerical accuracy of the EoS and the resulting integrals used to compute s^{EXC} have been verified using multiple computational methods, so we believe with high confidence that this effect is a genuine result of the subtle differences in the EoS that appear very close to the respective packing limits attained at $\hat{\phi}_c$ for each EoS. When the contribution of the excess entropy to the system-normalized entropy is computed (Figure 7-33, right panel), the difference in the results using the two EoS is less dramatic, as the multiplication of s^{EXC} by f offsets the numerical difference.

7.2.C   Excess Entropy Scaling

A strict exponential excess entropy scaling, spanning over nine orders of magnitude for Δ, is exhibited by the experimental GFLs, as depicted in Figure 7-34. The broader temperature range allows for confirmation of EES in the hard sphere partition from T_O down to below T_g. Although s^{EXC} differs significantly between the Speedy/Odriozola-Berthier and Liu EoS, the same scaling is obtained regardless of the choice of EoS. Based on the excess entropy scaling observed in model and experimental GFLs, the following generalized statement can be formulated: *The HSP method, which postulates $f = g(\sigma^+)^{-1}$, exhibits strict universal exponential scaling behavior with excess entropy s^{EXC} for all supercooled systems.* This is a new definition of a class of universal liquid behavior using the HPS method.
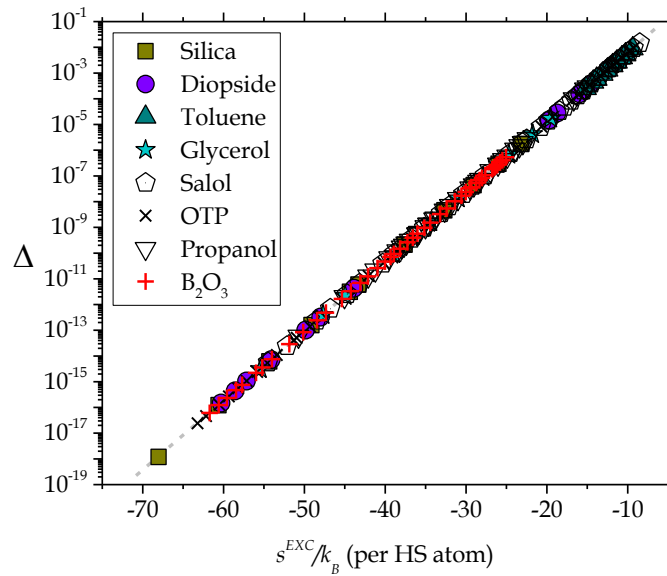
Figure 7-34:   Universal exponential excess entropy scaling as demonstrated by eight GFLs. Although the Speedy EoS is used for this evaluation, similar exponential scaling is observed with O-B and Liu equations of states.

Figure 4-35 shows the scaling behavior with $S^{EXC} = fs^{EXC}$. Expectedly, the contribution $fs^{EXC} = S^{EXC}$ becomes extremely small, as the hard sphere partition's contribution to the total entropy becomes nearly negligible as the vibrational HO modes become relatively dominant near and below T_g; for some GFLs, the HO modes becomes relatively dominant well-before T_g.
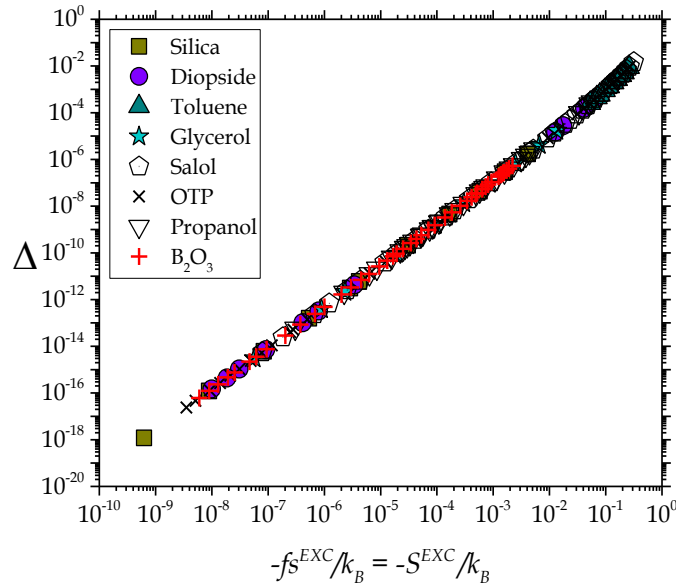
Figure 7-35: Excess entropy scaling with $fs^{EXC} = S^{EXC}$. An approximate power law scaling is observed for nearly the whole range of temperatures (from at or below T_g to the left, up to near and above the onset temperature T_O on the right).

Section 7.3　Discussion

Through the partitioning metric f and the Hard Sphere Partitioning (HSP) approach, we have established a formal method to idealize a glass forming liquid into two components – a set of non-interacting harmonic oscillators (HO) and a set of hard spheres (HS). It is postulated that f, which is the ratio of number of HS atoms to the total number of atoms ($f = N_{HS}/N$), is identically equal to the inverse of the HS radial distribution function at contact. Together with an appropriate equation of state for the metastable fluid branch, the HSP approach allows the development of formal jamming metrics including an effective packing fraction that converges to a certain critical packing fraction at temperatures close to T_c or T_g. The effective packing fraction of the conceptual hard sphere partition $\hat{\phi}$ shows an asymptotic approach to its maximum allowed value $\phi_c \sim \phi_{RCP}$ for both the model GFLs and experimental GFLs at low temperatures. Thus, the HSP model establishes an ideal HS partition that may be considered as indicators of the extent of thermal jamming in the liquid. This is a concept very distinct from the usual notion of jamming,

which is a static phenomenon based on geometric dimensions. Thermal jamming seeks to ascribe a jamming perspective to the slowing down phenomenology observed in supercooled liquids and GFLs. In this perspective, slow dynamics is a consequence of disappearance of the equivalent hard sphere atoms; strictly speaking, with decreasing temperature, the number of equivalent HS atoms decrease while the number of equivalent harmonic oscillators increase.

The HSP approach further allows the computation of excess entropy components. With the definition $s^{EXC} = s^{HS} - s^{IG}$, where s^{IG} is the ideal gas entropy, it is shown that dynamical variables in appropriate reduced forms show scaling with excess entropy. A remarkable and non-trivial observation is that all systems (model and real GFLs) that are investigated in this thesis show strict exponential (Rosenfeld) scaling with s^{EXC}. With a system normalized entropy $S^{EXC} = f s^{EXC}$, a strict scaling remains although approximated by a power-law form. The generality of the central definition of the partitioning metric, $f = N_{HS}/N$, leaves open a potentiality of numerous alternate formulations of this methodology in terms of other transport coefficients, or other hypotheses about the specific variation of f. Such assumptions will affect the quantitative establishment of the hard sphere partition and the calculation of s^{EXC}. It remains to be seen whether alternative formalisms would change the nature of entropy scaling behavior.

Chapter 8: Conclusions

The dramatic slowdown in the dynamics of supercooled and glass forming liquids can be described, under some conditions, through the 'thermal free volume', which is created by thermal energy working against pressure [132, 166]. In the thermal free volume conceptualization, the atoms may be thought of as becoming "thermally jammed" as temperature decreases. Relaxing the small pressure limit and insignificant overlap between the atoms, the dynamics can be characterized by using an effective hard sphere packing fraction at finite temperatures [166]. It is well-known that liquids can be approximated as a collection of hard spheres (HS) with a dominant repulsive potential and a weak attractive potential [37]. The collapse of structural and dynamic properties implies a quasi-universality in liquids that can be explained with model hard spheres [133, 134]; Dyre and coworkers have generalized this concept as the hard sphere paradigm [134].

In this work, we adopt the hard sphere paradigm and the point of view that thermal excitations create a thermal free volume which will decrease with decreasing temperature. However, departing from the established line of inquiry, it is posited that *only a subset* of the constituent atoms, modeled as hard spheres, in a supercooled liquid or glass forming liquid (GFL), will show the features of jammed conditions. ***Thus, the dynamic slowdown is posited to arise from the attrition of the thermally excited hard spheres with decreasing temperature (or increasing pressure) – we refer to this effect as thermal jammin**g*. The approach that is taken in this thesis differs from the path taken thus far – namely, to cast the structure and dynamics of the entire system comprising all the atoms/molecules into an equivalent system of hard spheres. Instead, a liquid system is portioned into a set of harmonic oscillators and a set of hard spheres. While the partitioning concept itself is not new, this approach diverges from the conventional wisdom of considering a liquid to be dominated by repulsive forces.

Thermal jamming is formalized using the Hard Sphere Partitioning (HSP) approach. We extend the original work of Lin, Blanco, and Goddard (LBG) [187] by carefully choosing the equations of state along the metastable fluid branch that are appropriate for supercooled liquids and GFLs. Unlike the traditional practice of considering the entire liquid state to be comprised of

equivalent hard spheres, the HSP approach postulates that any liquid system can be regarded to be comprised of a set of hard spheres (HS) and a set of harmonic oscillators (HO). Thus, any property of the liquid system then becomes a weighted average of the contributions from hard spheres and harmonic oscillators. For properties such as diffusivity there is no contribution from harmonic oscillators by construction, while for extensive properties such as entropy there are contributions from both harmonic oscillators and hard spheres. With this partitioning, the attractive forces now have a contribution to the properties of the liquid state – a significant departure from the traditional viewpoint of dense liquids as approximated by a set of hard spheres.

We first establish the definition of the hard sphere partition of the liquid using a "partitioning metric" f, which is the ratio of atoms in the liquid that behave effectively as hard spheres (N_{HS}) to the total number of atoms in the liquid (N). In principle, there could be multiple ways to plausibly compute N_{HS} for a liquid. In the HSP approach, the partitioning metric is identically equal to the inverse of the HS radial distribution function at contact, i.e., $f \equiv g(\sigma^+)^{-1}$. It is the shown that the partitioning postulate is in fact a mathematical conclusion that arises from the assumptions used to derive f in the original 2PT method [187]. The numerical bounds of f are as follows: as $f \rightarrow 1$, the system is entirely fluidic, meaning that the system behavior is represented entirely by hard spheres (the system is an hard sphere gas); in the other limit, $f \rightarrow 0$ entails no partitioning and the hard sphere component represents none of the system's behavior (the system is a solid modeled as a set of harmonic oscillators). With the partitioning approach, the liquid is deemed to have both solid-like (HO) and gas-like (HS) properties. Properties that depend on hopping across the potential energy basins such as diffusivity and viscosity are exclusively dependent on the HS partitioning, while properties that rely solely on vibrations are attributed to the HO partition. Thermodynamic properties such as entropy and free energy that depend on both can then be written as a superposition of the HS and HO contributions.

The hard sphere partitioning (HSP) method is devised to provide unambiguous jamming metrics to liquids in the supercooled states. The HSP approach presumes jamming *a priori* and provides the jamming metrics such as effective packing fraction and compressibility as the liquid traverses into the deeply supercooled states. This is done by incorporating three equations of states that are applicable in the metastable fluid branch – Speedy [151, 152], Odriozola and Berthier (O-B) [136] and Liu [148, 164]. The goal is to predict the ageing behavior of glass forming

liquids all the way to glass transition. The HSP approach does not postulate the significance of crossovers or discontinuities associated with the mode coupling critical temperature T_c or the glass transition temperature T_g.

The effective packing fraction $\hat{\phi}$ of the hard sphere partition of the liquid established by the HSP approach provides the extent of thermal jamming in the liquids in the supercooled states. When diffusivity of the liquid approaches zero, the partitioning metric $f \equiv N_{HS}/N$ also approaches zero and $\hat{\phi}$ approaches the critical packing fraction ϕ_c, which is close to the random-close-packed value ϕ_{RCP}. In general, the value depends on the choice of the hard sphere equation of state applied in the HSP approach. According to the hard sphere paradigm, the dynamics of simple liquids is well-described by association with the reference hard sphere system, and according to one of the prevailing notions in the field, the hard sphere fluid on the metastable branch undergoes a glass transition when the packing fraction approaches ϕ_{RCP}. In the HSP approach, we adopt this axiom but additionally incorporate an important caveat – only a subset of the atoms, as determined by the partitioning metric f, experiences the compressibility divergence. The partitioning metric, however, is expected to smoothly approach zero without exhibiting a discontinuity. Both the effective packing fraction and the partitioning metric are universally related for all glass forming liquids and supercooled liquids through the relation $f = \Delta^{\frac{3}{5}} \hat{\phi}^{\frac{2}{5}}$, where Δ is the non-dimensional diffusivity. The HSP approach also provides a method of establishing a universal description of liquid dynamics that is capable of spanning the entire range of liquid dynamics. The form of the non-dimensional diffusivity, which is determined from the kinetic theory of gases, is most appropriate for inquiry into any universal scaling relationships with effective packing fractions or excess entropy.

In Chapter 7 a two-pronged thermodynamic and dynamic analysis of supercooled liquids is undertaken using the HSP approach, from which the thermal jamming metrics are established for three model systems and eight real glass forming liquids (GFLs) using the assumptions within the methodology outlined in Chapter 4. Three model GFLs are featured in the first part of this analysis: the Kob-Andersen (KA) system [111], Weeks-Chandler-Andersen (WCA) system [203, 204], and the harmonic sphere (HARM) system [205, 206]. The eight experimental GFLs are: silica (SiO_2), glycerol ($C_3H_8O_3$), diopside ($MgCaSi_2O_6$), toluene (C_7H_8), o-terphenyl ($C_{18}H_{14}$), salol

$(C_{13}H_{10}O_3)$, boric oxide (B_2O_3), and n-Propanol (C_3H_8O); the references to the literature data used for these materials are shown in Table 7-2.

A divergence in the pressure or compressibility of the HS partition occurs as $\hat{\phi} \rightarrow \phi_c$. However, the divergence is not postulated to occur at a specific thermodynamic state. Therefore, there is no unique glass transition temperature or pressure in this approach, by construct. However, as shown in Chapter 7, the analysis of eight glass formers shows that non-dimensional diffusivity, the partitioning metric, compressibility, and excess entropy all tend to converge to specific values at the traditional laboratory glass transition temperature. Interestingly, with the Speedy EoS, the excess entropy of the hard sphere partition attains a value of approximately $\sim 60/k_B$ per HS atom for all the experimental GFLs near the laboratory glass transition temperature; this value corresponds to the attainment of approximately 10^{-10} for the partitioning metric f.

Excess entropy scaling is observed for the hard sphere components of the model and experimental GFLs, and critically, strict adherence to a single master curve is exhibited by all GFL systems. From this result, the following generalized non-trivial statement is formulated: *The HSP method, which postulates $f = g(\sigma^+)^{-1}$, exhibits strict universal exponential scaling behavior with excess entropy s^{EXC} for all supercooled systems.* The first-ever application of this methodology to GFLs in this work drives home the point that that the hard sphere partition becomes increasingly small as the dynamics of the liquid slows, and the harmonic oscillator partition dominates the total entropy of the liquid. In the HSP model, the dynamics becomes sluggish because the number of the participating diffusive (HS) atoms decreases precipitously on cooling. Relative to the existing theories, the HSP approach appears to be closest to the dynamic facilitation (DF) theory [117], although no formal correspondence is attempted in this work. No length scales are also identified in this approach although such metrics can possibly be constructed from the reduction of the HS atoms with decreasing temperature.

The HSP approach most importantly reveals an important attribute of liquids that seems to present a conflict with the seminal Van der Waals conception of liquids that are dominated by repulsive interactions among atoms. Numerous studies of simple liquids using the 2PT method, upon with the HSP approach is based, have indicated that the partitioning metric f for these liquids is not large, typically in the vicinity of 30-40%, meaning that 60-70% of the liquid's

dynamics is better modeled by a system of harmonic oscillators than by hard spheres. For the molecular GFLs studied in this work, f is significantly smaller than what is observed for simple liquids. As harmonic oscillators are characterized by attractive interactions as opposed to repulsive interactions, the calculation of f suggests that liquid behavior is dominated by solid-like vibrational modes instead of gas-like diffusion. From at least a practical standpoint, the HSP approach strongly suggests that liquid thermodynamics is better described by association of the liquid with solid-like vibrations in conjunction with HS gas-like diffusion.

From a different standpoint, the analysis of stringlike cooperative motion presented in Chapter 6. A general explanation for the findings presented in this work is that the dynamical behavior of string-like groups of atoms in glass formers changes in the vicinity of the crossover temperature T_S. The discrete tracking analysis conducted for strings in the three model GFLs indicates that long strings become increasingly critical for the relaxation of mobile atoms to occur as temperature decreases, while the prevalence of shorter strings is diminished. A peak in the non-monotonicity of the relative population of cooperative pairs, as well as crossovers in the populations of longer strings occurs at T_S, indicating that a crossover in string dynamics occurs at this temperature that is commensurate with other observed behavior at T_S, such as the liquid's deviation from the Stokes-Einstein relation. The increased reliance of mobile atoms on movement in the form of longer strings indicates the dominance of kinetically-constrained pathways that dominate relaxation behavior near the mode-coupling temperature T_c – a likely consequence of thermal jamming of the atoms in glass formers.

While this work serves to illuminate a new class of universal scaling in liquids, it also raises a number of important questions. First, how can the partitioning approach of the HSP method be used to better understand the important transitions in glass forming liquids that occur at T_S, T_g, or others among the numerous transition temperatures identified across the span of glassy dynamics (see Figure 1-4)? This work has identified one such association at the onset temperature T_O where the partitioning metric attains values approximately observed for simple, non-glassy liquids. In Chapter 7, particular values attained by f, Z, fZ and s^{EXC} at T_g for the experimental systems were identified – these are apparent convergence limits that are ***predicted*** by the HSP model commensurate with the attainment of a particular viscosity at T_g. Application of the HSP to a broader range of model GFLs, experimental liquids, and even materials such as superionic conductors that exhibit dynamics similar to that of glasses [17], could provide

sufficient information to identify transitions and crossovers in glassy liquids with metrics of the HSP method.

Secondly, a more concrete rationalization is desirable for the partitioning postulate. It would be interesting to inquire different functional forms and their effect on the strict universality that is presented in this thesis. While the inverse relationship between partition metric and the HS radial distribution function at contact is physically plausible, a firmer theoretical backing would strengthen the HSP approach. Finally, accurate equations of state in the metastable fluid branch are key to the success of the method. More refined equations of state would improve the predictive capability of the method. The preponderance of theoretical advancements provided in this work to establishing a class of universality in liquids, as well as the grounds provided by the HSP method for future work in advancing concepts of liquid physics, strongly warrants additional attention to the HSP approach in its broad application to glassy liquids and beyond.

References

[1]   V. Lubchenko, P.G. Wolynes, Theory of structural glasses and supercooled liquids, Ann. Rev. Phys. Chem. , 58 (2007) 235.

[2]   C.A. Angell, The old problems of glass and the glass transition, and the many new twists, Proceedings of the National Academy of Sciences, 92 (1995) 6675.

[3]   W. Kauzmann, The nature of the glassy state and the behavior of liquids at low temperatures, Chemical Reviews, 43 (1948) 219.

[4]   F.H. Stillinger, P.G. Debenedetti, Glass transition thermodynamics and kinetics, Annual Review of Condensed Matter Physics, 4 (2013) 263.

[5]   P.G. Debenedetti, F.H. Stillinger, Supercooled liquids and the glass transition, Nature, 410 (2001) 259.

[6]   M.I. Ojovan, W.E. Lee, Glassy wasteforms for nuclear waste immobilization, Metallurgical and Materials Transactions A, 42 (2011) 837.

[7]   W.J. Weber, Radiation and thermal ageing of nuclear waste glass, Procedia Materials Science, 7 (2014) 237.

[8]   W.J. Weber, R.C. Ewing, C.A. Angell, G.W. Arnold, A.N. Cormack, J.M. Delaye, D.L. Griscom, L.W. Hobbs, A. Navrotsky, D.L. Price, A.M. Stoneham, M.C. Weinberg, Radiation effects in glasses used for immobilization of high-level waste and plutonium disposition, Journal of Materials Research, 12 (1997) 1948.

[9]   N. Gravish, G. Gold, A. Zangwill, M.A. Goodisman, D.I. Goldman, Glass-like dynamics in confined and congested ant traffic, Soft matter, 11 (2015) 6552-6561.

[10]   I.K. Ono, C.S. O'Hern, D.J. Durian, S.A. Langer, A.J. Liu, S.R. Nagel, Effective temperatures of a driven system near jamming, Physical Review Letters, 89 (2002) 095703.

[11]   J. Goyon, A. Colin, G. Ovarlez, A. Ajdari, L. Bocquet, Spatial cooperativity in soft glassy flows, Nature, 454 (2008) 84.

[12]   L. Bécu, S. Manneville, A. Colin, Yielding and flow in adhesive and nonadhesive concentrated emulsions, Physical Review Letters, 96 (2006) 138302.

[13]   A.S. Keys, A.R. Abate, S.C. Glotzer, D.J. Durian, Measurement of growing dynamical length scales and prediction of the jamming transition in a granular material, Nat Phys, 3 (2007) 260-264.

[14]   D.S. Grebenkov, M.P. Ciamarra, M. Nicodemi, A. Coniglio, Flow, ordering, and jamming of sheared granular suspensions, Physical Review Letters, 100 (2008) 078001.

[15]   G. D'Anna, G. Gremaud, The jamming route to the glass state in weakly perturbed granular media, Nature, 413 (2001) 407-409.

[16]   A. Annamareddy, J. Eapen, Low dimensional string-like relaxation underpins superionic conduction in fluorites and related structures, Sci. Reports, 7 (2017) 44149.

[17]   V.A. Annamareddy, P.K. Nandi, X. Mei, J. Eapen, Waxing and waning of dynamical heterogeneity in the superionic state, Phys. Rev. E, 89 (2014) 010301.

[18]   A. Annamareddy, J. Eapen, Mobility propagation and dynamic facilitation in superionic conductors, J. Chem. Phys., 143 (2015) 194502.

[19]   A. Annamareddy, J. Eapen, Ion Hopping and Constrained Li Diffusion Pathways in the Superionic State of Antifluorite Li_2O, Entropy, 19 (2017) 227.

[20]   A. Annamareddy, J. Eapen, Disordering and dynamic self-organization in stoichiometric UO_2 at high temperatures, Journal of Nuclear Materials, 483 (2017) 132-141.

[21] K. Nagel, M. Schreckenberg, A cellular automaton model for freeway traffic, Journal de Physique I, 2 (1992) 2221-2229.

[22] O. Biham, A.A. Middleton, D. Levine, Self-organization and a dynamical transition in traffic-flow models, Physical Review A, 46 (1992) R6124.

[23] A. Kushima, J. Eapen, J. Li, S. Yip, T. Zhu, Time scale bridging in atomistic simulation of slow dynamics: viscous relaxation and defect activation, Eur. Phys. J. B, 82 (2011) 271.

[24] S.A. Kivelson, G. Tarjus, In search of a theory of supercooled liquids, Nature Materials, 7 (2008) 831-833.

[25] E.D. Zanotto, J.C. Mauro, The glassy state of matter: Its definition and ultimate fate, Journal of Non-Crystalline Solids, 471 (2017) 490-495.

[26] X. Mei, W. Mohamed, J. Eapen, Approach to local thermodynamic equilibrium and the evolution to a glassy core following neutron/ion radiation impact, Philosophical Magazine, 98 (2018) 2701.

[27] M.H. Cohen, G. Grest, Liquid-glass transition, a free-volume approach, Physical Review B, 20 (1979) 1077.

[28] C. Angell, J. Tucker, Heat capacity changes in glass-forming aqueous solutions and the glass transition in vitreous water, The Journal of Physical Chemistry, 84 (1980) 268-272.

[29] C.A. Angell, Perspective on the glass transition, Journal of Physics and Chemistry of Solids, 49 (1988) 863-871.

[30] J.C. Mauro, R.J. Loucks, S. Sen, Heat capacity, enthalpy fluctuations, and configurational entropy in broken ergodic systems, The Journal of Chemical Physics, 133 (2010) 164503.

[31] A. Cavagna, Supercooled liquids for pedestrians, Physics Reports, 476 (2009) 51.

[32] M.D. Ediger, P. Harrowell, Perspective: Supercooled liquids and glasses, The Journal of Chemical Physics, 137 (2012) 080901.

[33] V. Lubchenko, P.G. Wolynes, Theories of structural glass dynamics: mosaics, jamming and all that, in: P.G. Wolynes, V. Lubchenko (Eds.) Structural Glasses and Supercooled liquids, John Wiley and Sons, Inc., Hoboken, New Jersey, 2012.

[34] L. Berthier, J.P. Garrahan, Real space origin of temperature crossovers in supercooled liquids, Physical Review E, 68 (2003) 041201.

[35] A. Kushima, X. Lin, J. Li, J. Eapen, J.C. Mauro, X. Qian, P. Diep, S. Yip, Computing the viscosity of supercooled liquids, The Journal of Chemical Physics, 130 (2009) 224504.

[36] R.H. Doremus, Viscosity of silica, Journal of Applied Physics, 92 (2002) 7619.

[37] J.-P. Hansen, I.R. McDonald, Theory of Simple Fluids, Elsevier, London, 1986.

[38] J.P. Boon, S. Yip, Molecular Hydrodynamics, Dover, New York, 1991.

[39] M.G. Mazza, N. Giovambattista, H.E. Stanley, F.W. Starr, Connection of translational and rotational dynamical heterogeneities with the breakdown of the Stokes-Einstein and Stokes-Einstein-Debye relations in water, Physical Review E, 76 (2007) 031203.

[40] J.C. Mauro, Y. Yue, A.J. Ellison, P.K. Gupta, D.C. Allan, Viscosity of glass-forming liquids, Proceedings of the National Academy of Sciences, DOI (2009) pnas. 0911705106.

[41] G. Adam, J.H. Gibbs, On the temperature dependence of cooperative relaxation properties in glass-forming liquids, J. Chem. Phys., 43 (1965) 139.

[42] J.H. Gibbs, E.A. DiMarzio, Nature of the glass transition and the glassy state, The Journal of Chemical Physics, 28 (1958) 373.

[43] L.M. Martinez, C.A. Angell, A thermodynamic connection to the fragility of glass-forming liquids, Nature, 410 (2001) 663.

[44] S. Sastry, The relationship between fragility, configurational entropy and the potential energy landscape of glass-forming liquids, Nature, 409 (2001) 164.

[45]   S. Sastry, P.G. Debenedetti, F.H. Stillinger, Signatures of distinct dynamical regimes in the energy landscape of a glass-forming liquid, Nature, 393 (1998) 554.

[46]   F.H. Stillinger, T.A. Weber, Hidden structure in liquids, Physical Review A, 25 (1982) 978.

[47]   F.H. Stillinger, T.A. Weber, Packing Structures and Transitions in Liquids and Solids, Science, 225 (1984) 983-989.

[48]   M. Goldstein, Viscous liquids and the glass transition: a potential energy barrier picture, J. Chem. Phys., 51 (1969) 3728.

[49]   G. Tarjus, S.A. Kivelson, Z. Nussinov, P. Viot, The frustration-based approach of supercooled liquids and the glass transition: a review and critical assessment, J. Phys. Condens. Matter, 17 (2005) R1143.

[50]   F. Mallamace, C. Branca, C. Corsaro, N. Leone, J. Spooren, S.-H. Chen, H.E. Stanley, Transport properties of glass-forming liquids suggest that dynamic crossover temperature is as important as the glass transition temperature Proc. Nat. Acad. Sci., 107 (2010) 22457.

[51]   T.R. Kirkpatrick, D. Thirumalai, Colloquium: Random first order transition theory concepts in biology and physics, Reviews of Modern Physics, 87 (2015) 183.

[52]   F. Stickel, E.W. Fischer, R. Richert, Dynamics of glass-forming liquids. II. Detailed comparison of dielectric relaxation, dc-conductivity, and viscosity data, The Journal of Chemical Physics, 104 (1996) 2043.

[53]   C.M. Roland, Characteristic relaxation times and their invariance to thermodynamic conditions, Soft Matter, 4 (2008) 2316.

[54]   L. Berthier, G. Biroli, Theoretical perspective on the glass transition and amorphous materials, Rev. Mod. Phys., 83 (2011) 587.

[55]   W. Gotze, Complex Dynamics of Glass Forming Liquids, Oxford University Press, Oxford, 2009.

[56]   W. Götze, The essentials of the mode-coupling theory for glassy dynamics, Condensed Matter Physics 1(1998) 873.

[57]   B. Bagchi, Dynamics in the crossover region of supercooled liquids, in: V. Lubchenko, P.G. Wolynes (Eds.) Structural Glasses and Supercooled Liquids, John Wiley and Sons, Inc., Hoboken, New Jersey, 2012., 2012.

[58]   E. Flenner, H. Staley, G. Szamel, Universal features of dynamic heterogeneity in supercooled liquids, Phys. Rev. Lett., 112 (2014) 097801.

[59]   E. Flenner, G. Szamel, Dynamic heterogeneities above and below the mode-coupling temperature: Evidence of a dynamic crossover, J. Chem. Phys., 138 (2013) 12A523.

[60]   W. Kob, S. Roldán-Vargas, L. Berthier, Non-monotonic temperature evolution of dynamic correlations in glass-forming liquids, Nature Physics, 8 (2011) 164.

[61]   G.M. Hocky, L. Berthier, W. Kob, D.R. Reichman, Crossovers in the dynamics of supercooled liquids probed by an amorphous wall, Phys. Rev. E, 89 (2014) 052311.

[62]   M.D. Ediger, Spatialy Heterogeneous Dynamics in Supercooled Liquids, Annual Review of Physical Chemistry, 51 (2000) 99.

[63]   W. Kob, H.C. Andersen, Testing mode-coupling theory for a supercooled binary Lennard-Jones mixture. II. Intermediate scattering function and dynamic susceptibility, Physical Review A, 52 (1995) 4134.

[64]   N.P. Bailey, T.B. Schroder, J.C. Dyre, Exponential distributions of collective flow-event properties in viscous liquid dynamics, Physical Review Letters, 102 (2009) 055701.

[65] T. Hecksher, A.I. Nielsen, N.B. Olsen, J.C. Dyre, Little evidence for dynamic divergences in ultraviscous molecular liquids, Nature Physics, 4 (2008) 737-741.

[66] J.C. Dyre, T. Hechsher, K. Niss, A brief critique of the Adam-Gibbs entropy model, J. Non-crystal. solids, 355 (2009) 624.

[67] E. Masiewicz, A. Grzybowski, K. Grzybowska, S. Pawlus, J. Pionteck, M. Paluch, Adam-Gibbs model in the density scaling regime and its implications for the configurational entropy scaling, Scientific Reports, 5 (2015) 13998.

[68] C.M. Roland, S. Capaccioli, M. Lucchesi, R. Casalini, Adam–Gibbs model for the supercooled dynamics in the ortho-terphenyl ortho-phenylphenol mixture, The Journal of Chemical Physics, 120 (2004) 10640.

[69] F.W. Starr, J.F. Douglas, S. Sastry, The relationship of dynamical heterogeneity to the Adam-Gibbs and random first-order transition theories of glass formation, J. Chem. Phys., 138 (2013) 12A541.

[70] S. Karmakar, C. Dasgupta, S. Sastry, Growing length and time scales in glass-forming liquids, Proceedings of the National Academy of Sciences, 106 (2009) 3675.

[71] S. Sastry, Liquid limits: Glass transition and liquid-gas spinodal boundaries of metastable liquids, Phys. Rev. Lett., 85 (2000) 590.

[72] D. Kivelson, H. Reiss, Metastable systems in thermodynamics: consequences, role of constraints, Journal of Physical Chemistry B, 103 (1999) 8337.

[73] H. Reiss, Apparent entropy, residual entropy, causality, metastability, constraints, and the glass transition, Journal of Non-Crystalline Solids, 355 (2009) 617.

[74] J.C. Mauro, P.K. Gupta, R.J. Loucks, A.K. Varshneya, Non-equilibrium entropy of glasses formed by continuous cooling, Journal of Non-Crystalline Solids, 355 (2009) 600.

[75] M. Goldstein, On the reality of the residual entropies of glasses and disordered crystals: Counting microstates, calculating fluctuations, and comparing averages, The Journal of Chemical Physics, 134 (2011) 124502.

[76] I. Gutzow, J.W.P. Schmelzer, The Third Principle of thermodynamics and the zero-point entropy of glasses: History and new developments, Journal of Non-Crystalline Solids, 355 (2009) 581.

[77] G.P. Johari, J. Khouri, Entropy change on the cooling and heating paths between liquid and glass and the residual entropy, The Journal of Chemical Physics, 134 (2011) 034515.

[78] G.P. Johari, Specific heat relaxation-based critique of isothermal glass transition, zero residual entropy and time-average formalism for ergodicity loss, Thermochimica Acta, 523 (2011) 97.

[79] T.V. Tropin, J.W. Schmelzer, V.L. Aksenov, Modern aspects of the kinetic theory of glass transition, Physics-Uspekhi, 59 (2016) 42.

[80] P. Richet, Residual and configurational entropy: Quantitative checks through applications of Adam–Gibbs theory to the viscosity of silicate melts, Journal of Non-Crystalline Solids, 355 (2009) 628.

[81] S.V. Nemilov, Zero-point entropy of glasses as physical reality, Journal of Non-Crystalline Solids, 355 (2009) 607.

[82] F. Sciortino, W. Kob, P. Tartaglia, Inherent Structure Entropy of Supercooled Liquids, Phys. Rev. Lett., 83 (1999) 3214.

[83] S. Srikanth, Evaluation of the configurational entropy of a model liquid from computer simulations, Journal of Physics: Condensed Matter, 12 (2000) 6515.

[84] L. Berthier, D. Coslovich, Novel approach to numerical measurements of the configurational entropy in supercooled liquids, Proc. Nat. Acad. Sci., 111 (2014) 11668.

[85]   D.A. McQuarrie, Statistical Mechanics, University Science Books, California, 2000.

[86]   M.T. Cicerone, M. Ediger, Relaxation of spatially heterogeneous dynamic domains in supercooled ortho-terphenyl, The Journal of Chemical Physics, 103 (1995) 5684-5692.

[87]   D. Johnston, Stretched exponential relaxation arising from a continuous sum of exponential decays, Physical Review B, 74 (2006) 184430.

[88]   S. Karmakar, C. Dasgupta, S. Sastry, Analysis of dynamic heterogeneity in a glass former from the spatial correlations of mobility, Physical Review Letters, 105 (2010) 015701.

[89]   C. Toninelli, M. Wyart, L. Berthier, G. Biroli, J.-P. Bouchaud, Dynamical susceptibility of glass formers: Contrasting the predictions of theoretical scenarios, Physical Review E, 71 (2005) 041505.

[90]   E.V. Russell, N. Israeloff, Direct observation of molecular cooperativity near the glass transition, Nature, 408 (2000) 695.

[91]   J. Clauss, K. Schmidt-Rohr, H.W. Spiess, Determination of domain sizes in heterogeneous polymers by solid-state NMR, Acta Polymerica, 44 (1993) 1-17.

[92]   S. Karmakar, C. Dasgupta, S. Sastry, Growing length scales and their relation to timescales in glass-forming liquids, Annual Review of Condensed Matter Physics, 5 (2014) 255.

[93]   C.K. Mishra, K. Hima Nagamanasa, R. Ganapathy, A.K. Sood, S. Gokhale, Dynamical facilitation governs glassy dynamics in suspensions of colloidal ellipsoids, Proceedings of the National Academy of Sciences, 111 (2014) 15362.

[94]   S. Gokhale, K. Hima Nagamanasa, R. Ganapathy, A.K. Sood, Growing dynamical facilitation on approaching the random pinning colloidal glass transition, Nature Communications, 5 (2014).

[95]   H. Zhang, D.J. Srolovitz, J.F. Douglas, J.A. Warren, Grain boundaries exhibit the dynamics of glass-forming liquids, Proceedings of the National Academy of Sciences, 106 (2009) 7735.

[96]   H. Zhang, M. Khalkhali, Q. Liu, J.F. Douglas, String-like cooperative motion in homogeneous melting, The Journal of Chemical Physics, 138 (2013) 12A538-516.

[97]   C. Donati, J.F. Douglas, W. Kob, S.J. Plimpton, P.H. Poole, S.C. Glotzer, Stringlike cooperative motion in a supercooled liquid, Physical Review Letters, 80 (1998) 2338.

[98]   J.D. Stevenson, J. Schmalian, P.G. Wolynes, The shapes of cooperatively rearranging regions in glass-forming liquids, Nature Physics, 2 (2006) 268.

[99]   D.J. Ashton, J.P. Garrahan, Relationship between vibrations and dynamical heterogeneity in a model glass former: Extended soft modes but local relaxation, The European Physical Journal E, 30 (2009) 303.

[100]   G.S. Matharoo, M.G. Razul, P.H. Poole, Structural and dynamical heterogeneity in a glass-forming liquid, Physical Review E, 74 (2006) 050502.

[101]   D. Chandler, J.P. Garrahan, Dynamics on the way to forming glass: bubbles in space-time, Annual Review of Physical Chemistry, 61 (2010) 191-217.

[102]   A.S. Keys, L.O. Hedges, J.P. Garrahan, S.C. Glotzer, D. Chandler, Excitations are localized and relaxation is hierarchical in glass-forming liquids, Physical Review X, 1 (2011) 021013.

[103]   T. Salez, J. Salez, K. Dalnoki-Veress, E. Raphaël, J.A. Forrest, Cooperative strings and glassy interfaces, Proceedings of the National Academy of Sciences, 112 (2015) 8227.

[104]   J.S. Langer, Theories of glass formation and the glass transition, Reports on Progress in Physics, 77 (2014) 042501.

[105] M.H. Cohen, D. Turnbull, Molecular transport in liquids and glasses, J. Chem. Phys., 31 (1959) 1164.

[106] D. Turnbull, M.H. Cohen, On the free-volume model of the liquid-glass transition, The Journal of Chemical Physics, 52 (1970) 3038-3041.

[107] M. Goldstein, Some thermodynamic aspects of the glass transition: Free Volume, entropy, and enthalpy theories, The Journal of Chemical Physics, 39 (1963) 3369.

[108] R.P. White, J.E.G. Lipson, How free volume does influence the dynamics of glass forming liquids, ACS Macro Letters, 6 (2017) 529.

[109] D.R. Reichman, P. Charbonneau, Mode-Coupling Theory, Journal of Statistical Mechanics: Theory and Experiment, 2005 (2005).

[110] L.M.C. Janssen, Mode-coupling theory of the glass transition: a primer, Frontiers in Physics, 6 (2018).

[111] W. Kob, H.C. Andersen, Testing mode-coupling theory for a supercooled binary Lennard-Jones mixture I: The van Hove correlation function, Physical Review E, 51 (1995) 4626.

[112] S. Sastry, Onset temperature of slow dynamics in glass forming liquids, PhysChemComm, 3 (2000) 79-83.

[113] V. Lubchenko, Theory of the structural glass transition: a pedagogical review, Advances in Physics, 64 (2015) 283-443.

[114] T.R. Kirkpatrick, P.G. Wolynes, Stable and metastable states in mean-field Potts and structural glasses, Physical Review B, 36 (1987) 8552.

[115] T.R. Kirkpatrick, D. Thirumalai, p-spin-interaction spin-glass models: Connections with the structural glass problem, Physical Review B, 36 (1987) 5388.

[116] T.R. Kirkpatrick, D. Thirumalai, P.G. Wolynes, Scaling concepts for the dynamics of viscous liquids near an ideal glassy state, Physical Review A, 40 (1989) 1045.

[117] J.P. Garrahan, D. Chandler, Coarse-grained microscopic model of glass formers, Proceedings of the National Academy of Sciences, 100 (2003) 9710.

[118] J.P. Garrahan, D. Chandler, Geometrical explanation and scaling of dynamical heterogeneities in glass forming systems, Physical Review Letters, 89 (2002) 035704.

[119] J. Jäckle, S. Eisinger, A hierarchically constrained kinetic ising model, Zeitschrift für Physik B Condensed Matter, 84 (1991) 115-124.

[120] A.S. Keys, J.P. Garrahan, D. Chandler, Calorimetric glass transition explained by hierarchical dynamic facilitation, Proc. Nat. Acad. Sci., 110 (2013) 4482.

[121] G. Parisi, F. Zamponi, Mean-field theory of hard sphere glasses and jamming, Rev. Mod. Phys., 82 (2010) 789.

[122] S. Torquato, F.H. Stillinger, Jammed hard-particle packings: From Kepler to Bernal and beyond, Reviews of Modern Physics, 82 (2010) 2633.

[123] C. Roland, R. Casalini, Density scaling of the dynamics of vitrifying liquids and its relationship to the dynamic crossover, Journal of Non-Crystalline Solids, 351 (2005) 2581-2587.

[124] R. Casalini, C.M. Roland, Viscosity at the Dynamic Crossover in o-Terphenyl and Salol under High Pressure, Physical Review Letters, 92 (2004) 245702.

[125] R. Casalini, C.M. Roland, Scaling of the supercooled dynamics and its relation to the pressure dependences of the dynamic crossover and the fragility of glass formers, Phys. Rev. B, 71 (2005) 014210.

[126] R. Casalini, S. Capaccioli, C.M. Roland, What Can We Learn by Squeezing a Liquid?, The Journal of Physical Chemistry B, 110 (2006) 11491-11495.

[127]   R. Casalini, C.M. Roland, Thermodynamical scaling of the glass transition dynamics, Physical Review E, 69 (2004) 062501.

[128]   T.S. Ingebrigtsen, T.B. Schrøder, J.C. Dyre, What Is a simple liquid?, Phys. Rev. X, 2 (2012) 011011.

[129]   N. Gnan, T.B. Schrøder, U.R. Pedersen, N.P. Bailey, J.C. Dyre, Pressure-energy correlations in liquids. IV. "Isomorphs" in liquid phase diagrams, J. Chem. Phys., 131 (2009) 234504.

[130]   U.R. Pedersen, N.P. Bailey, T.B. Schroder, J.C. Dyre, Strong pressure-energy correlations in van der Waals liquids, Phys. Rev. Lett., 100 (2008) 015701.

[131]   J.C. Dyre, Hidden scale invariance in condensed matter, J. Phys. Chem. B, 118 (2014) 10007.

[132]   N. Xu, T.K. Haxton, A.J. Liu, S.R. Nagel, Equivalence of glass transition and colloidal glass transition in the hard-sphere limit, Phys. Rev. Lett., 103 (2009) 245701.

[133]   A.K. Bacher, T.B. Schrøder, J.C. Dyre, Explaining why simple liquids are quasi-universal, Nat Commun, 5 (2014) 5424.

[134]   J.C. Dyre, Simple liquids' quasiuniversality and the hard-sphere paradigm, J. Phys. Condens. Matter, 28 (2016) 323001.

[135]   N. Michael, M.A. Ankur, G. Orkoulas, A Monte Carlo study of the freezing transition of hard spheres, J. Phys. Condens. Matter, 23 (2011) 325106.

[136]   G. Odriozola, L. Berthier, Equilibrium equation of state of a hard sphere binary mixture at very large densities using replica exchange Monte Carlo simulations, J. Chem. Phys., 134 (2011) 054504.

[137]   M. Rintoul, S. Torquato, Metastability and crystallization in hard-sphere systems, Physical Review Letters, 77 (1996) 4198.

[138]   D. Frenkel, B. Smit, Understanding Molecular Simulation, Academic Press, New York, 2002.

[139]   B. Alder, T. Wainwright, Phase transition for a hard sphere system, The Journal of chemical physics, 27 (1957) 1208-1209.

[140]   B. Alder, T. Wainwright, Velocity autocorrelations for hard spheres, Physical Review Letters, 18 (1967) 988.

[141]   A.J. Liu, S.R. Nagel, The jamming transition and the marginally jammed solid, Annual Review of Condensed Matter Physics, 1 (2010) 347-369.

[142]   A.J. Liu, S.R. Nagel, Nonlinear dynamics: Jamming is not just cool any more, Nature, 396 (1998) 21-22.

[143]   C.S. O'hern, L.E. Silbert, A.J. Liu, S.R. Nagel, Jamming at zero temperature and zero applied stress: The epitome of disorder, Physical Review E, 68 (2003) 011306.

[144]   L. Berthier, T.A. Witten, Glass transition of dense fluids of hard and compressible spheres, Phys. Rev. E, 80 (2009) 021502.

[145]   P. Chaudhuri, L. Berthier, S. Sastry, Jamming transitions in amorphous packings of frictionless spheres occur over a continuous range of volume fractions, Physical Review Letters, 104 (2010) 165701.

[146]   Y. Song, R.M. Stratt, E. Mason, The equation of state of hard spheres and the approach to random closest packing, The Journal of Chemical Physics, 88 (1988) 1126-1133.

[147]   L.E. Silbert, D. Ertaş, G.S. Grest, T.C. Halsey, D. Levine, Geometry of frictionless and frictional sphere packings, Physical Review E, 65 (2002) 031304.

[148]   Theory and simulation of hard-sphere fluids and related systems, in: A. Mulero (Ed.) Lecture Notes in Physics, Springer, Berlin, 2008.

[149] N.F. Carnahan, K.E. Starling, Thermodynamic properties of a rigid-sphere fluid, The Journal of Chemical Physics, 53 (1970) 600-603.

[150] Y. Song, E. Mason, R.M. Stratt, Why does the Carnahan-Starling equation work so well?, The Journal of Physical Chemistry, 93 (1989) 6916-6919.

[151] R.J. Speedy, On the reproducibility of glasses, J. Chem. Phys., 100 (1994) 6684.

[152] R.J. Speedy, Quench rate independence of the hard sphere glass transition, Mol. Phys., 83 (1994) 591.

[153] G.-W. Wu, R.J. Sadus, Hard sphere compressibility factors for equation of state development, AIChE Journal, 51 (2005) 309-313.

[154] J. Kolafa, S. Labík, A. Malijevský, Accurate equation of state of the hard sphere fluid in stable and metastable regions, PCCP, 6 (2004) 2335.

[155] A. Santos, S.B. Yuste, M.L.d. Haro, Communication: Inferring the equation of state of a metastable hard-sphere fluid from the equation of state of a hard-sphere mixture at high densities, J. Chem. Phys., 135 (2011) 181102.

[156] A. Luca, F. Giuseppe, Configurational entropy of hard spheres, J. Phys.: Conden. Matter, 19 (2007) 256207.

[157] A. Santos, S.B. Yuste, M.L.d. Haro, Contact values of the radial distribution functions of additive hard-sphere mixtures in d dimensions: A new proposal, J. Chem. Phys., 117 (2002) 5785.

[158] Z.W. Salsburg, W.W. Wood, Equation of state of classical hard spheres at high density, J. Chem. Phys., 37 (1962) 798.

[159] A. Donev, F.H. Stillinger, S. Torquato, Configurational entropy of binary hard-disk glasses: Nonexistence of an ideal glass transition, J. Chem. Phys., 127 (2007) 124509.

[160] L. Berthier, T.A. Witten, Compressing nearly hard sphere fluids increases glass fragility, EPL (Europhysics Letters), 86 (2009) 10001.

[161] L. Berthier, H. Jacquin, F. Zamponi, Microscopic theory of the jamming transition of harmonic spheres, Phys. Rev. E, 84 (2011) 051103.

[162] A.J. Liu, S.R. Nagel, Jamming and Rheology: Constrained Dynamics on Microscopic and Macroscopic Scales Taylor and Francis, New York, 2001.

[163] N.F. Carnahan, K.E. Starling, Equation of state for nonattracting rigid spheres, J. Chem. Phys., 51 (1969) 635.

[164] H. Liu, A very accurate hard sphere equation of state over the entire stable and metstable region, arXiv:cond-mat/0605392, DOI (2006).

[165] Á. Mulero, Theory and simulation of hard-sphere fluids and related systems, Springer 2008.

[166] M. Schmiedeberg, T.K. Haxton, S.R. Nagel, A.J. Liu, Mapping the glassy dynamics of soft spheres onto hard-sphere behavior, EPL, 96 (2011) 36010.

[167] F. de J. Guevara-Rodríguez, M. Medina-Noyola, Dynamic equivalence between soft- and hard-core Brownian fluids, Phys. Rev. E, 68 (2003) 011405.

[168] P.E. Ramírez-González, L. López-Flores, H. Acuña-Campa, M. Medina-Noyola, Density-temperature-softness scaling of the dynamics of glass-forming soft-sphere liquids, Phys. Rev. Lett., 107 (2011) 155701.

[169] R. Mari, F. Krzakala, J. Kurchan, Jamming versus Glass Transitions, Phys. Rev. Lett., 103 (2009) 025701.

[170] H.C. Andersen, J.D. Weeks, D. Chandler, Relationship between the hard-sphere fluid and fluids with realistic repulsive forces, Phys. Rev. A, 4 (1971) 1597.

[171] G.L. Hunter, E.R. Weeks, The physics of the colloidal glass transition, Rep. Prog. Phys., 75 (2012) 066501.

[172] P.N. Pusey, W. van Megen, Phase behaviour of concentrated suspensions of nearly hard colloidal spheres, Nature, 320 (1986) 340.

[173] L. Marshall, C.F. Zukoski, Experimental studies on the rheology of hard-sphere suspensions near the glass transition, J. Phys. Chem., 94 (1990) 1164.

[174] T. Voigtmann, A.M. Puertas, M. Fuchs, Tagged-particle dynamics in a hard-sphere system: mode-coupling theory analysis, Phys. Rev. E, 70 (2004) 061506.

[175] F. Weysser, A.M. Puertas, M. Fuchs, T. Voigtmann, Structural relaxation of polydisperse hard spheres: comparison of the mode-coupling theory to a Langevin dynamics simulation, Phys. Rev. E, 82 (2010) 011504.

[176] J. Budzien, J.D. McCoy, D.B. Adolf, Solute mobility and packing fraction: A new look at the Doolittle equation for the polymer glass transition, J. Chem. Phys., 119 (2003) 9269.

[177] G.B. McKenna, Glass dynamics: Diverging views on glass transition, Nat Phys, 4 (2008) 673-673.

[178] L. López-Flores, H. Ruíz-Estrada, M. Chávez-Páez, M. Medina-Noyola, Dynamic equivalences in the hard-sphere dynamic universality class, Phys. Rev. E, 88 (2013) 042301.

[179] Y. Rosenfeld, Relation between the transport coefficients and the internal entropy of simple systems, Physical Review A, 15 (1977) 2545.

[180] J.C. Dyre, Perspective: Excess-entropy scaling, The Journal of Chemical Physics, 149 (2018) 210901.

[181] M. Dzugutov, A universal scaling law for atomic diffusion in condensed matter, Nature, 381 (1996) 137.

[182] C. Qi-Long, H. Duo-Hui, Y. Jun-Sheng, W. Ming-Jie, W. Fan-Hou, Transport properties and the entropy-scaling law for liquid tantalum and molybdenum under high pressure, Chinese Physics Letters, 31 (2014) 066202.

[183] R. Chopra, T.M. Truskett, J.R. Errington, Excess entropy scaling of dynamic quantities for fluids of dumbbell-shaped particles, The Journal of Chemical Physics, 133 (2010) 104506.

[184] Y.D. Fomin, V. Ryzhov, N. Gribova, Breakdown of excess entropy scaling for systems with thermodynamic anomalies, Physical Review E, 81 (2010) 061201.

[185] V.V. Vasisht, J. Mathew, S. Sengupta, S. Sastry, Nesting of thermodynamic, structural, and dynamic anomalies in liquid silicon, The Journal of Chemical Physics, 141 (2014) 124501.

[186] S. Higuchi, D. Kato, D. Awaji, K. Kim, Connecting thermodynamic and dynamical anomalies of water-like liquid-liquid phase transition in the Fermi–Jagla model, The Journal of Chemical Physics, 148 (2018) 094507.

[187] S.-T. Lin, M. Blanco, W.A. Goddard III, The two-phase model for calculating thermodynamic properties of liquids from molecular dynamics: Validation for the phase diagram of Lennard-Jones fluids, The Journal of Chemical Physics, 119 (2003) 11792-11805.

[188] J. Wang, B. Chakraborty, J. Eapen, Absolute thermodynamic properties of molten salts using the two-phase thermodynamic (2PT) superpositioning method, Physical Chemistry Chemical Physics, 16 (2014) 3062-3069.

[189]   S.-T. Lin, P.K. Maiti, W.A. Goddard, Dynamics and thermodynamics of water in PAMAM dendrimers at subnanosecond time scales, The Journal of Physical Chemistry B, 109 (2005) 8663-8672.

[190]   T.A. Pascal, S.-T. Lin, W.A. Goddard III, Thermodynamics of liquids: standard molar entropies and heat capacities of common solvents from 2PT molecular dynamics, Physical Chemistry Chemical Physics, 13 (2011) 169-181.

[191]   T. Sun, J. Xian, H. Zhang, Z. Zhang, Y. Zhang, Two-phase thermodynamic model for computing entropies of liquids reanalyzed, The Journal of Chemical Physics, 147 (2017).

[192]   P. Bak, C. Tang, K. Wiesenfeld, Self-organized criticality, Physical review A, 38 (1988) 364.

[193]   J.J. Erpenbeck, W.W. Wood, Molecular dynamics calculations of the hard-sphere equation of state, Journal of Statistical Physics, 35 (1984) 321-340.

[194]   A. Rahman, Correlations in the Motion of Atoms in Liquid Argon, The Physical Review, 136 (1964).

[195]   B.J. Alder, T.E. Wainwright, Studies in molecular dynamics. I. General method, The Journal of Chemical Physics, 31 (1959) 459-466.

[196]   D.S. Cerutti, D.A. Case, Molecular dynamics simulations of macromolecular crystals, Wiley Interdisciplinary Reviews: Computational Molecular Science, 9 (2019) e1402.

[197]   K.E. Kennedy, N. Shafique, J.F. Douglas, F.W. Starr, Cooperative dynamics in a model DPPC membrane arise from membrane layer interactions, Emergent Materials, 2 (2019) 1-10.

[198]   C. Scalliet, L. Berthier, F. Zamponi, Nature of excitations and defects in structural glasses, arXiv preprint arXiv:1906.06894, DOI (2019).

[199]   D.C. Rapaport, The art of molecular dynamics simulation, Cambridge university press2004.

[200]   M.P. Allen, D.J. Tildesley, Computer simulation of liquids, Oxford University Press2017.

[201]   R.E. Rudd, J.Q. Broughton, Coarse-grained molecular dynamics and the atomic limit of finite elements, Physical Review B, 58 (1998) R5893.

[202]   S. Whitelam, L. Berthier, J.P. Garrahan, Dynamic criticality in glass-forming liquids, Physical Review Letters, 92 (2004) 185705.

[203]   J.D. Weeks, D. Chandler, H.C. Andersen, Role of repulsive forces in determining the equilibrium structure of simple liquids, The Journal of Chemical Physics, 54 (1971) 5237-5247.

[204]   E. Flenner, G. Szamel, H. Staley, Universal features of dynamic heterogeneity: Supplemental Material, Physical Review Letters, 112 (2014).

[205]   M. Dzugutov, Monatomic model of icosahedrally ordered metallic glass formers, Journal of Non-Crystalline Solids, 156 (1993) 173-176.

[206]   M.N. Bergroth, M. Vogel, S.C. Glotzer, Examination of dynamic facilitation in molecular dynamics simulations of glass-forming liquids, The Journal of Physical Chemistry B, 109 (2005) 6748-6753.

[207]   W. Kob, C. Donati, S.J. Plimpton, P.H. Poole, S.C. Glotzer, Dynamical heterogeneities in a supercooled Lennard-Jones liquid, Physical Review Letters, 79 (1997) 2827.

[208]   M. Aichele, Y. Gebremichael, F.W. Starr, J. Baschnagel, S. Glotzer, Polymer-specific effects of bulk relaxation and stringlike correlated motion in the dynamics of a supercooled polymer melt, The Journal of Chemical Physics, 119 (2003) 5290-5304.

[209]   M.P. Ciamarra, R. Pastore, A. Coniglio, Particle jumps in structural glasses, Soft Matter, 12 (2016) 358-366.

[210] Y. Gebremichael, M. Vogel, S. Glotzer, Particle dynamics and the development of string-like motion in a simulated monoatomic supercooled liquid, The Journal of Chemical Physics, 120 (2004) 4415-4427.

[211] J.J. Duderstadt, L.J. Hamilton, Nuclear reactor analysis, Wiley New York 1976.

[212] P. Mohazzabi, A.G. Mansoori, Nonextensivity and nonintensivity in nanosystems: A molecular dynamics simulation, Journal of Computational and Theoretical Nanoscience, 2 (2005) 138-147.

[213] R.G. Della Valle, E. Venuti, Quasiharmonic lattice-dynamics and molecular-dynamics calculations for the Lennard-Jones solids, Physical Review B, 58 (1998) 206.

[214] M.P. Desjarlais, First-principles calculation of entropy for liquid metals, Physical Review E, 88 (2013) 062145.

[215] K. Rah, Generalized excluded volume and the diffusivity and viscosity of supercooled liquids and glasses over the entire fragility spectrum, Physica A: Statistical Mechanics and its Applications, 378 (2007) 167-182.

[216] R. Brueckner, Properties and structure of vitreous silica. I, Journal of Non-Crystalline Solids, 5 (1970) 123-175.

[217] Y. Bottinga, P. Richet, D. Weill, Calculation of the density and thermal expansion coefficient of silicate liquids, Bulletin de Minéralogie, 106 (1983) 129-138.

[218] I.V. Blazhnov, N.P. Malomuzh, S.V. Lishchuk, Temperature dependence of density, thermal expansion coefficient and shear viscosity of supercooled glycerol as a reflection of its structure, The Journal of Chemical Physics, 121 (2004) 6435-6441.

[219] A. Karamanov, M. Pelino, Induced crystallization porosity and properties of sintereds diopside and wollastonite glass-ceramics, Journal of the European Ceramic Society, 28 (2008) 555-562.

[220] E. Rössler, Corresponding states analysis for viscosity and nuclear magnetic resonance data in the glass transition regime, The Journal of Chemical Physics, 92 (1990) 3725-3735.

[221] A. Barlow, J. Lamb, A. Matheson, Viscous behaviour of supercooled liquids, Proceedings of the Royal Society of London. Series A. Mathematical and Physical Sciences, 292 (1966) 322-342.

[222] W. Laughlin, D.R. Uhlmann, Viscous flow in simple organic liquids, The Journal of Physical Chemistry, 76 (1972) 2317-2325.

[223] M. Cukierman, J. Lane, D.R. Uhlmann, High-temperature flow behavior of glass-forming liquids: A free-volume interpretation, The Journal of Chemical Physics, 59 (1973) 3639-3644.

[224] R. Greet, D. Turnbull, Glass Transition in o-Terphenyl, The Journal of Chemical Physics, 46 (1967) 1243-1251.

[225] N. Ray, Composition—property relationships in inorganic oxide glasses, Journal of Non-Crystalline Solids, 15 (1974) 423-434.

[226] A. Napolitano, P. B. Macedo, E.G. Hawkins, Viscosity and density of boron trioxide, Journal of the American Ceramic Society, 48 (1965) 613-616.

[227] D.R. Uhlmann, R. Shaw, The thermal expansion of alkali borate glasses and the boric oxide anomaly, Journal of Non-Crystalline Solids, 1 (1969) 347-359.

[228] G.C. Benson, O. Kiyohara, Thermodynamics of aqueous mixtures of nonelectrolytes. I. Excess volumes of water-n-alcohol mixtures at several temperatures, Journal of Solution Chemistry, 9 (1980) 791-804.

[229] O. Kiyohara, G.C. Benson, Ultrasonic speeds and isentropic compressibilities of n-alkanol+ n-heptane mixtures at 298.15 K, The Journal of Chemical Thermodynamics, 11 (1979) 861-873.

Appendices

Appendix A: Simulation Details for Supercooled Liquids

The model supercooled liquids featured in this work are described in this section. They are: the Kob-Andersen [111] and Weeks-Chandler-Andersen system [203, 204] and the harmonic sphere (HARM) system [205, 206]. For these model systems, all simulation parameters are reported in reduced MD units.

A.1   Kob-Andersen System

N = 10,976 (14×14×14 FCC unit cells as initial configuration)

ρ = 1.204

Δt = 0.001443375

r_{cut} = $2.5\sigma_{AA}$

Potential parameters are those used in [111]. The total correlation time used to collect the velocity autocorrelation function is 1,500,000 simulation time steps. Simulations were run in the NVT ensemble for equilibration and in the NVE ensemble for data collection. The following table indicates the number of independent runs (with different initial velocities) conducted for each temperature:

No. of Ind. Runs: KA System	Temperatures
200	0.42, 0.43, 0.44, 0.46
100	0.48, 0.50, 0.52, 0.55, 0.60
20	0.65, 0.70
10	0.80, 1.00, 1.20, 1.40

Final results were produced as the average of the results from each of these independent

simulations. For the analysis of stringlike cooperative motion the same simulation parameters listed above were used, except the number of atoms was set to N = 6,912 (12×12×12 FCC unit cells), and the time step was doubled to Δt = 0.00288675. The temperatures studied were T = 0.48, 0.50, 0.52, 0.55, 0.60, 0.70, 0.80, and 1.00. For each temperature, the simulations were equilibrated in the NVT ensemble for 750,000 time steps, and data was collected over a period of over 500,000 time steps in the NVE ensemble. Configuration snapshots were printed every 100 time steps. Results were averaged over four independent runs per temperature.

A.2   Weeks-Chandler-Andersen System

N = 10,976 (14×14×14 FCC unit cells as initial configuration)

ρ = 1.204

Δt = 0.001443375

r_{cut} = $2.5\sigma_{AA}$

Potential parameters are those used in [111], where the potential is shifted and truncated so that only repulsive interactions are considered among the atoms. The total correlation time used for the velocity autocorrelation function is 1,500,000 simulation time steps. Simulations were run in the NVT ensemble for equilibration and in the NVE ensemble for data collection. The following table indicates the number of independent runs (with different initial velocities) conducted per temperature:

No. of Ind. Runs: WCA System	Temperatures
200	0.28, 0.29
50	0.30, 0.32, 0.34, 0.36
20	0.38, 0.40, 0.42, 0.45, 0.50, 0.55, 0.60

Results were averaged over the results from each of these independent simulations. For the analysis of stringlike cooperative motion the same simulation parameters listed above were used, except the number of atoms was set to N = 6,912 (12×12×12 FCC unit cells), and the time step was

doubled to Δt = 0.00288675. The temperatures studied were T = 0.36, 0.38, 0.40, 0.42, 0,45, 0.50, 0.60, 0.70, 0.80, and 1.00. For each temperature, the simulations were equilibrated in the NVT ensemble for 500,000 time steps, and data was collected over a period of over 500,000 time steps in the NVE ensemble. Configuration snapshots were printed every 100 time steps. Results were averaged over four independent runs per temperature.

A.3 Harmonic Sphere (HARM) System

N = 10,648 (22×22×22 cubic unit cells as initial configuration)

ρ = 0.675

Δt = 0.01

$r_{cut} = \sigma$

Potential parameters are those used in [59]. The total correlation time used to compute the velocity autocorrelation function is 1,000,000 simulation time steps. Simulations were run in the NVT ensemble for cooling, and equilibration and in the NVE ensemble for data collection. Results are averaged over 5 independent runs per temperature. For the analysis of stringlike cooperative motion the same simulation parameters listed above were used, except the number of atoms was set to N = 4,096 (16×16×16 cubic unit cells), and the time step was doubled to Δt = 0.02. The temperatures studied were T = 5.0, 5.5, 6.0, 6.5, 7.0, 8.0, 9.0, 10.0, 12.0, 15.0, 20.0, 25.0, and 30.0. For each temperature, the simulations were equilibrated in the NVT ensemble for 150,000 time steps, and data was collected over a period of over 1,000,000 time steps in the NVE ensemble. Configuration snapshots were printed every 100 time steps. Results were averaged over four independent runs per temperature.

A.4 Dzugutov System

N = 2,048 (8×8×8 cubic unit cells as initial configuration)

ρ = 0.85

Δt = 0.01

$r_{cut} = \sigma$

Potential parameters are those used in [205]. Only results for stringlike cooperative motion were compiled for the Dzugutov system. A relatively small system size was used, as larger systems exhibit an increased likelihood of partial crystallization. For this reason, many independent runs with different initial velocities were conducted, and of those runs the several simulations whose potential energy exhibited a constant value after cooling were selected to perform the post-processing analysis. To perform the explicit cooling, the system was equilibrated at a high temperature of T = 1.6 for 50,000 time steps to erase memory of the initial configuration. Then, at intervals of 50 time steps the temperature was reduced by 0.001 temperature units until the final desired temperature is reached, upon which data collection was begun immediately in the NVT ensemble. The temperatures studied were T = 0.42, 0.43, 0.46, 0.49, 0.52, 0.55, 0.65, 0.80, and 1.00. Data was collected over a period of over 100,000 time steps. Configuration snapshots were printed every 20 time steps. Results were averaged over four independent runs per temperature. Dzugutov system is used only for string tracking analysis.

Appendix B: Internal Consistency of the Hard Sphere Partitioning Method

Some of the assumptions upon which the hard sphere partitioning (HSP) approach warrant additional investigation and verification. As noted above, the partitioning metric can be shown to be $f = D(T, \rho)/D_0^{HS}(T, \rho)$, where D is the diffusion coefficient of the system, and D_0^{HS} is the theoretical diffusivity of a system of hard spheres at the same density as that of the true system and at zero pressure.
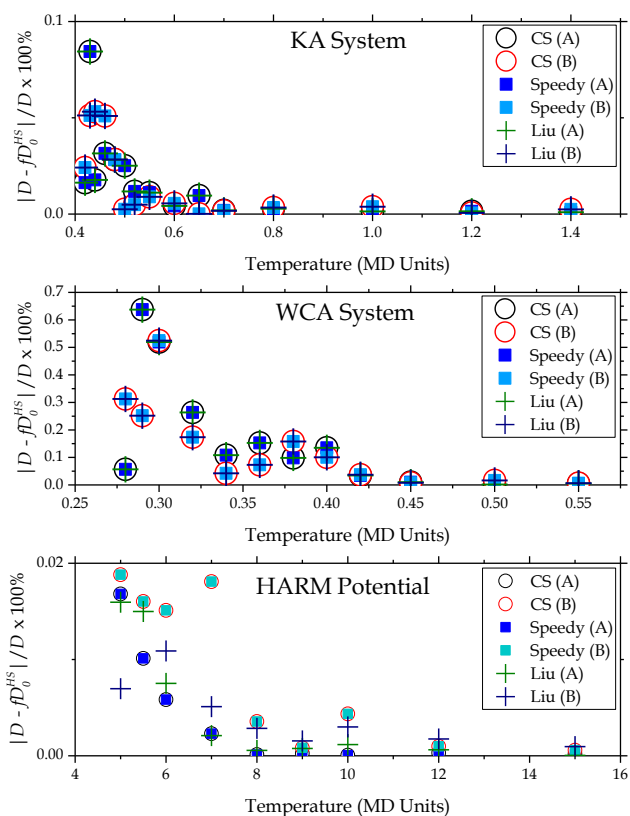

Figure A-1: Calculation of the error E_D^1 for the KA [111], WCA [203], and HARM [204] systems, using the Carnahan-Starling, Speedy, and Liu equations of state.

There is one relation of specific interest: the relative error in the hard sphere diffusion coefficient given by

$$E_D^1 = \left| \frac{fD_0^{HS}(T,\rho) - D(T,\rho)}{D(T,\rho)} \right| \tag{A-1}$$

This error metric quantifies the extent to which the relationship $fD_0^{HS}(T,\rho)$ deviates from the diffusivity of the actual system (evaluated from MD simulations).

The error E_D^1, which is shown in Figure A-1 increases with decreasing temperature, as accurate calculation of the diffusion coefficient, and thus the HSP parameters including the partitioning metric f, becomes more difficult. However, at worst, this error never exceeds 1% for any of the three model systems for any temperature. The Carnahan-Starling, Speedy, and Liu equations produce nearly the same errors for all systems and temperatures.